Computer Simulation of Nonadiabatic Dynamics by means of the Quantum-Classical Liouville Equation

---

by

Daniel A. Uken

Submitted in fulfilment of the
requirements for the degree of
Doctor of Philosophy
in the
School of Chemistry and Physics
University of KwaZulu-Natal
Pietermaritzburg

December 2013

As the candidate's supervisor I have approved this thesis for submission.

Signed: Name: Dr. A. Sergi Date:

Abstract

Simulation of quantum dynamics for many-body systems is an open area of research. For interacting many-body quantum systems, the computer memory necessary to perform calculations has an astronomical value, so that approximated models are needed to reduce the required computational resources. A useful approximation that can often be made is that of quantum-classical dynamics, where the majority of the degrees are treated classically, while a few of them must be treated quantum mechanically. When energy is exchanged very quickly between the quantum subsystem and classical environment, the dynamics is nonadiabatic. Most theories for nonadiabatic dynamics are unsatisfactory, as they fail to properly describe the quantum backreaction of the subsystem on the environment. However, an approach based on the quantum-classical Liouville equation solves this problem. Even so, nonadiabatic dynamics is difficult to implement on a computer, and longer simulation times are often inaccessible due to statistical error. There is thus a need for improved algorithms for nonadiabatic dynamics. In this thesis, two algorithms that utilise the quantum-classical Liouville equation will be qualitatively and quantitatively compared. In addition, stochastic sampling schemes for nonadiabatic transitions will be studied, and a new sampling scheme is introduced [D. A. Uken *et al.*, Phys. Rev. E. **88**, 033301 (2013)] which proves to have a dramatic advantage over existing techniques, allowing far longer simulation times to be calculated reliably.

Preface

The computational work described in this thesis was carried out in the School of Chemistry and Physics, University of KwaZulu-Natal, Pietermaritzburg, from January 2011 to November 2013, under the supervision of Dr Alessandro Sergi.

These studies represent original work by the author and have not otherwise been submitted in any form for any degree or diploma to any tertiary institution. Where use has been made of the work of others it is duly acknowledged in the text.

Declaration 1 - Plagiarism

I, ... declare that

- The research reported in this thesis, except where otherwise indicated, is my original research.
- This thesis has not been submitted for any degree or examination at any other university.
- This thesis does not contain other persons data, pictures, graphs or other information, unless specifically acknowledged as being sourced from other persons.
- This thesis does not contain other persons' writing, unless specifically acknowledged as being sourced from other researchers. Where other written sources have been quoted, then:

  a. Their words have been re-written but the general information attributed to them has been referenced

  b. Where their exact words have been used, then their writing has been placed in italics and inside quotation marks, and referenced.
- This thesis does not contain text, graphics or tables copied and pasted from the Internet, unless specifically acknowledged, and the source being detailed in the thesis and in the Bibliography.

Signed: .....

Declaration 2 - Publications

Details of contribution to publications that form part and/or include research presented in this thesis:

Publication 1 - D. A. Uken, A. Sergi and F. Petruccione, "Stochastic simulation of long-time nonadiabatic dynamics "

Status: Published in *Physica Scripta* (2011).

Computational work performed by D. A. Uken, paper written by A. Sergi, in consultation with D. A. Uken and F. Petruccione.

Publication 2 - D. A. Uken and A. Sergi, "Momentum Shift in Nonadiabatic Dynamics"

Status: Published in *Modern Physics Letters B* (2011).

Computational work performed by D. A. Uken, paper written by A. Sergi and D. A. Uken.

Publication 3 - D. A. Uken, A. Sergi and F. Petruccione, "Filtering schemes in the quantum-classical Liouville approach to nonadiabatic dynamics"

Status: Published in *Physical Review E* (2013).

Computational work performed by D. A. Uken, paper written by D. A. Uken and A. Sergi, in consultation with F. Petruccione.

Signed: .....

Declaration 3 - Conferences and Presentations

Details of conferences attended while a PhD student and presentations given that include research presented in this thesis:

Conferences attended:

- "Quantum Information Processing, Communication and Control 2", Pumula Beach Hotel, South Coast, KZN, 25 - 29 November 2013.
- "Research Workshop on Dissipative Quantum Computing and State Engineering", NIThePKZN and School of Chemistry and Physics, UKZN, 25 - 28 September 2012.
- "Quantum Africa 2, Quantum Science and Technology", Mont Aux Sources Hotel, Northern Drakensberg, South Africa, 3 - 7 September 2012.
- "23rd Chris Engelbrecht Summer School on Quantum Biology", Salt Rock Hotel, Durban, South Africa, 18 - 28 January, 2012.
- "Research Workshop on Quantum Biology", NIThePKZN and School of Physics, UKZN, 7 - 11 November 2011.
- "Workshop on Foundations of Quantum Theory: measurement, the quantum to classical transition, and the flow of time", NIThePStellenbosch, 26 - 28 October, 2011.
- "Research Workshop: Relativistic Quantum Information", NIThePKZN and School of Physics, UKZN, 7 - 11 March 2011.

No conference proceedings.

Signed: .....

Presentations delivered:

- **Title**: Nonadiabatic Dynamics of Quantum-Classical Systems

  Date: 11 June 2012

  Venue: University of Messina, Italy

- **Title**: Algorithms for Simulation of Nonadiabatic Dynamics of Quantum-Classical Systems

  Date: 23 November 2012

  Venue: NITheP, University of Stellenbosch, South Africa

Signed: .....

Contents

Acknowledgements

I would like to begin by thanking my supervisor, Dr. Alessandro Sergi, for his assistance in understanding the theory and always keeping me motivated to give of my best. His constant enthusiasm for our work and long philosophical conversations throughout my PhD studies have inspired my great interest in my line of study.

Secondly to my family, and girlfriend Paula, for their understanding and support throughout my PhD. Without their care I would not have been able to accomplish what I have.

I would also like to thank Binky for help with proof reading of the thesis, and finding those errors that I could not.

Finally, I would like to acknowledge the National Institute for Theoretical Physics (NITheP) for the bursary they awarded me, without which I would not have been able to complete my PhD in Physics.

Chapter 1

Introduction - Simulation of Quantum Dynamics

Despite the huge advances made since the advent of the computer, both in computational technology and in the development of algorithms, simulation of many-body quantum systems remains a great challenge, and is an open area of research today [1]. While almost all classical systems can be solved using a similar technique, due to the complexity of quantum mechanics, there is no overarching method for studying the dynamics of quantum systems. In general, numerical methods for solving quantum dynamics have to be decided on a system by system basis.

Soon after the computer was invented in the mid 20^{th} century, the idea of Molecular Dynamics (MD) simulation was introduced by Alder and Wainwright [2][3] to study the dynamics of molecules or atoms from a classical perspective. Although, as the name implies, MD is the simulation of small particles such as molecules or atoms, it can be applied in essentially the same way to interacting many-body systems for macroscopic bodies, such as planets in the solar system, as it based simply on the numerical solution of Newton's equations of motion for some interaction potential. Molecular dynamics simulation essentially solved the problem of being unable to analytically solve many-body interacting systems, being very successful at simulating

dynamics of systems with very large numbers of particles. Indeed the only limitation on system particle number is computational resources. Unfortunately, however, the incredible success of conventional MD applies only to dynamics of systems that can be treated classically.

Due to the intrinsic classical treatment of particles by MD simulation, it is unable to successfully simulate systems where quantum effects, such as energy-quantisation and tunnelling are important. In systems containing heavier atoms and molecules, the classical treatment is often sufficient, but when considering smaller particles, especially in the case of Hydrogen, a proper quantum mechanical description is required [4].

In principle, this is resolved by performing a full quantum mechanical treatment of the system of study. However, this is unfeasible, and in many cases impossible for any but the simplest of quantum systems. Indeed, even solving three-body quantum systems can be a formidable task. The problems are two fold. Firstly, quantum mechanics itself is difficult to implement on a computer due to its complex mathematical nature. It is formulated not in terms of functions, as in the case of classical mechanics, but in terms of operators which do not necessarily commute. Secondly, the computational expense rises extremely rapidly with increasing number of particles. While in the case of classical mechanics, the computational resources needed to simulate a system can increase as slowly as linearly with number of particles, in the case of quantum systems, the resources required generally increases exponentially due to the increase in the size of the Hilbert space of the system. Indeed it has been estimated [1] that to simulate only 64 electrons in a lattice would require approximately 10^{28}Gb of memory to store a single eigenvector. Even the fastest supercomputers today have of the order of 10^{6}Gb of memory available to them, a far cry from what is required. This stands in contrast to classical simulations, where systems of up to the order of thousands of particles can be simulated on a modern day home computer.

Because of this severe limitation on the simulation of quantum dynamics, one

is forced to resort to approximations to simplify the system of study in some way. One of the first approximations developed was the Born-Oppenheimer approximation, where electronic and nuclear motions are decoupled. This decoupling means that nuclear dynamics occurs on only a single potential energy surface, and the electronic dynamics is for a single quantum state. Techniques such as the Hartree-Fock method [5][6] and Density Functional Theory [7][8] both utilise this approximation and have enjoyed much success.

In many cases, however, this treatment of the quantum dynamics is not sufficient. This occurs especially when nonadiabatic effects in the system are important. When this is the case, dynamics no longer occurs on a single potential energy surface, but on many. There are many examples of such systems, such as photochemical processes and proton transfer, which are inherently nonadiabatic due to avoided crossings in the energy level structure.

In response to this failure of the Born-Oppenheimer approximation to describe nonadiabatic processes, quantum-classical methods such as the Ehrenfest mean-field approach [9] and surface-hopping techniques [10]-[13] were developed. Quantum-classical methods [14] are based on a partitioning of a system of study into two parts. The first part contains the most essential aspects of the system that one is interested, and requires a full quantum treatment. The remainder is then treated in a classical way, and generally comprises heavier, slower moving particles. This approximation thus reduces the many-body quantum problem to just a few essential degrees of freedom that need to be treated quantum mechanically. This makes numerical simulation feasible, as opposed to impossible, since it is a simple matter to simulate a large number of degrees of freedom classically.

Quantum-classical methods have proven highly successful, as a wide range of systems in condensed matter can be reduced to a quantum subsystem interacting with a classical-like environment. Examples of such systems are found in a variety of research areas such as quantum information processing [15][16], quantum optics [17][18], and condensed matter physics [19]. It has also been demonstrated that

rate constants and transport coefficients for chemical processes can be determined using quantum-classical techniques [20][21].

More recently, evidence of coherent quantum effects for energy transfer in photosynthetic systems [22] has resulted in a resurgence of interest in quantum biology [23]. It is naturally not possible to study the large scale, noisy, dissipative environments found in photosynthetic systems in a fully quantum way, and one can therefore think of numerically simulating such systems in a quantum-classical manner, where excited electrons are treated quantum mechanically in an environment of classically treated proteins.

Quantum-classical methods do have their drawbacks, however. Mean-field methods have the problem of being unable to accurately simulate dynamics when the potential energy surfaces of the system are too dissimilar. Surface-hopping schemes solve this problem, but in most cases implement the quantum backreaction - the effect of the subsystem on the environment when a nonadiabatic transition occurs - in an ad hoc fashion [24]. In addition to this, they suffer from large statistical error at longer simulation times. This large error is result of implementation of stochastic sampling schemes for nonadiabatic transitions, and is the biggest limiting factor of current surface-hopping methods.

More recently, a surface-hopping scheme was developed, based on the quantum-classical Liouville equation [25]-[33]. This equation results in a formulation which realises the statistical mechanics of the quantum-classical dynamics in terms of a density matrix, not a wavefunction. It is also able to describe the quantum backreaction in a more rigorous way than previous surface-hopping algorithms. Currently, two separate algorithms have been developed within this formalism, the Sequential Short-time Propagation algorithm [34], and the Trotter Based Quantum-Classical algorithm [35].

These algorithms, however, still suffer from large statistical error at longer times. Recently, it has been shown that, with use of intelligent stochastic sampling schemes for nonadiabatic transitions, it is possible to reduce the statistical error at longer

times [36][37].

In this thesis, a detailed study is performed, analysing the two algorithms within the quantum-classical Liouville equation approach. The two algorithms are compared from both a qualitative and quantitative perspective. In addition to this, a study of current sampling schemes for nonadiabatic transitions is presented, and current methods are compared to a newly devised hybrid scheme [38]. It will be shown that the new scheme greatly outperforms previous techniques, allowing far longer simulation times to be reliably calculated than was previously possible.

The layout of the thesis is as follows. In Chapter 2, the two basic types of quantum-classical methods are discussed - mean-field approaches and surface-hopping methods. In particular, the Ehrenfest mean-field method, and surface-hopping with the fewest switches algorithm proposed by Tully will be considered. Chapter 3 presents a method of representing quantum dynamics in phase space, by means of the Wigner representation. The partial Wigner representation is then discussed, as well as a comparison between Hamiltonian and non-Hamiltonian bracket structures. The quantum-classical Liouville equation is then introduced in Chapter 4, and the non-Hamiltonian quantum-classical bracket is defined. In this chapter, the adiabatic basis is also defined, and the form of the quantum-classical Liouville equation in this basis is given. Chapter 5 outlines the two algorithms within the quantum-classical Liouville approach that are being compared, namely the Sequential Short-time Propagation algorithm and the Trotter Based Quantum-Classical algorithm. In Chapter 6, the original sampling schemes for nonadiabatic transition used by each algorithm are discussed, as well as the newer improved sampling schemes. Chapter 7 presents the spin-boson system. This is the model that was used in the simulations to compare the different algorithms and sampling schemes. In Chapter 8, the results of the numerical calculations are given. Finally in Chapter 9, the results are discussed, and perspectives on future work are given.

Chapter 2

Molecular Dynamics and Methods for Quantum-Classical Systems

2.1 Molecular Dynamics

Developed in the late 1950s by Alder and Wainwright [2][3], Molecular Dynamics is a method for simulating the dynamics of systems comprising many interacting atoms by means of numerical integration of classical equations of motion. It is a powerful method that has been applied to a wide range of systems with much success, including modelling of liquids, biological systems such as proteins, and performing simulations at constant pressure or temperature. It is also used in X-ray crystallography and NMR for determining molecular and crystal structures.

To simulate exactly the dynamics of a many body atomic system, one would need to solve the time-dependent Schrödinger equation for both the nuclear and electronic degrees of freedom. Currently, this is impossible to do for a system comprising more than three atoms and more than one electronic state. It is, however, possible to simulate the approximate dynamics of such systems using MD methods. Molecular

Dynamics techniques are based on two fundamental approximations. The first is the assumption that the motion of the atoms is governed by classical mechanics, and the second is the Born-Oppenheimer approximation.

Despite its success, it is indeed these two approximations that limit the applicability of conventional MD to a wider range of systems and processes. The classical treatment of the nuclei means that intrinsically quantum effects such as tunnelling and zero-point motion are neglected. Molecular Dynamics is thus insufficient if these effects have a large influence in dynamics, such as determining rate constants in proton transfer, as well as low temperature processes.

Due to the Born-Oppenheimer approximation, MD also fails for any system whose dynamics is inherently nonadiabatic, in other words, a system where the nuclear dynamics occurs on multiple potential energy surfaces. Examples of such systems are nonradiative relaxation in large molecules, any system involving electron or charge transfer processes, as well as photochemical systems. The Born-Oppenheimer approximation is explained in more detail below.

2.1.1 Born-Oppenheimer Approximation

The Born-Oppenheimer approximation is based on the assumption that the motions of the slower nuclei and the faster electrons are separable. In other words, the electrons are taken to respond instantaneously to any changes in the nuclear configuration. As a consequence of this, the dynamics of the atomic nuclei occur on only one potential energy surface corresponding to a single electronic state, as opposed to many potential energy surfaces. In general, this potential energy surface is the ground state, and is calculated by solving the time-independent Schrödinger equation for fixed nuclear configurations.

Consider a non-relativistic system comprising N nuclei and n electrons. The positions of the nuclei are given by the vector R, and have masses given by M. The electronic positions are given by r. Note that a notation where N, n and M are multidimensional has been used for simplicity. The total Hamiltonian of such a

system is

$$\hat{H}(r,R) = \hat{T}_n(R) + \hat{T}_e(r) + V(R) + V(r) + V(r,R)\,, \tag{2.1}$$

where $\hat{T}_n(R)$ and $\hat{T}_e(r)$ are the kinetic energy operators for the nuclei and electrons respectively, and $V(R)$, $V(r)$ and $V(r,R)$ are the potential energy of internuclear repulsion, interelectronic repulsion and electronic-nuclear attraction respectively. To exactly simulate the dynamics of this system, the time-dependent Schrödinger equation would need to be solved for this Hamiltonian:

$$\hat{H}\Psi(r,R,t) = i\hbar\frac{\partial}{\partial t}\Psi(r,R,t)\,. \tag{2.2}$$

Since this is not possible, instead the fixed-nuclei approximation is made, and the electronic Hamiltonian is defined as

$$\hat{H}_e(r,R) = \hat{T}_e(r) + V(R) + V(r) + V(r,R)\,. \tag{2.3}$$

Assume that $\psi_i(r,R)$, the eigenfunction solutions to the time-independent Schrödinger equation for the electronic Hamiltonian, are known, and

$$\int_{-\infty}^{\infty} \psi_i^*(r,R)\psi_j(r,R)\,dr = \delta_{ij}\,, \tag{2.4}$$

in other words, the eigenfunctions are orthonormal. Because the eigenfunctions form a complete set, the wavefunction for the total system can be written in terms of them:

$$\Psi(r,R,t) = \sum_i \phi_i(R,t)\psi_i(r,R)\,. \tag{2.5}$$

The eigenfunctions $\psi(r,R)$ are dependent on the electronic position coordinates, but also depend parametrically on the nuclear positions R. Substitution of Eq. (2.5) into Eq. (2.2) gives:

$$\hat{H}\sum_i \phi_i(R,t)\psi_i(r,R) = i\hbar\frac{\partial}{\partial t}\sum_i \phi_i(R,t)\psi_i(r,R)\,. \tag{2.6}$$

The next step is to multiply both sides on the left by $\psi_j^*(r,R)$ and integrating over the electronic coordinates:

$$\begin{aligned}\sum_i \int_{-\infty}^{\infty} \psi_j^*\hat{H}\psi_i\phi_i\,dr &= i\hbar\sum_i\int_{-\infty}^{\infty}\psi_j^*\psi_i\frac{\partial}{\partial t}\phi_i\,dr \\ &= i\hbar\frac{\partial}{\partial t}\phi_j\,. \end{aligned}\tag{2.7}$$

In the final line above, the orthonormality of the eigenfunctions ψ_i has been used. Now consider the left hand side of Eq. (2.7). Using $\hat{H} = \hat{T}_n + \hat{H}_e$, and the fact that ψ_i are the eigenfunctions of $\hat{H}_e$, one can write

$$\begin{aligned}\sum_i \int_{-\infty}^{\infty} \psi_j^*\hat{H}\psi_i\phi_i\,dr &= \sum_i\int_{-\infty}^{\infty}\psi_j^*\hat{T}_n\psi_i\phi_i\,dr + \sum_i\int_{-\infty}^{\infty}\psi_j^*\hat{H}_e\psi_i\phi_i\,dr \\ &= \sum_i\int_{-\infty}^{\infty}\psi_j^*\hat{T}_n\psi_i\phi_i\,dr + E_j\phi_j\,, \end{aligned}\tag{2.8}$$

where orthonormality has again been used. Focus now on the first term on the right hand side above, containing $\hat{T}_n$. The nuclear kinetic energy operator $\hat{T}_n$ contains a double derivative with respect to the R coordinate. Since both ψ_i and ϕ_i depend on

R, the product rule of differentiation must be used to obtain

$$\begin{aligned}
\sum_i \int_{-\infty}^{\infty} \psi_j^* \hat{T}_n \psi_i \phi_i \, dr &= \sum_i \int_{-\infty}^{\infty} \psi_j^* \psi_i \, dr \, \hat{T}_n \phi_i \\
&\quad -2 \sum_i \frac{\hbar^2}{2M} \int_{-\infty}^{\infty} \psi_j^* \frac{\partial}{\partial R} \psi_i \, dr \, \frac{\partial}{\partial R} \phi_i \\
&\quad + \sum_i \int_{-\infty}^{\infty} \psi_j^* \hat{T}_n \psi_i \, dr \, \phi_i \\
&= \hat{T}_n \phi_j \\
&\quad + \sum_i \left[\int_{-\infty}^{\infty} \psi_j^* \hat{T}_n \psi_i \, dr - \frac{\hbar^2}{M} \int_{-\infty}^{\infty} \psi_j^* \frac{\partial}{\partial R} \psi_i \, dr \, \frac{\partial}{\partial R} \right] \phi_i \\
&= \hat{T}_n \phi_j + \sum_j \mathcal{C}_{ji} \phi_i \, . \qquad (2.9)
\end{aligned}$$

The term $\mathcal{C}_{ji}$, defined in the final line above, is known as the coupling operator. Substitution of Eq. (2.9) into Eq. (2.8) and subsequent substitution of Eq. (2.8) into Eq. (2.7) yields

$$i\hbar \frac{\partial}{\partial t} \phi_j = \hat{T}_n \phi_j + E_j \phi_j + \sum_i \mathcal{C}_{ji} \phi_i \, , \qquad (2.10)$$

which is a set of coupled differential equations. However, if the coupling operator $\mathcal{C}_{ji}$ is negligible for all j, the coupling term can be dropped, giving

$$i\hbar \frac{\partial}{\partial t} \phi_j(R,t) = \hat{T}_n(R) \phi_j(R,t) + E_j(R) \phi_j(R,t) \, . \qquad (2.11)$$

The differential equations are now uncoupled, and nuclear dynamics occurs on a single potential energy surface.

Although there are a wide range of systems and situations where the Born-Oppenheimer approximation is applicable, it completely breaks down when nonadiabatic effects are important, in other words, when the coupling between different

adiabatic energy surfaces is no longer negligible. This is most notably the case when there is an avoided crossing (see Fig. 2.1) in the energy level profile. Avoided crossings occur when diabatic energy curves cross, and in this region, adiabatic energy curves come close together with non-negligible coupling. Because of this inability to describe nonadiabatic effects, the Born-Oppenheimer approximation completely fails to describe any system or process containing electronic excitations.

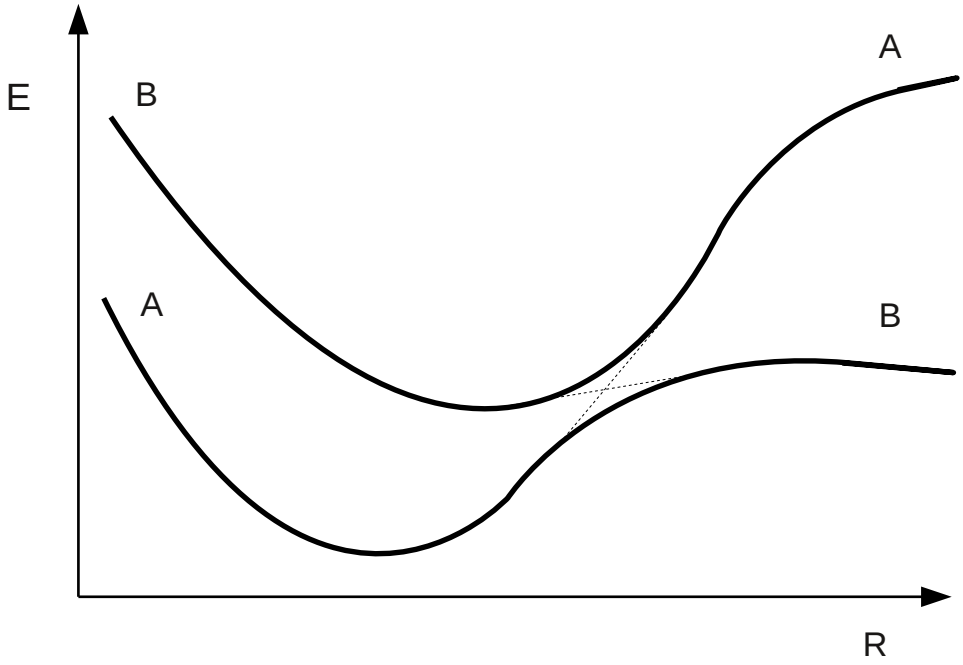

Figure 2.1: Energy profile as a function of nuclear coordinates R for an arbitrary two-state system with two configurations, A and B, corresponding to the diabatic states. The thick solid lines denote the adiabatic potential energy surfaces. The thin dashed lines denote where the diabatic states cross. At this point, an avoided crossing occurs. The adiabatic surfaces come close to each other and are strongly coupled.

Naturally the problems mentioned above are resolved by a full quantum mechanical treatment of all degrees of freedom, but, as mentioned before, this is generally impossible. One of the solutions to this problem is to employ a mixed quantum-classical description of the dynamics. In this description, a small part of the total system of study is treated in a full quantum-mechanical way, with the remainder of the system treated in the conventional MD classical manner.

There are a number of techniques that utilise a quantum-classical description, where the dynamics of the classically treated particles cause transitions in the quantum subsystem. Many of these, however, fail to incorporate the back-reaction of the quantum subsystem onto the classical part of the system [39]-[42]. In cases where the energies of the classical particles is far greater than that of the subsystem, this is acceptable, since the quantum back-reaction has little effect on the classical particles. Nevertheless, for many processes, this is not the case, and the quantum back-reaction must be included in the description of the dynamics.

Two of the main methods which are able to incorporate the quantum back-reaction are the Ehrenfest mean-field method, and the surface-hopping approach. Both techniques have regimes where they are highly successful, and it is perhaps not possible to say if one is superior to the other. A discussion of both is presented below.

2.2 The Ehrenfest Mean-Field Method

It was first Paul Ehrenfest who, in 1927, showed that averages of certain quantum observables follow the same equations of motion as their classical counterparts [43]. This discovery was what lead to the idea of mean-field dynamics, where classical particles evolve in the field of the average of the energy for a quantum system [44, 45]. Possibly the most widely used and successful of these methods is the Ehrenfest mean-field approach [9],[46]-[48]. The derivation presented below follows the method outlined in [4].

It begins by making the standard approximation for mean-field methods that the wavefunction of the total system can be split into a product of two wavefunctions - one for the faster, lighter particles, and another for the (to be classical) slower, heavier particles:

$$\Psi(r,R,t) = \psi(r,t)\phi(R,t)e^{\frac{i}{\hbar}\int^t E_e(t')\,dt'}\,. \tag{2.12}$$

Again, the convention has been used where r and R denote the fast and slow particles respectively, and a multidimensional notation has been used. Both the fast and slow wavefunctions are assumed to be normalised at all times t. The phase term, containing the term $E_e(t)$ is arbitrary, but it is convenient to define it as the expectation value of the total Hamiltonian excluding the kinetic energy of the slow particles. Thus

$$E_e(t) = \int_R \int_r \psi^*(r,t)\phi^*(R,t) H_e(r,R) \psi(r,t)\phi(R,t)\, dr\, dR\,, \tag{2.13}$$

where H_e is, as before, the Hamiltonian that describes the motion of the fast particles in the static field of the slow particles, and is given by Eq. (2.3). The next step is to substitute the approximation for the total wavefunction into the time-dependent Schrödinger equation:

$$\begin{aligned} i\hbar \frac{\partial}{\partial t}\left(\psi(r,t)\phi(R,t) e^{\frac{i}{\hbar}\int^t E_e(t')\,dt'}\right) &= \left(\hat{T}_e(R) + \hat{T}_n(r) + V(r,R)\right) \times \\ & \qquad \psi(r,t)\phi(R,t) e^{\frac{i}{\hbar}\int^t E_e(t')\,dt'}\,. \end{aligned} \tag{2.14}$$

The term $V(r,R)$ comprises the potential energy of the slow particles, the fast particles as well as the potential energy of interaction between the two.

Consider the left-hand side of Eq. (2.14). By the product rule

$$\begin{aligned} \frac{\partial}{\partial t}\left(\psi(r,t)\phi(R,t) e^{\frac{i}{\hbar}\int^t E_e(t')\,dt'}\right) &= \psi(r,t) e^{\frac{i}{\hbar}\int^t E_e(t')\,dt'} \frac{\partial \phi(R,t)}{\partial t} \\ &+ \phi(R,t) e^{\frac{i}{\hbar}\int^t E_e(t')\,dt'} \frac{\partial \psi(r,t)}{\partial t} \\ &+ \frac{i}{\hbar}\psi(r,t)\phi(R,t) E_e(t) e^{\frac{i}{\hbar}\int^t E_e(t')\,dt'}\,. \end{aligned} \tag{2.15}$$

Substituting this back into (2.14), and dividing both sides by the phase term gives

$$\begin{aligned} i\hbar\phi(R,t)\frac{\partial\psi(r,t)}{\partial t} &= \phi(R,t)\hat{T}_e(r)\psi(r,t) + \psi(r,t)\left(\hat{T}_n(R) + V(r,R)\right)\phi(R,t) \\ &- i\hbar\psi(r,t)\frac{\partial\phi(R,t)}{\partial t} + E_e(t)\psi(r,t)\phi(R,t)\,. \end{aligned} \tag{2.16}$$

Next, multiply both sides by $\phi^*(R,t)$ on the left, and integrate over the slow particle coordinates R, using the fact that $\phi(R,t)$ is normalised with the respect to R. From this, one obtains an effective Schrödinger equation for the fast-particle wavefunction $\psi(r,t)$:

$$\begin{aligned} i\hbar\frac{\partial\psi(r,t)}{\partial t} &= \hat{T}_e(r)\psi(r,t) + \left[\int_R \phi^*(R,t)\left(\hat{T}_n(R) + V(r,R)\right)\phi(R,t)\,dR\right]\psi(r,t) \\ &- i\hbar\left[\int_R \phi^*(R,t)\frac{\partial\phi(R,t)}{\partial t}\,dR\right]\psi(r,t) + E_e(t)\psi(r,t)\,. \end{aligned} \tag{2.17}$$

A similar, effective Schrödinger equation for the slow particle wavefunction $\phi(R,t)$ can also be derived by multiplying both sides of Eq. (2.16) by $\psi^*(r,t)$ on the left, and integrating over r:

$$\begin{aligned} i\hbar\frac{\partial\phi(R,t)}{\partial t} &= \hat{T}_n(R)\phi(R,t) + \left[\int_R \psi^*(r,t)\left(\hat{T}_e(r) + V(r,R)\right)\psi(r,t)\,dR\right]\phi(R,t) \\ &- i\hbar\left[\int_R \psi^*(R,t)\frac{\partial\psi(r,t)}{\partial t}\,dR\right]\phi(r,t) + E_e(t)\phi(r,t)\,. \end{aligned} \tag{2.18}$$

Equations (2.17) and (2.18) resemble mean-field equations, except for the derivative integral terms. These terms can be eliminated by considering the following. Because the individual wavefunctions are assumed to be normalised, the derivative integral terms in the square brackets are pure imaginary. Thus, when they are multiplied by the factor $i\hbar$, they become pure real. Now multiplying Eq. (2.17) by $\psi(r,t)$ on the left, and integrating over r:

$$
\begin{aligned}
& i\hbar \int_r \psi^*(r,t) \frac{\partial \psi(r,t)}{\partial t}\, dr + i\hbar \int_r \psi^*(r,t)\psi(r,t)\, dr \int_R \phi^*(R,t) \frac{\partial \phi(R,t)}{\partial t}\, dR \\
= \quad & \int_r \int_R \psi^*(r,t)\phi(R,t) \left(\hat{T}_n + \hat{T}_e + V(r,R) \right) \phi(R,t)\psi_i(r,t)\, dR\, dr \\
+ \quad & E_e(t) \int_r \psi^*(r,t)\psi(r,t)\, dr \,. \qquad (2.19)
\end{aligned}
$$

Again, the fact that the wavefunctions are normalised can be used, as well as the definition of the total Hamiltonian $\hat{H}(r,R) = \hat{T}_n(R) + \hat{T}_e(r) + V(r,R)$, to give

$$
\begin{aligned}
i\hbar \int_r \psi^*(r,t) \frac{\partial \psi(r,t)}{\partial t}\, dr \quad + \quad & i\hbar \int_R \phi^*(R,t) \frac{\partial \phi(R,t)}{\partial t}\, dR - E_e(t) \\
= \quad & \int_r \int_R \psi^*(r,t)\phi(R,t)\hat{H}(r,R)\phi(R,t)\psi(r,t)\, dR\, dr \\
= \quad & E \,, \qquad (2.20)
\end{aligned}
$$

where E is the total energy of the system, including fast and slow particles. This equation is the only constraint on the derivative integral terms, and can be chosen arbitrarily. For reasons that will become apparent, it is convenient to define these terms in following way:

$$
i\hbar \int_r \psi^*(r,t) \frac{\partial \psi(r,t)}{\partial t}\, dr = E_e(t) \,, \qquad (2.21)
$$

and

$$
i\hbar \int_R \phi^*(R,t) \frac{\partial \phi(R,t)}{\partial t}\, dR = E \,. \qquad (2.22)
$$

Substituting these definitions back into Eqs. (2.17) and (2.18) yields

$$i\hbar\frac{\partial\psi(r,t)}{\partial t} = \hat{T}_e(r)\psi(r,t) + \left[\int_R \phi^*(R,t)V(r,R)\phi(R,t)\,dR\right]\psi(r,t)\,, \tag{2.23}$$

and

$$i\hbar\frac{\partial\phi(R,t)}{\partial t} = \hat{T}_n(R)\phi(R,t) + \left[\int_r \psi^*(r,t)\hat{H}_e(r,R)\psi(r,t)\,dr\right]\phi(R,t)\,. \tag{2.24}$$

These equations are of a general form for a mean-field theory. They are effective Schrödinger equations, where the wavefunction for the fast particles is calculated using the mean-field of the slow particles, and the slow particle wavefunction is determined using the mean-field of the fast particles. In this manner, there is a feedback in both directions between the slow and fast particles. This is, however, still not a quantum-classical description, as both slow and fast degrees of freedom are still being treated quantum-mechanically. To obtain the Ehrenfest mean-field equations, the classical limit needs to be taken for the effective Schrödinger equation for the slow particles, Eq. (2.24).

To this end, the wavefunction for the slow particles is factored into its amplitude and phase:

$$\phi(R,t) = A(R,t)e^{\frac{i}{\hbar}S(R,t)} \tag{2.25}$$

Equation (2.24) then becomes

$$i\hbar\frac{\partial}{\partial t}\left(Ae^{\frac{i}{\hbar}S}\right) = -\frac{\hbar^2}{2M}\frac{\partial^2}{\partial R^2}\left(Ae^{\frac{i}{\hbar}S}\right) + \left[\int_r \psi^*(r,t)\hat{H}_e\psi(r,t)\,dr\right]Ae^{\frac{i}{\hbar}S}\,. \tag{2.26}$$

Note that A and S still depend on R and t, even though the dependence is no longer

shown. It is easier to deal with each term separately, so first consider the left-hand side of Eq. (2.26):

$$i\hbar\frac{\partial}{\partial t}\left(Ae^{\frac{i}{\hbar}S}\right) = i\hbar e^{\frac{i}{\hbar}S}\frac{\partial A}{\partial t} - Ae^{\frac{i}{\hbar}S}\frac{\partial S}{\partial t}\,. \tag{2.27}$$

The first term on the right-hand side of Eq. (2.26) can also be expanded using the product rule:

$$\begin{aligned} -\frac{\hbar^2}{2M}\frac{\partial^2}{\partial R^2}\left(Ae^{\frac{i}{\hbar}S}\right) &= -\frac{\hbar^2}{2M}e^{\frac{i}{\hbar}S}\frac{\partial^2 A}{\partial R^2} - \frac{i\hbar}{M}e^{\frac{i}{\hbar}S}\frac{\partial A}{\partial t}\frac{\partial S}{\partial t} \\ &- \frac{i\hbar}{2M}Ae^{\frac{i}{\hbar}S}\frac{\partial^2 S}{\partial R^2} + \frac{1}{2M}Ae^{\frac{i}{\hbar}S}\left(\frac{\partial S}{\partial R}\right)^2 \end{aligned} \tag{2.28}$$

Substituting Eqs. (2.27) and (2.28) into Eq. (2.26) and dividing both sides by $e^{\frac{i}{\hbar}S}$ gives

$$\begin{aligned} i\hbar\frac{\partial A}{\partial t} - A\frac{\partial S}{\partial t} &= -\frac{\hbar^2}{2M}\frac{\partial^2 A}{\partial R^2} - \frac{i\hbar}{M}\frac{\partial A}{\partial R}\frac{\partial S}{\partial R} - \frac{i\hbar}{A}\frac{\partial^2 S}{\partial R^2} + \frac{1}{2M}A\left(\frac{\partial S}{\partial R}\right)^2 \\ &+ A\int_r \psi^*(r,t)H_e(r,R)\psi(r,t)\,dr. \end{aligned} \tag{2.29}$$

This equation can be split into two equations, one for the real components, and another for the imaginary terms. Equating the real terms, and dividing through by A yields

$$\frac{\partial S}{\partial t} + \frac{1}{2M}\left(\frac{\partial S}{\partial R}\right)^2 + \int_r \psi^*(r,t)H_e(r,R)\psi(r,t)\,dr = \frac{\hbar^2}{2M}\frac{1}{A}\frac{\partial^2 A}{\partial R^2}\,. \tag{2.30}$$

Secondly, equating the imaginary terms and dividing through by $\hbar$ gives

$$\frac{\partial A}{\partial t} + \frac{1}{M}\frac{\partial A}{\partial t}\frac{\partial S}{\partial t} + \frac{1}{2M}A\frac{\partial^2 S}{\partial R^2} = 0\,. \tag{2.31}$$

The two equations above still describe the evolution of a wavefunction, and are interchangeable with the effective Schrödinger equation for the slow particles, Eq. (2.24). The particles are thus still treated quantum mechanically at this point. In order to ensure classical treatment of the slow particles, the classical limit is taken in the usual way, by setting $\hbar \to 0$. Equation (2.30) then becomes

$$\frac{\partial S}{\partial t} + \frac{1}{2M}\left(\frac{\partial S}{\partial R}\right)^2 + \int_r \psi^*(r,t)H_e(r,R)\psi(r,t)\,dr = 0\,. \tag{2.32}$$

This is simply a Hamilton-Jacobi Equation, and is completely equivalent to Newton's equations of motion, where the potential is given by the average value (mean-field) of the energy of the fast particles:

$$\frac{dP}{dt} = -\frac{\partial}{\partial R}\left(\int_r \psi^*(r,t)H_e(r,R)\psi(r,t)\,dr\right)\,. \tag{2.33}$$

Note however, that the description is not yet complete, as the effective Schrödinger equation for the fast particles still contains the wavefunction for the slow particles. The customary solution to this is to assume that the wavefunction $\phi(R,t)$ can be replaced by $\delta(R)$. The effective Schrödinger equation for the fast particles is thus

$$i\hbar\frac{\partial\psi(r,R,t)}{\partial t} = H_e(r,R)\psi(r,R,t)\,. \tag{2.34}$$

Since the equation includes the classical positions of the slow particles, the dependence on R has been included here.

The Ehrenfest mean-field method is defined by Eqs. (2.33) and (2.34). The slow particle dynamics are given by classical trajectories that move in the mean-field of the fast particles, (see Fig. 2.2) and the wavefunctions for the fast particles are calculated in the static field of the slow particles. Although the slow particles are treated completely classically, the fast particles, which are generally the subsystem that one is most interested in studying are still treated in a full quantum way. From the equations it can be seen that energy can flow in both directions, from the classical part to the quantum subsystem, and vice versa. The Ehrenfest approach thus includes the quantum back-reaction which is neglected by many other quantum-classical techniques.

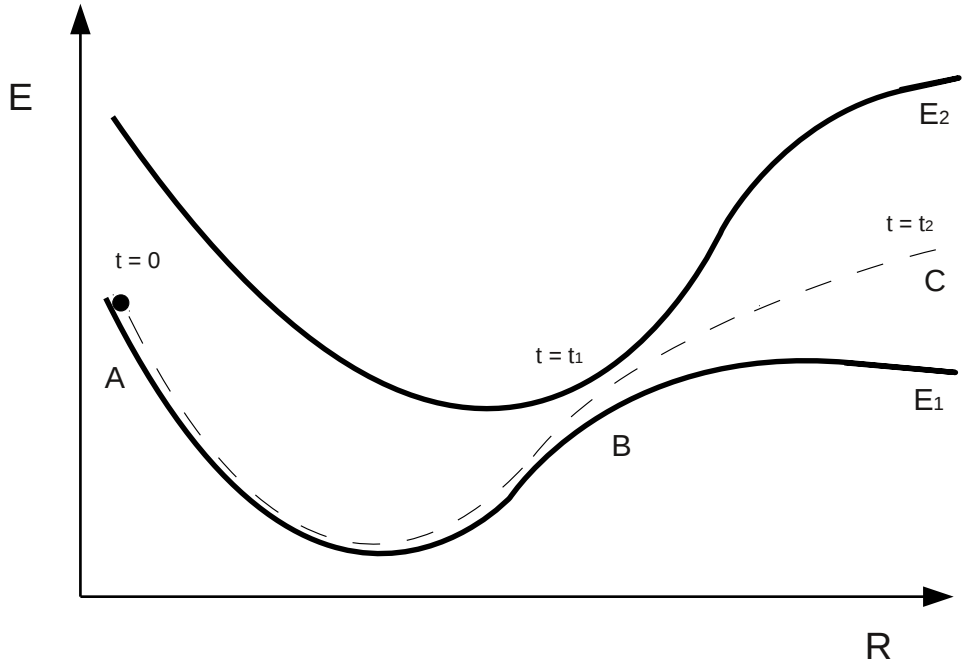

Figure 2.2: Example of a classical trajectory in the Ehrenfest method for a two-state system. In this example, the trajectory begins at configuration A in a pure ground state at time zero. Because the initial state is pure ground state, the mean-field, given by the dashed line, resembles the ground state. At time t_1 in the trajectory, it encounters an avoided crossing at B, and the coupling results in some amplitude for the excited state. The mean-field now has contributions from both the ground state and excited state, and at time t_2, the classical trajectory is in configuration C, and is evolving on a completely mixed mean-field surface.

Note further that although certain techniques include representing the equations

in the adiabatic basis, this is not necessary. The equations can be implemented numerically as is, by propagating a wave packet.

The Ehrenfest approach has shown success for a number of systems and processes, most notably the dynamics involved in energy transfer at metal surfaces. The most common example is that of a carbon monoxide (CO) molecule adsorbed to the face of a copper crystal [49][50][51]. In this case, conventional MD calculates a lifetime for the CO stretching mode that is many orders of magnitude too large, because it fails to include the inherent nonadiabatic effects involved. The Ehrenfest method however, has proved to be quite accurate [4]. This is due to the fact that the individual adiabatic potential energy surfaces are close to being parallel. In fact, whenever the adiabatic potential energy surfaces are very similar, the Ehrenfest approach tends to perform well. This is due to the fact that the classical particle dynamics governed by the mean-field is close to the dynamics on any particular adiabatic potential energy surface.

This is, however, one of two serious limitations of the Ehrenfest mean-field method. Despite its success, it is only accurate when the potential energy surfaces which determine the classical particle dynamics are not too dissimilar. When the surfaces are significantly different, the classical dynamics on individual potential surfaces diverge, and the dynamics according to the mean-field fails to describe the classical dynamics correctly. This problem becomes particularly apparent when one wishes to study a pathway which has a low probability. Because the mean-field is weighted by the populations of the different states, the dynamics will always be similar to the dynamics on the high probability pathways, and thus fail to describe channels of low probability.

The second problem of the Ehrenfest method is that it fails to satisfy the condition of microscopic reversibility. To illustrate this, consider a two state system where the adiabatic potential energy surfaces are weakly coupled. Dynamics of the system when it is initially in state 1 and then develops amplitude in state 2 is governed by a mean-field potential that is very different to the reverse path where the

system is initially in state 2. Since the dynamics for the forward and reverse path are governed by different mean-field surfaces, their dynamics will diverge, and microscopic reversibility will not be satisfied. In an effort to resolve these problems encountered by the Ehrenfest method, a new quantum-classical approach for dealing with nonadiabatic dynamics was developed, namely surface-hopping.

2.3 Surface-hopping Approach

The surface-hopping approach to nonadiabatic dynamics was first proposed by Tully and Preston in 1971, and applied to the reaction of protons with D_2 molecules [10]. It can be viewed as an extension of conventional MD, as dynamics is calculated similarly to MD, except it occurs on multiple potential energy surfaces, as opposed to one.

The derivation of the surface hopping approach begins similarly to that of the Born-Oppenheimer approximation above, by expressing the total wavefunction of the system by a sum over states. Although it is not required, it is convenient to use the adiabatic basis, as it helps facilitate interpretation of the surface-hopping method. The total wavefunction can thus be written as

$$\Psi(r, R, t) = \sum_i \psi_i(r, R)\phi_i(R, t)\,, \tag{2.35}$$

where all the symbols have the same meaning as used previously. The terms $\phi_i(R, t)$ are the wavefunctions of the slow particles, but note that they are not orthonormal, as integrating the modulus square of $\phi_i(R, t)$ gives the population of fast particle quantum state $\psi_i(r, R)$ at time t.

The next step is to substitute Eq. (2.35) into the time-dependent Schrödinger equation and, as before, premultiply both sides by $\psi_j^*(r, R)$ and integrate over fast particle coordinate r. This yields Eq. (2.10), however, in the surface-hopping case it is more convenient to right it in the form

$$
\begin{aligned}
i\hbar\frac{\partial\phi_j(R,t)}{\partial t} &= -\frac{\hbar^2}{2M}\frac{\partial^2}{\partial R^2}\phi_j(R,t) + E_j\phi_j(R,t) \\
&+ \frac{\hbar^2}{2M}\sum_i D_{ji}(R)\phi_i(R,t) - \frac{\hbar^2}{M}\sum_{i\neq j} d_{ji}(R)\frac{\partial}{\partial R}\phi_i(R,t)\,,
\end{aligned}
\tag{2.36}
$$

where $D_{ji}(R)$ and $d_{ji}(R)$ are defined as

$$
D_{ji}(R) = -\int_r \psi_j^*(r,R)\frac{\partial^2}{\partial R^2}\psi_i(r,R)\,dr\,, \tag{2.37}
$$

and

$$
d_{ji}(R) = \int_r \psi_j^*(r,R)\frac{\partial}{\partial R}\psi_i(r,R)\,dr\,. \tag{2.38}
$$

The term $d_{ji}(R)$ is known as the nonadiabatic coupling vector, and it indicates coupling strength between states i and j. The first two terms on the right-hand side of Eq. (2.36) describe adiabatic dynamics of the slow particles on potential energy surface j. The final two terms govern the change in population of state j due to coupling with other states. These are the terms that are dropped in the Born-Oppenheimer approximation.

The next step is to take the classical limit for the slow particles, as in the case of the Ehrenfest method. This is performed in a similar way as before, that is, to write the wavefunction for the slow particles as a product of amplitude and phase (Eq. (2.25)). Substitution into Eq. (2.36) and subsequent splitting of real and imaginary terms yields

$$\frac{\partial S_j}{\partial t} + \frac{1}{2M}\left(\frac{\partial S_j}{\partial R}\right)^2 + E_j = \frac{\hbar^2}{2M}\frac{1}{A}\frac{\partial^2 A_j}{\partial R^2} - \frac{\hbar^2}{2M}\sum_i \frac{A_i}{A_j} D_{ji} e^{\frac{i}{\hbar}(S_i - S_j)} + \frac{\hbar^2}{M}\frac{1}{A_j} d_{ji}\frac{\partial A_i}{\partial R} e^{\frac{i}{\hbar}(S_i - S_j)}\,, \tag{2.39}$$

and

$$\frac{\partial A_j}{\partial t} + \frac{1}{M}\frac{\partial A_j}{\partial R}\frac{\partial S_j}{\partial R} + \frac{1}{2M} A_j \frac{\partial^2 S_j}{\partial R^2} + \frac{1}{M}\sum_i A_i d_{ji}\frac{\partial S_i}{\partial R} e^{\frac{i}{\hbar}(S_i - S_j)} = 0\,. \tag{2.40}$$

The classical limit is achieved by setting the reduced Planck constant to zero in Eq. (2.39). All the terms on the right hand side then disappear, giving a Hamilton-Jacobi equation,

$$\frac{\partial S_j}{\partial t} + \frac{1}{2M}\left(\frac{\partial S_j}{\partial R}\right)^2 + E_j = 0\,, \tag{2.41}$$

similar to the case of the Ehrenfest method. This equation is thus equivalent to Newton's equations for the slow particles. In the Ehrenfest method, however, the dynamics occurred on the mean of the adiabatic potential energy surfaces, where as in the surface-hopping case, this Hamilton-Jacobi equation is for a single surface. Equation (2.40), containing the nonadiabatic coupling vector $d_{ji}(R)$, governs the values of the coefficients A_j, the modulus square of which are the populations of the adiabatic states.

Equation (2.41), representing the classical dynamics on a single adiabatic surface is easy to perform on a computer as it is simply dynamics in the Born-Oppenheimer approximation. However, implementation of Eq. (2.40) is, in general, far more difficult. Surface-hopping algorithms attempt to solve this by using a swarm of independent trajectories, which evolve on a single adiabatic state, with a hopping

algorithm which determines when nonadiabatic transitions or 'hops' occur between states (see Fig 2.3). This is done in a way which approximately preserves the correct populations of the swarm in each adiabatic state.

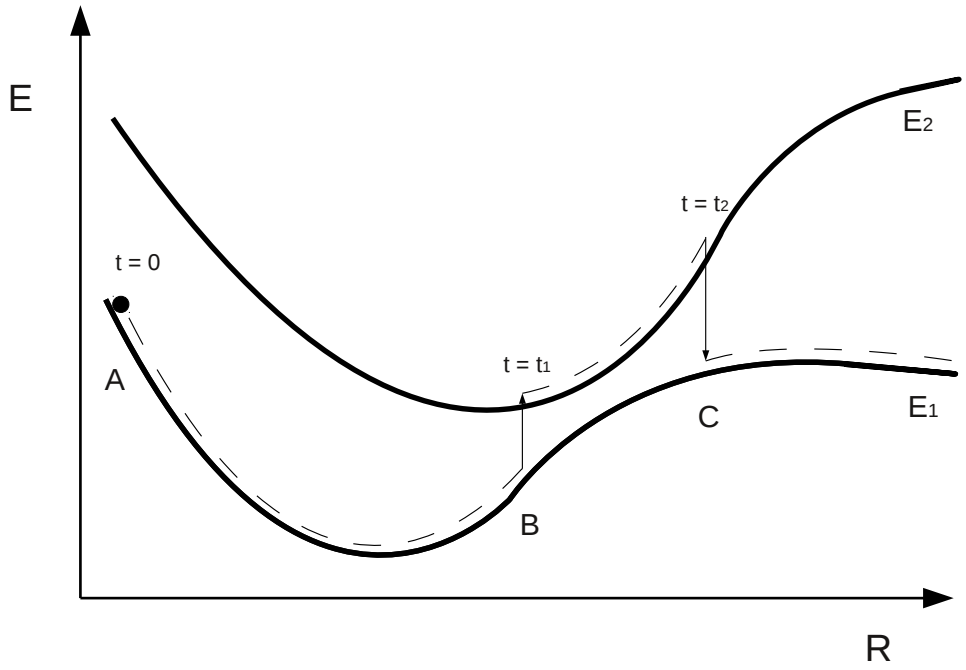

Figure 2.3: Example of a classical trajectory in the surface-hopping approach for a two-state system. In this example, the trajectory, given by the dashed line, begins at configuration A in the ground state at time zero. At time t_1 in the trajectory, at configuration B, a nonadiabatic transition occurs from the ground state to the excited. Between times t_1 and t_2, the trajectory evolves on the excited state energy surface. At time t_2 at configuration C, another transition occurs down to the ground state. After this the trajectory evolves on the ground state surface. Although transitions can occur at any point in configuration space, they are most likely to occur around the avoided crossing, where coupling between the surfaces is strong.

It is the way these nonadiabatic transitions are implemented that is the most defining characteristic of a specific surface-hopping scheme. They are generally performed using a stochastic algorithm, which uses some probability which determines whether or not a transition will occur. In the original surface-hopping scheme by Tully and Preston [10], hops between states could only occur at predetermined locations. These were, in general at the location of an avoided crossing where there is strong coupling, and thus large probability of transition between states.

This limitation was later removed by the introduction of the so-called "fewest switches" algorithm. This algorithm provides a way of obtaining the correct populations at each time t in the simulation using only the fewest number of transitions needed to obtain them. The populations are calculated using numerical integration, and the algorithm is derived by imposing the fewest switches rule. To derive this, consider a case where N trajectories are being propagated. At some time t, there will be some fraction N_i/N of the trajectories that are in state i. Since $|A_i|^2$ is the fractional population of each state,

$$N_i(t) = |A_i(t)|^2 N \,. \tag{2.42}$$

If, after a time step δt, the population $|A_i(t+\delta t)|^2$ is greater than $|A_i(t)|^2$, then the probability of transition from state i to any other state is set to zero. If, however, the population is smaller, then the probability of a trajectory in state i moving to another state is given by

$$P_i(t+\delta t) = \frac{\delta N}{N_i(t)} \,, \tag{2.43}$$

where $\delta N = N_i(t) - N_i(t+\delta t)$. This can be rewritten in terms of the population coefficients:

$$\begin{aligned} P_i(t+\delta t) &= \frac{|A_i(t)|^2 - |A_i(t+\delta t)|^2}{|A_i(t)|^2} \\ &\approx -\frac{\delta t}{|A_i(t)|^2} \frac{d|A_i(t)|^2}{dt} \,, \end{aligned} \tag{2.44}$$

where, in the last line, a first order approximation for the time derivative has been made. The probability of a trajectory undergoing a transition from state i to a specific other state j is then determined by the nonadiabatic coupling element for states

i and j. The probability given in Eq. (2.44) ensures that the correct population is kept at each time t. The algorithm fails to achieve the correct populations, however, when transitions would occur in regions where it is energetically forbidden. When these so-called classical forbidden transitions would occur, the usual way of dealing with them is to stay on the initial energy surface. This leads to discrepancies in the calculated and analytical populations, although the error caused by this problem is generally small.

A point of contention for surface-hopping schemes is the backreaction of the fast, quantum particles on the slow, classical particles. Although surface-hopping algorithms do include the backreaction, as opposed to some other quantum-classical methods, it is generally implemented in an ad hoc way. In most surface-hopping algorithms, when a transition occurs, the velocity is instantaneously adjusted in such a way that energy of the total system is conserved. Most commonly, the velocity is rescaled in the direction of the nonadiabatic coupling vector $d_{ji}(R)$. This non-rigorous way of describing the quantum backreaction is generally considered a flaw in the surface-hopping method.

A further point worthy of note is that the surface-hopping approach is more computationally expensive than the Ehrenfest method. Since dynamics in the Ehrenfest method occurs on only a single mean surface, only one trajectory is required for each classical degree of freedom. In the case of surface-hopping, however, depending on the number of adiabatic states accessible, there may be many different trajectories.

Despite these problems, surface-hopping algorithms remain a valuable tool for simulation of quantum-classical dynamics, especially in cases where the Ehrenfest method fails. Due to the nature of the surface-hopping approach, all potential pathways are investigated, and not just the mean-field pathway. Surface-hopping schemes have been used very effectively for describing proton transfer [21][52] for example, a process where the Ehrenfest method is known to be unsuccessful.

More recently, methods have been proposed based on partial Wigner transforms. This has led to the so-called quantum-classical Liouville approach, which, while

mainly surface-hopping in nature, also exhibits some mean-field properties. It has been shown to be quite successful, and has removed some of the problems with the classic surface-hopping algorithms.

Chapter 3

Quantum Mechanics in Phase Space

3.1 Phase Space Representation of Quantum Mechanics

It has long been known that, in certain conditions (generally when the limit $\hbar \to 0$ is taken), probability distributions for many dynamical quantum variables approach their classical counterparts [53]. This can be performed using either a configuration space representation or a momentum space representation, but it still does not provide a full classical description of quantum mechanics. In classical mechanics, one can see from the equations of motion that the position and momentum are inherently linked:

$$\begin{aligned} \frac{dp}{dt} &= \frac{\partial}{\partial q} H(q,p,t) \ , \\ \frac{dq}{dt} &= \frac{\partial}{\partial p} H(q,p,t) \ , \end{aligned} \tag{3.1}$$

and probability distributions do not have to be functions of only position or momentum, but indeed of both and are known as phase space distribution functions.

In order to represent quantum mechanics in a more classical fashion, it would thus be desirable to obtain a phase space like distribution for a quantum system. One of the most successful attempts to achieve this is provided by the work of Hermann Weyl and Eugene Wigner [54][55].

3.1.1 The Wigner Representation

In Schrödinger's formulation of quantum mechanics, wavefunctions and probability densities are, in general, given as functions of position space [56]:

$$\psi(x) = \langle x|\psi\rangle, \quad P(x) = |\psi(x)|^2 \, . \tag{3.2}$$

To obtain the wavefunction, and thus probability density, in momentum space, one simply has to perform a Fourier transform for the position space wavefunction:

$$\psi(p) = \frac{1}{\sqrt{\hbar}} \int e^{-ixp/\hbar} \psi(x) dx \, . \tag{3.3}$$

As mentioned above, however, it would be desirable to represent the probability densities as functions of both position and momentum at the same time. To be interpreted as a probability distribution, this phase space function would need to be both normalised over phase space, as well as be pointwise positive. In addition to this, it must be possible to use the function to calculate expectation values, since all the information of a quantum system is given by quantum averages of physical observables. The Wigner function satisfies all these properties, except for the pointwise positivity condition. Despite this, it has some very useful properties.

In order to define the Wigner function, the Weyl transform first needs to be introduced. For an arbitrary operator $\hat{\chi}$, the Weyl transform [55] is given by

$$\tilde{\chi}(x,p) = \int e^{-ipy/\hbar} \langle x + y/2|\hat{\chi}|x - y/2\rangle dy \, , \tag{3.4}$$

where a tilde is used to denote the Weyl transform of an operator. Here the operator

being transformed was represented in the position basis, but exactly the same result is achieved for an operator in the momentum basis:

$$\tilde{\chi}(x,p) = \int e^{ixy/\hbar} \langle p + y/2 | \hat{\chi} | p - y/2 \rangle dy \; . \tag{3.5}$$

The Weyl transform therefore provides a method of representing a quantum operator as a function of phase space, which was a historical step in the field of quantum mechanics. Prior to this representation, quantum mechanics was described only using operators acting on wave functions in configurational space (Schrödinger), or operators given by matrices (Heisenberg). When Weyl first introduced this transform in 1931 and later Wigner the Wigner function in 1932, it was the first time that it was proven that quantum mechanics could be described by functions, and not only as operators.

An important property of the Weyl transform is the fact that integration of the product of the Weyl transforms of two operators over phase space yields the trace of the product of two operators untransformed [56]:

$$\mathrm{Tr}\left(\hat{A}\hat{B}\right) = \frac{1}{h} \int \int \tilde{A}(x,p) \tilde{B}(x,p) dx \, dp \; . \tag{3.6}$$

This is a highly important identity since, as will be shown later, it allows for the determination of expectation values using the Wigner function.

The Wigner function for a pure state is defined as the Weyl transform of the density matrix divided by Planck's constant [54]:

$$\begin{aligned} W(x,p,t) = \frac{\tilde{\rho}(x,p,t)}{h} &= \frac{1}{h} \int e^{-ipy/\hbar} \langle x + y/2 | \hat{\rho}(t) | x - y/2 \rangle \, dy \\ &= \frac{1}{h} \int e^{-ipy/\hbar} \langle x + y/2 | \psi \rangle \langle \psi | x - y/2 \rangle \, dy \\ &= \frac{1}{h} \int e^{-ipy/\hbar} \psi(x + y/2) \psi^*(x - y/2) \, dy \; , \end{aligned}$$

(3.7)

and has some interesting properties. Firstly, it is a simple matter to recover either the position space or momentum space probability distribution through a simple integration [57]:

$$\int W(x,p,t)\,dp = |\psi(x,t)|^2\,, \quad \int W(x,p,t)\,dx = |\psi(p,t)|^2\,, \tag{3.8}$$

and secondly, using Eq. (3.6), it is possible to show that integrating the product of the Wigner transform and the Weyl transform of an operator over phase space yields its expectation value.

$$\begin{aligned} \langle\chi\rangle = \text{Tr}\ (\hat{\rho}\hat{\chi}) &= \frac{1}{h}\int\int \tilde{\rho}(x,p)\tilde{\chi}(x,p)dx\,dp \\ &= \int\int W(x,p)\tilde{\chi}(x,p)dx\,dp\,, \end{aligned} \tag{3.9}$$

Equation (3.9) shows that the Wigner function satisfies the third condition for it to be interpreted as a phase space probability density. It is quite simple to show that the Wigner function is also normalised over phase space, the first condition given above.

Taking the Weyl transform of the identity matrix, it can be shown that it is unity:

$$\begin{aligned} \tilde{1} &= \int e^{-ipy/\hbar}\langle x+y/2|\hat{1}|x-y/2\rangle \\ &= \int e^{-ipy/\hbar}\delta(y)\,dy = 1\,. \end{aligned} \tag{3.10}$$

Using this fact, in conjunction with the identity for the trace of operator products in Eq. (3.6), one obtains

$$\begin{aligned}\int\int W(x,p)dx\,dp &= \frac{1}{h}\int\int \tilde{\rho}(x,p)\tilde{1}dx\,dp \\ &= \mathrm{Tr}\left(\hat{\rho}\hat{1}\right) = 1 \end{aligned} \tag{3.11}$$

Using the Wigner function, it is also possible to determine whether or not the system is in a pure state, analogous to the $\mathrm{Tr}\,(\hat{\rho}^2) = 1$ condition for pure states. If the integral over phase space of the square of the Wigner function multiplied by Planck's constant is equal to one, then the state is pure. This is shown by the following:

$$\begin{aligned} h\int\int W(x,p)^2 dx\,dp &= \left(\frac{1}{h}\int\int \tilde{\rho}(x,p)\tilde{\rho}(x,p)dx\,dp\right) \\ &= \mathrm{Tr}\,(\hat{\rho}^2)\begin{cases} = 1 & \text{if pure state} \\ < 1 & \text{if mixed state} \end{cases} . \end{aligned} \tag{3.12}$$

Unlike the Schrödinger wavefunction representation, mixed states are easy to represent with the Wigner formulation. Consider a mixed state with density matrix

$$\hat{\rho} = \sum_j P_j |\psi_j\rangle\langle\psi_j| \,, \tag{3.13}$$

where P_j is the probability that the system is in state $|\psi_j\rangle$. The Wigner function for this mixed state is given by

$$\begin{aligned} W(x,p) &= \frac{\tilde{\rho}}{h} \\ &= \frac{1}{h}\sum_j P_j\tilde{\rho}_j \\ &= \sum_j P_j W_j(x,p)\,, \end{aligned} \tag{3.14}$$

where $\tilde{\rho}_j$ and $W_j(x,p)$ are the Weyl transformed density matrix and Wigner function respectively for state $|\psi_j\rangle$.

Since the Wigner function is normalised, and the fact that one can use it to determine expectation values, it would be tempting to interpret the Wigner function as a phase space probability density. It is, however, not possible to do so, due to one particular characteristic - the fact that it is not guaranteed to be pointwise positive.

Consider two orthogonal states of a system ψ_1 and ψ_2 with corresponding density operators given by $\hat{\rho}_1$ and $\hat{\rho}_2$. Using Eq. (3.6), one obtains

$$\mathrm{Tr}\,(\hat{\rho}_1\hat{\rho}_2) = \frac{1}{h}\int\int hW_1(x,p)hW_2(x,p)dx\,dp\;. \tag{3.15}$$

But $\mathrm{Tr}\,(\hat{\rho}_1\hat{\rho}_2) = |\langle\psi_1|\psi_2\rangle|^2$, which is zero for orthogonal states. Therefore,

$$h\int\int W_1(x,p)W_2(x,p)dx\,dp = 0\;. \tag{3.16}$$

Since Wigner functions cannot be zero for all of phase space, this implies that $W_1(x,p)$ or $W_2(x,p)$, or even both, must be negative for some regions of phase space. Indeed, for any orthogonal set of states, for Eq (3.16) to hold, at most only one state in the set may have an associated Wigner function that is positive for all phase space. This is the case for the quantum harmonic oscillator, where the ground state Wigner function is pointwise positive, but all other states have Wigner functions with negative values for some regions of phase space.

Since probabilities are only meaningful if they are positive, naturally the fact that the Wigner function may be negative denies its interpretation as a probability density. The Wigner function is thus generally labelled as a quasidistribution.

Because equations of motion in quantum mechanics are given in terms of products of operators, it must be possible to represent this in the Wigner representation as well. If one considers two operators $\hat{A}$ and $\hat{B}$, the Weyl transform of their product is [20]

$$\begin{aligned}(\widetilde{\hat{A}\hat{B}}) &= A(R,P)e^{\frac{\hbar\Lambda}{2i}}B(R,P) \\ &= B(R,P)e^{-\frac{\hbar\Lambda}{2i}}A(R,P)\,, \end{aligned} \tag{3.17}$$

where the symbol Λ is the negative of the Poisson bracket.

One final important characteristic of the Weyl transform is the manner in which operators that depend on either $\hat{x}$ or $\hat{p}$, but not both, are transformed. Consider an operator $\hat{A}$ which only depends on the operator $\hat{x}$. The Weyl transform of this operator is [56]

$$\begin{aligned}\widetilde{\hat{A}(\hat{x})} &= \int e^{-ipy/\hbar}\langle x+y/2|\hat{A}(\hat{x})|x-y/2\rangle\, dy \\ &= \int e^{-ipy/\hbar}A(x-y/2)\delta(y)\, dy = A(x)\,. \end{aligned} \tag{3.18}$$

Similarly, for operators that depend only on the momentum operator,

$$\widetilde{\hat{B}(\hat{p})} = B(p) \tag{3.19}$$

Therefore, one can perform the Weyl transform on any operator that depends only on $\hat{x}$ by simply replacing the operator $\hat{x}$ with x, and similarly for purely momentum based operators, by replacing $\hat{p}$ with p. This also applies to sums of operators where all the individual operators depend on either $\hat{x}$ or $\hat{p}$. This makes it easy to represent any Hamiltonian of the form $\hat{H}(\hat{x},\hat{p}) = \hat{T}(\hat{p}) + \hat{U}(\hat{x})$ in the Wigner representation, as one replaces the operators $\hat{x}$ and $\hat{p}$ with phase space variables to obtain $H(x,p) = T(p) + U(x)$. This is useful when using the partial Wigner representation.

3.1.2 The Partial Wigner Representation

The partial Wigner representation is highly useful when attempting to study quantum-classical dynamics [34][58] and is derived from the more general Wigner representation of quantum mechanics. One can think of general open quantum systems, where the system being studied can be divided into a quantum subsystem of interest, and an environment with which the quantum subsystem interacts. Much of the time, the environment contains far too many degrees of freedom for it to be possible to solve the dynamics in a full quantum way. When the particles that constitute the environment are significantly more massive than those of the subsystem, it is far more practical to treat the environmental degrees of freedom classically, or in classical-like fashion. The partial Wigner transform is perfectly suited to this situation. A partial Wigner representation is obtained by taking the Weyl function over only certain degrees of freedom of the system (in this case the environmental degrees of freedom). In this way, a hybrid representation is achieved, where the subsystem is still described in terms of operators, but the remainder is given in terms of phase space functions. The Hamiltonian of the system is thus converted from a full operator to an operator of the Hilbert space of the subsystem, as well as a function of phase space variables for the bath:

$$\hat{H}(\hat{R}, \hat{P}, \hat{q}, \hat{p}) \rightarrow H_W(R, P, \hat{q}, \hat{p}) \ , \tag{3.20}$$

where the W subscript denotes the partial Wigner representation. The (R, P) are the bath coordinates, and $(\hat{r}, \hat{p})$ are the position and momentum operators for the subsystem. The operators of the quantum subsystem remain unchanged, and the subsystem is still treated in a full quantum way, as desired. In fact, at this point, the environment is still being treated quantum-mechanically, but the partial Wigner representation allows for treatment of the bath in a more classical-like way.

For a system comprising a quantum subsystem coupled to an environment of N particles, the partial Wigner transform for the density matrix is given by

$$\hat{\rho}_W(R,P) = h^{-3N} \int dz e^{iP\cdot z/\hbar} \langle R - \frac{z}{2}|\hat{\rho}|R + \frac{z}{2}\rangle \ . \tag{3.21}$$

Note that $\hat{\rho}_W(R,P) \equiv W(R,P)$, but henceforth the notation $\hat{\rho}_W(R,P)$ will be used for the Wigner function. The factor in front of the integral in the above equation has changed from h^{-1} to h^{-3N} due to the fact that density matrix is for N particles, and all variables must be interpreted as vectors of dimension $3N$ [53].

For an arbitrary operator of the system $\hat{\chi}$, its partial Wigner transform is

$$\hat{\chi}(R,P) = \int dz e^{iP\cdot z/\hbar} \langle R - \frac{z}{2}|\hat{\chi}|R + \frac{z}{2}\rangle \ . \tag{3.22}$$

As in the case of the density matrix, the operator $\hat{\chi}$ is both an operator on the Hilbert space of the subsystem and a function of phase space. This hybrid form for the density matrix and operators is ideal for treating a system in a quantum-classical fashion, due to its ability to treat the environmental degrees of freedom in a classical-like way. A point to note, however, is that since the forms of the operator and density matrix have been altered, their respective equations of motion change as well. Indeed, their time evolution is no longer governed by the quantum commutator in the Heisenberg and von Neumann equations. Instead, a mixed quantum-classical formulation is required to describe the time evolution of these hybrid objects. This formulation will be introduced in the next chapter. It will be shown that in deriving this quantum-classical representation, one obtains a quantum-classical bracket that is non-Hamiltonian (or approximately Hamiltonian) in nature. The difference between Hamiltonian and non-Hamiltonian algebras will be discussed below.

3.2 Hamiltonian Theory and Non-Hamiltonian Theory

3.2.1 Hamiltonian Theory

The purpose of describing any system mathematically, whether in the realm of classical mechanics or quantum mechanics, is to be able to predict values for system properties that are experimentally measurable. In general, a system of study is subject to some external influence, and the theory must be able to describe how this system evolves in time, and thus predict observable quantities. These measurable properties are given by ensemble averages. In either quantum or classical mechanics, linear response theory can be used to obtain ensemble averages in terms of time correlation functions [59]. Linear response theory, however, requires that the mathematical theory used to describe the dynamics of the system has the property of being invariant under time translation. Any structure that is a Lie, or Hamiltonian, algebra possesses this time translation invariance property [60][61].

For a theory to be Hamiltonian, the algebra of its bracket must constitute a Lie algebra. To define a Lie algebra, consider a mathematical space, to which objects $\{A, B, C\}$ belong. An algebra of this space is a Lie algebra if it possesses the following properties [61]:

$$(A, B) = -(B, A) \ , \tag{3.23}$$

$$\lambda(A, B) = (\lambda A, B) = (A, \lambda B) \ , \tag{3.24}$$

$$(A + B, C) = (A, C) + (B, C) \ , \tag{3.25}$$

where $(.., ..)$ is the bracket that defines this algebra and the symbol λ is a c-number. In addition to these 3 properties, for the algebra to be Hamiltonian, and specifically

for time translation invariance to hold, the brackets must satisfy

$$\mathcal{J} = ((A, B), C) + ((C, A), B) + ((B, C), A) = 0 \ , \tag{3.26}$$

which is the Jacobi relation.

An algebra may thus satisfy the first three properties given in Eqs. (3.23-3.25), and still not be Hamiltonian. It is only a Lie algebra (and consequently a Hamiltonian theory) if it also satisfies the Jacobi relation. Equations. (3.24) and (3.25) imply that the bracket is a linear operator of its space, as well as of complex numbers. The antisymmetric property of the bracket, given by Eq. (3.23) is important for time evolution [61]. When the elements of the space of the bracket are not explicitly dependent on time, time evolution can be given choosing an element H, and defining the equations of motion by [61]:

$$\frac{dA}{dt} = (A, H) \ , \tag{3.27}$$

where H is typically the Hamiltonian.

It can be shown that if the Jacobi relation is satisfied, then the algebra is time translation invariant. Consider the two elements A and B, which are in the space of the algebra defined by the bracket $(.., ..)$. They are constants of motion if and only if

$$\dot{A} = (A, H) = 0 \qquad \dot{B} = (B, H) = 0 \ , \tag{3.28}$$

where the dot accent is used to denote derivation with respect to time. If the theory is time translation invariant, then Eq. (3.28) implies that (A, B) is also a constant of motion, which would be expressed in the following way:

$$((A, B), H) = 0 \ . \tag{3.29}$$

It can be seen, however, that Eq. (3.29) follows directly from the Jacobi relation:

$$\begin{aligned}((A,B),H) &= -((H,A),B) - ((B,H),A) \\ &= ((A,H),B) - ((B,H),A) \\ &= (\dot{A},B) - (\dot{B},A) = 0\,, \end{aligned} \tag{3.30}$$

thus proving that any theory that is Hamiltonian is consequently time translation invariant as well.

Both the quantum commutator and the classical Poisson bracket which govern their respective algebras are Hamiltonian, and thus time translation invariant. It is this property which allows for the success of linear response theory.

3.2.2 Non-Hamiltonian Theory

With the requirements for a Hamiltonian theory defined, it is now possible to define a non-Hamiltonian theory. A non-Hamiltonian algebra is one whose bracket satisfies the antisymmetric and linear properties outlined in Eqs. (3.23), (3.24) and (3.25), but does not satisfy the Jacobi relation:

$$\mathcal{J} = ((A,B),C) + ((C,A),B) + ((B,C),A) = \lambda\,, \tag{3.31}$$

where λ is some non-zero c-number. Defining C to be the Hamiltonian, and A and B as constants of motion, one obtains

$$\begin{aligned}((A,B),H) &= -((H,A),B) - ((B,H),A) + \lambda \\ &= (\dot{A},B) - (\dot{B},A) + \lambda \\ &= \lambda \neq 0\,. \end{aligned} \tag{3.32}$$

The fact that A and B are constants of motion thus no longer implies that (A,B) is also a constant of motion, and time translation invariance is violated. This shows

that the Jacobi relation is indeed the requirement for time translation invariance.

This drawback to non-Hamiltonian theories might make it counter intuitive to ever choose to use a non-Hamiltonian theory over a Hamiltonian one. To see the advantages a non-Hamiltonian theory might have, consider dynamics in a thermal bath. In real life experiments, systems are generally studied at constant temperature, not constant energy [61]. This implies that numerical calculations should be performed in the canonical ensemble. Molecular dynamics performs simulations using the microcanonical ensemble, which only converges with the canonical ensemble in the thermodynamic limit. However, it is not possible, due to lack of computational resources, to perform calculations, even classically, for that large a number of degrees of freedom. Consequently, the calculations that are performed at constant energy for Hamiltonian dynamics deviate from those conducted at constant temperature [62].

In the case of classical mechanics, it was shown that, using a non-Hamiltonian formalism it is possible to simulate an infinite thermal bath using only a small number of degrees of freedom [63]. More recently, this formalism was extended to the quantum case [60][64]. In quantum dynamics, it can be a highly computationally expensive task to simulate even a relatively small number of degrees of freedom by classical standards, and larger numbers are essentially impossible to currently simulate. In particular cases, this problem has been solved by formulating non-Hamiltonian quantum-classical methods.

3.2.3 The Quantum and Classical Brackets

Due to the fact that a quantum-classical formalism must be able to describe dynamics that comprises both a classical and a quantum element, it would not be unreasonable to assume that it possesses a bracket structure that is similar to that of the classical Poisson bracket or quantum commutator, or some hybrid thereof. It would thus be of interest to consider the structures of the quantum and classical brackets.

The classical Poisson bracket has a symplectic nature, which lends itself to being cast into matrix form [65][66]. For any two arbitrary functions of phase space f and g, one has

$$\{f,g\} = \begin{bmatrix} \frac{\partial f}{\partial R} & \frac{\partial g}{\partial P} \end{bmatrix} \cdot \mathcal{B}^c \cdot \begin{bmatrix} \frac{\partial f}{\partial P} \\ \frac{\partial g}{\partial R} \end{bmatrix} , \tag{3.33}$$

where $\mathcal{B}^c$ is known as the symplectic matrix

$$\mathcal{B}^c = \begin{bmatrix} 0 & 1 \\ -1 & 0 \end{bmatrix} . \tag{3.34}$$

There are indeed great similarities between the quantum and classical bracket structure, as the quantum commutator also has this symplectic form [60], and can be written in the following form:

$$[A,B] = \begin{bmatrix} A & B \end{bmatrix} \cdot \mathcal{B}^c \cdot \begin{bmatrix} A \\ B \end{bmatrix} . \tag{3.35}$$

It is worth noting that while the symplectic form for the bracket is a requirement for its equations of motion to be canonical, it is not a requirement for it to be a Lie bracket. Conversely, however, if a bracket is symplectic, then it constitutes a Lie algebra.

As shall be shown in the next chapter, the quantum-classical bracket can indeed be written in similar matrix form, however, because it loses its Hamiltonian nature, it can no longer be written in terms of the symplectic matrix.

Chapter 4

The Quantum-Classical Liouville Approach

4.1 The Quantum-Classical Liouville Equation

The quantum-classical Liouville approach is a method of obtaining a mixed quantum-classical representation of dynamics through use of a partial Wigner transform. The resulting quantum-classical Liouville equation defines the quantum-classical bracket, which is non-Hamiltonian in nature, and thus not symplectic. The equation is obtained by making a quantum-classical approximation, however, as shall be shown below, it is exact for a certain subset of Hamiltonians.

This approach is highly useful when considering systems that can be split into a small subsystem which one wishes to treat quantum mechanically, and an environment which comprises slower, heavier particles, the dynamics of which one is less interested. This is due to the natural way that the bath degrees of freedom are represented in terms of phase space variables, while still maintaining the mathematical operator structure for the subsystem.

Consider a system defined by the total Hamiltonian operator

$$\hat{H}(\hat{R},\hat{P}) = \hat{H}_S + \hat{H}_B(\hat{R},\hat{P}) + \hat{H}_{SB}(\hat{R}) \; , \tag{4.1}$$

where the subscripts S, B and SB stand for the subsystem, bath and coupling potential respectively. It is assumed that the Hamiltonian depends upon a pair of canonically conjugate operators $(\hat{R},\hat{P})$ through the bath Hamiltonian, and the interaction Hamiltonian with form $\hat{H}_{SB}(\hat{R})$. The Hamiltonian also depends on some quantum operators for the system, but these are not shown here, since the partial Wigner transform will only be taken over the environmental degrees of freedom. Using the symplectic matrix form for the quantum commutator, the equation of motion for the density matrix $\hat{\rho}$, the von Neumann equation, is given by

$$\frac{\partial\hat{\rho}}{\partial t} = -\frac{i}{\hbar}\left[\begin{array}{cc} \hat{H} & \hat{\rho} \end{array}\right]\cdot\mathcal{B}^c\cdot\left[\begin{array}{c} \hat{H} \\ \hat{\rho} \end{array}\right] \; . \tag{4.2}$$

At this point, in order to obtain a mixed quantum-classical representation of the dynamics, the partial Wigner transform is taken over the bath coordinates $\hat{R}$ and $\hat{P}$. Using the fact that each term in the Hamiltonian is an operator of either $\hat{R}$ or $\hat{P}$, but not both, the partial Wigner transformed Hamiltonian of the system is given by

$$\hat{H}_W(X) = \hat{H}_S + H_{W,B}(X) + \hat{H}_{W,SB}(R) \; , \tag{4.3}$$

where the symbol X has been used to denote the canonically conjugate classical phase space variables (R,P). Making use of the identity given in Eq. (3.17) for the Weyl transform of a product of operators, the evolution equation for the density matrix becomes:

$$\frac{\partial}{\partial t}\hat{\rho}_W(X,t) \;\; = \;\; -\frac{i}{\hbar}\left[\begin{array}{cc} \hat{H}_W(X) & \hat{\rho}_W(X,t) \end{array}\right]\cdot\mathcal{D}\cdot\left[\begin{array}{c} \hat{H}_W(X) \\ \hat{\rho}_W(X,t) \end{array}\right] \; ,$$

(4.4)

where the matrix $\mathcal{D}$ is given by

$$\mathcal{D} = \begin{bmatrix} 0 & e^{\frac{i\hbar}{2}\overleftarrow{\partial}_k \mathcal{B}^c_{kj} \overrightarrow{\partial}_j} \\ -e^{\frac{i\hbar}{2}\overleftarrow{\partial}_k \mathcal{B}^c_{kj} \overrightarrow{\partial}_j} & 0 \end{bmatrix} . \tag{4.5}$$

The symbols $\overleftarrow{\partial}_k = \overleftarrow{\partial} / \partial X_k$ and $\overrightarrow{\partial}_j = \overrightarrow{\partial} / \partial X_j$ denote the operators of derivation with respect to the phase space point coordinates, acting to left and right respectively, and the repeated indices imply summation. Note that although the matrix $\mathcal{D}$ has an off-diagonal form, it is not the symplectic matrix, and hence the associated equations of motion are not canonical. However, the bracket defined by Eq. (4.4) satisfies the Jacobi relation, and is thus still Hamiltonian in nature.

The evolution given in Eq. (4.4) is still not a mixed quantum-classical representation of dynamics. It would be more accurate to describe it as quantum-classical-like. Although the bath degrees of freedom are represented in a classical-like phase space way, this mixed Wigner-Heisenberg representation is completely equivalent to that of Heisenberg. In other words it is still a fully quantum evolution. However, calculations using Eq. (4.4) are usually very difficult to perform, so at this point the quantum-classical approximation is made. This amounts to taking a linear order approximation for the exponential terms in the matrix $\mathcal{D}$:

$$\mathcal{D}_{lin} = \begin{bmatrix} 0 & 1 + \frac{i\hbar}{2} \overleftarrow{\partial}_k \, \mathcal{B}^c_{kj} \, \overrightarrow{\partial}_j \\ -1 - \frac{i\hbar}{2} \overleftarrow{\partial}_k \, \mathcal{B}^c_{kj} \, \overrightarrow{\partial}_j & 0 \end{bmatrix} . \tag{4.6}$$

In this approximation, the evolution equation for the density matrix becomes

$$\frac{\partial}{\partial t}\hat{\rho}_W(X,t) = -\frac{i}{\hbar} \begin{bmatrix} \hat{H}_W(X) & \hat{\rho}_W(X,t) \end{bmatrix} \cdot \mathcal{D}_{lin} \cdot \begin{bmatrix} \hat{H}_W(X) \\ \hat{\rho}_W(X,t) \end{bmatrix} . \tag{4.7}$$

This form for the evolution equation is far easier to simulate on a computer than Eq. (4.4). The approximation essentially neglects higher order quantum correction terms to the evolution of the bath degrees of freedom. In certain cases, however, Eq (4.7) is exact. If the Hamiltonian for the bath is at most quadratic in R and P, and the interaction Hamiltonian is of the form

$$\hat{H}_{W,SB} = V_B(R) \otimes \hat{H}'_S \ , \tag{4.8}$$

where V_B depends only on the positions of the environmental degrees of freedom, and $\hat{H}'_S$ acts only in the Hilbert space of the subsystem, then the linear expansion of the exponential terms in the matrix $\mathcal{D}$ is exact. Therefore, Eq (4.7) is exact for this class of Hamiltonians. The higher order terms of the expansion for the exponentials go to zero when operated on $\hat{H}_W(X)$.

Equation (4.7) is known as the quantum-classical Liouville equation, and it can also be expressed in terms of the quantum commutator bracket and the classical Poisson bracket. Performing the matrix multiplication in Eq. (4.7) yields

$$\begin{aligned} \frac{\partial}{\partial t}\hat{\rho}_W(X,t) &= -\frac{i}{\hbar}[\hat{H}_W, \hat{\rho}_W] + \frac{1}{2}\left(\{\hat{H}_W, \hat{\rho}_W\} - \{\hat{\rho}_W, \hat{H}_W\}\right) \\ &= -\left(\hat{H}_W, \hat{\rho}_W\right)_{QC} \\ &= -i\mathcal{L}\hat{\rho}_W(X,t) \ , \end{aligned} \tag{4.9}$$

where the quantum-classical bracket has been defined in the second line. The last line defines the quantum-classical Liouville operator $\mathcal{L}$. As was surmised previously, the quantum-classical bracket is indeed a combination of both the quantum commutator, and the Poisson bracket. The commutator acts on the quantum subsystem, while the Poisson bracket acts on the classical phase space functions of the bath.

However, the quantum-classical bracket does not obey the Jacobi relation [60], and is therefore non-Hamiltonian. The violation is due to the quantum-classical approximation that is made. The bracket obeys the Jacobi relation to first order in

$\hbar$ though, and a more accurate description for the bracket would perhaps be approximately Hamiltonian. This accounts for the fact that certain dynamical properties of systems that require linear response theory can still be computed within this formalism [20][21].

Note that if either the bath or the subsystem is removed, then the Hamiltonian structure is recovered. Removing the quantum degrees of freedom, leaves only the bath, and the commutator becomes zero. All that then remains is the Hamiltonian Poisson bracket of classical mechanics. Similarly, by removing the classical degrees of freedom results in the Poisson bracket becoming zero, leaving only the quantum commutator, which is also Hamiltonian.

The Heisenberg equation is converted into the partial Wigner representation in exactly the same way as that of the von Neumann equation, since the two equations are exactly the same apart from the change in sign. The evolution equation for an arbitrary operator $\hat{\chi}$ in the partial Wigner representation is therefore given by

$$\frac{\partial}{\partial t}\hat{\chi}_W(X,t) \;=\; \left(\hat{H}_W, \hat{\chi}_W\right)_{QC} = i\mathcal{L}\hat{\chi}_W(X,t)\;. \tag{4.10}$$

It has been assumed thus far that the total Hamiltonian for the system of study is time-independent. If this is indeed the case, then the quantum-classical Liouville operator is also time-independent. When the quantum-classical Liouville operator is time-independent, Eqs. (4.9) and (4.10) have the following formal solutions:

$$\hat{\rho}_W(R,P,t) \;=\; e^{-i\hat{\mathcal{L}}t}\hat{\rho}_W(R,P,0)\;, \tag{4.11}$$

$$\hat{\chi}_W(R,P,t) \;=\; e^{i\hat{\mathcal{L}}t}\hat{\chi}_W(R,P,0)\;. \tag{4.12}$$

In the case of time-dependent Hamiltonians, solutions are not as simple, since

the quantum-classical Liouville operator also becomes explicitly dependent on time.

In the current form, Eqs. (4.11) and (4.12) are not expressed in any basis. In order to to obtain a form that is suitable for numerical simulations, it is useful to first rotate them into a convenient basis.

4.2 The Adiabatic Basis

Consider an arbitrary set of linearly independent basis vectors $|\alpha\rangle$, spanning the Hilbert space of the quantum subsystem of interest - in other words, a complete basis set. Equations (4.11) and (4.12) rotated into this basis become:

$$\hat{\rho}_W^{\alpha\alpha'}(R,P,t) = \sum_{\beta\beta'} \left(e^{-i\hat{\mathcal{L}}t}\right)_{\alpha\alpha',\beta\beta'} \hat{\rho}_W^{\beta\beta'}(R,P,0) \,, \tag{4.13}$$

and

$$\hat{\chi}_W^{\alpha\alpha'}(R,P,t) = \sum_{\beta\beta'} \left(e^{i\hat{\mathcal{L}}t}\right)_{\alpha\alpha',\beta\beta'} \hat{\chi}_W^{\beta\beta'}(R,P,0) \,. \tag{4.14}$$

In general, the basis chosen to represent the equations depends on both the system being studied, and the algorithm that is being used to perform the numerical calculations. When the algorithm being used is a surface-hopping, and especially in the case of the quantum-classical Liouville approach, the adiabatic basis is most convenient. This is due to the fact that, when represented in the adiabatic basis, the quantum-classical Liouville operator splits naturally into two parts. The first part is responsible for purely adiabatic dynamics, in other words, dynamics that occurs on a single adiabatic potential energy surface. The second part is responsible for nonadiabatic transitions in the subsystem and accompanying changes in the energy of the environment. This splitting of terms allows for easy implementation in surface-hopping algorithms.

Recall from Chapter 2 that the adiabatic Hamiltonian $\hat{h}_W$ is defined as all the terms of the total system Hamiltonian except for the kinetic energy of the bath:

$$\hat{h}_W(R) = \hat{H}_W(R,P) - \frac{P^2}{2M}\,. \tag{4.15}$$

Therefore, for an arbitrary quantum subsystem coupled to an environment, the adiabatic Hamiltonian is given by

$$\hat{h}_W(R) = \hat{h}_s + V_b(R) + \hat{V}_c(R)\;, \tag{4.16}$$

where $\hat{h}_s$ is the Hamiltonian of the subsystem and $V_b(R)$ is the potential energy of the bath and a function of the bath coordinates. The term $\hat{V}_c(R)$ is the potential energy due to the coupling between the subsystem and the bath, and is both an operator of the subsystem and function of the bath coordinates.

The adiabatic basis is defined as the solution to the eigenvalue equation for the adiabatic Hamiltonian:

$$\hat{h}_W(R)|\alpha;R\rangle = E_\alpha(R)|\alpha;R\rangle\;. \tag{4.17}$$

Note that the both the adiabatic basis vectors $|\alpha;R\rangle$ and the adiabatic energy surfaces $E_\alpha(R)$ are dependent only on the position coordinate of the bath, and not the momentum. This is because the adiabatic Hamiltonian only depends on R.

4.3 Representation of the Quantum-Classical Liouville Equation in the Adiabatic Basis

Now that the adiabatic basis has been defined, the next step is to represent the quantum-classical Liouville equation into this basis. The derivation is quite long, and so only the most relevant equations are given in this section. The full derivation

can be found in Appendix A.

Representing the quantum-classical Liouville equation into the adiabatic basis essentially amounts to representing the quantum-classical Liouville operator in the adiabatic basis. In this basis, the operator takes the form

$$\begin{aligned} -i\mathcal{L}_{\alpha\alpha',\beta\beta'} &= -\left(i\omega_{\alpha\alpha'} + iL_{\alpha\alpha'}\right)\delta_{\alpha\beta}\delta_{\alpha'\beta'} + J_{\alpha\alpha',\beta\beta'} \\ &= -i\mathcal{L}^0_{\alpha\alpha'}\delta_{\alpha\beta}\delta_{\alpha'\beta'} + J_{\alpha\alpha',\beta\beta'}\,, \end{aligned} \tag{4.18}$$

where $\mathcal{L}^0$ is the adiabatic quantum-classical Liouville operator. The quantum-classical Liouville operator thus comprises two terms. The first term is responsible for adiabatic evolution of the system. It comprises two terms - the Bohr frequency, which depends on the differences in energies of adiabatic states α and α':

$$\omega_{\alpha\alpha'} = \frac{E_\alpha(R) - E_{\alpha'}(R)}{\hbar}\,, \tag{4.19}$$

and the classical-like Liouville operator $L_{\alpha\alpha'}$. This operator evolves the dynamics of the bath according the average of the Hellmann-Feynman forces for states α and α', and is given by

$$iL_{\alpha\alpha'} = \frac{P}{M}\cdot\frac{\partial}{\partial R} + \frac{1}{2}\left(F^{\alpha}_{W} + F^{\alpha'}_{W}\right)\cdot\frac{\partial}{\partial P}\,. \tag{4.20}$$

This term is relatively easy to implement in numerical simulation.

The final term of the quantum-classical Liouville operator is the J operator:

$$
\begin{aligned}
J_{\alpha\alpha',\beta\beta'} &= -\frac{P}{M}\cdot d_{\alpha\beta}(R)\left(1+\frac{1}{2}\frac{\Delta E_{\alpha\beta}(R)\hat{d}_{\alpha\beta}(R)}{\frac{P}{M}\cdot\hat{d}_{\alpha\beta}(R)}\cdot\frac{\partial}{\partial P}\right)\delta_{\alpha'\beta'} \\
&\quad -\frac{P}{M}\cdot d^{*}_{\alpha'\beta'}(R)\left(1+\frac{1}{2}\frac{\Delta E_{\alpha'\beta'}(R)\hat{d}^{*}_{\alpha'\beta'}(R)}{\frac{P}{M}\cdot\hat{d}^{*}_{\alpha'\beta'}(R)}\cdot\frac{\partial}{\partial P}\right)\delta_{\alpha\beta}\,,
\end{aligned}
\tag{4.21}
$$

where $\Delta E_{\alpha\beta}(R) = E_{\alpha}(R) - E_{\beta}(R)$, and $d_{\alpha\beta}$ is the nonadiabatic coupling matrix element, given by

$$
\langle\alpha;R|\frac{\partial}{\partial R}|\beta;R\rangle\,. \tag{4.22}
$$

The symbol $\hat{d}_{\alpha\beta}$ denotes the normalised nonadiabatic coupling matrix element.

The J, or transition, operator is responsible for nonadiabatic transitions between energy levels in the quantum subsystem, and concomitant changes in the momenta of the bath degrees of freedom. Implementation of the J operator is the most challenging aspect of numerically simulating dynamics using the quantum-classical Liouville equation. It will be discussed in greater detail in the following chapters.

Chapter 5

Quantum-Classical Propagators

5.1 Dyson Integral Equation Method

As it stands, the evolution equation for the density matrix is

$$\rho_W^{\alpha\alpha'}(R,P,t) = e^{\left[(-i\omega_{\alpha\alpha'}-iL_{\alpha\alpha'})\delta_{\alpha\beta}\delta_{\alpha'\beta'}+J_{\alpha\alpha',\beta\beta'}\right]t}\rho_W^{\beta\beta'}(R,P,0)\ . \tag{5.1}$$

This equation is difficult to implement in numerical calculations in this form, specifically because dealing with the exponentiated form of the J operator numerically is challenging. One method of solving this problem, developed by Kapral and Ciccotti [31], was a surface-hopping description arising from use of the Dyson operator identity, given by

$$e^{(\hat{A}+\hat{B})t} = e^{\hat{A}t} + \int_0^t dt' e^{\hat{A}(t-t')}\hat{B}e^{(\hat{A}+\hat{B})t'}\ . \tag{5.2}$$

Applying the identity to $e^{-i\mathcal{L}t}$ yields

$$\begin{aligned}(e^{-i\mathcal{L}t})_{\alpha\alpha',\beta\beta'} &= e^{-i\mathcal{L}^0_{\alpha\alpha'}t}\delta_{\alpha\beta}\delta_{\alpha'\beta'} \\ &+ \sum_{\nu\nu'}\int_0^t dt' e^{-i\mathcal{L}^0_{\alpha\alpha'}(t-t')}J_{\alpha\alpha',\nu\nu'}\left(e^{-i\mathcal{L}t'}\right)_{\nu\nu',\beta\beta'}\ ,\end{aligned} \tag{5.3}$$

where

$$\begin{aligned} e^{i\mathcal{L}^0_{\alpha\alpha'}(t_2-t_1)} &= e^{i\omega_{\alpha\alpha'}+iL_{\alpha\alpha'}} \\ &= e^{i\int_{t_1}^{t_2}\omega_{\alpha\alpha'}\,dt}e^{iL_{\alpha\alpha'}(t_2-t_1)} \\ &\equiv \mathcal{W}_{\alpha\alpha'}(t_1,t_2)e^{iL_{\alpha\alpha'}(t_2-t_1)}\,. \end{aligned} \tag{5.4}$$

The term $\mathcal{W}_{\alpha\alpha'}(t_1,t_2)$ is a phase factor associated with a trajectory segment between t_1 and t_2. Equation (5.3) provides a form that is far easier to deal with, because the J operator only occurs linearly, not exponentially. Substitution of Eq. (5.3) into Eq. (5.1) gives

$$\begin{aligned} \rho_W^{\alpha\alpha'}(R,P,t) &= e^{-i\mathcal{L}^0_{\alpha\alpha'}t}\rho_W^{\alpha\alpha'}(R,P,0) \\ &+ \sum_{\nu\nu'}\int_0^t dt' e^{-i\mathcal{L}^0_{\alpha\alpha'}(t-t')}J_{\alpha\alpha',\beta\beta'}\rho_W^{\beta\beta'}(R,P,t') \end{aligned} \tag{5.5}$$

The Dyson integral form for the evolution operator thus provides a way of solving the evolution equation in an iterative way. The full solution at some time t becomes

$$\begin{aligned} \rho_W^{\alpha_0\alpha_0'}(R,P,t) &= e^{-i\mathcal{L}^0_{\alpha_0\alpha_0'}t}\rho_W^{\alpha_0\alpha_0'}(R,P) + \sum_{n=1}^{\infty} \\ &\times \sum_{(\alpha_1\alpha_1')\ldots(\alpha_n\alpha_n')}\int_0^{t_0}dt_1\int_0^{t_1}dt_2\ldots\int_0^{t_{n-1}}dt_n \\ &\times \prod_{k=1}^{n}\left[e^{-i\mathcal{L}^0_{\alpha_{k-1}\alpha_{k-1}'}(t_{k-1}-t_k)}J_{\alpha_{k-1}\alpha_{k-1}',\alpha_k\alpha_k'}\right] \\ &\times e^{-i\mathcal{L}^0_{\alpha_n\alpha_n'}t_n}\rho_W^{\alpha_n\alpha_n'}(R,P)\,, \end{aligned} \tag{5.6}$$

where $\rho_W^{\alpha\alpha'}(R,P)$ is the value of the density matrix element at time $t=0$. For an operator, the solution to the evolution equation looks identical, apart from an additional term due to the difference in sign between the von Neumann equation

and the Heisenberg equation. For an arbitrary operator $\hat{\chi}$ at time t, the solution is

$$\begin{aligned}
\chi_W^{\alpha_0\alpha_0'}(R,P,t) &= e^{i\mathcal{L}^0_{\alpha_0\alpha_0'}t}\chi_W^{\alpha_0\alpha_0'}(R,P) + \sum_{n=1}^{\infty}(-1)^n \\
&\times \sum_{(\alpha_1\alpha_1')\ldots(\alpha_n\alpha_n')} \int_0^{t_0} dt_1 \int_0^{t_1} dt_2 \ldots \int_0^{t_{n-1}} dt_n \\
&\times \prod_{k=1}^{n}\left[e^{i\mathcal{L}^0_{\alpha_{k-1}\alpha_{k-1}'}(t_{k-1}-t_k)} J_{\alpha_{k-1}\alpha_{k-1}',\alpha_k\alpha_k'}\right] \\
&\times e^{i\mathcal{L}^0_{\alpha_n\alpha_n'}t_n}\chi_W^{\alpha_n\alpha_n'}(R,P)\ . \qquad (5.7)
\end{aligned}$$

Equations (5.6) and (5.7) provide a series solution where the dynamics can be calculated in a perturbative way, using a hybrid Monte Carlo-Molecular Dynamics surface-hopping algorithm. The first term on the right hand side describes trajectories that undergo pure Born-Oppenheimer dynamics on a single adiabatic potential energy surface - in other words, that do not contain any nonadiabatic transitions. The integral terms on the right hand side of Eqs. (5.6) and (5.7) are then perturbative terms describing trajectories which have undergone an increasing number of nonadiabatic transitions. In between nonadiabatic transitions, the evolution of the trajectories is governed by the mean Hellmann-Feynman forces of adiabatic states α and α'. A phase factor is associated with each trajectory segment, determined by the frequency $\omega_{\alpha\alpha'}$. If $\alpha = \alpha'$, then the phase factor is zero, and dynamics for that specific trajectory segment is on a single adiabatic energy surface. If the J operator is set to zero (adiabatic approximation), then the integral terms all fall away, leaving only the first term on the right-hand side, and the dynamics is purely adiabatic.

A point to note is that, in the above equations, the sum over all nonadiabatic contributions goes up to infinity. Naturally this is impossible to simulate, so generally a cut-off is defined, above which higher order nonadiabatic contributions are neglected. This is justified by the fact that higher order terms in the sequence contribute diminishingly to the value of the density matrix/observable.

While this method has garnered some success, it has some serious limitations. Firstly, the full series solution has to be calculated for each time t in the simulation, which naturally means this algorithm is very computationally expensive. It would be far more desirable to devise an algorithm that calculates the trajectory in a more continuous fashion. The second issue with this approach is that it is only accurate for cases where there are few nonadiabatic transitions. The algorithm becomes unstable when higher order terms are included in the calculation. This limits the length of time the algorithm can reliably simulate, as higher order contributions become more important at later times, when more nonadiabatic transitions have occurred. These terms can therefore no longer be neglected from the calculation.

In an effort to resolve the issues encountered by the Dyson integral equation approach, a new algorithm was developed to solve Eq. (5.1), known as the Sequential Short-Time-Propagation, or SSTP algorithm [34].

5.2 The SSTP Algorithm

Proposed in 2002 by MacKernan *et al.* [34], the SSTP algorithm is a large improvement over the Dyson integral equation approach to the quantum-classical Liouville equation. While it does still utilise the Dyson operator identity in its derivation, it is based on the decomposition of the evolution operator into sequential short-time propagators. This is possible due to the fact that the quantum-classical Liouville operator is time-independent. The evolution operator can be split into propagators of arbitrary time-length which are not necessarily equal.

Consider some finite simulation time t, which is divided into N time-steps of length $\tau_j = t_j - t_{j-1}$. The evolution operator can be rewritten as

$$\left(e^{-i\mathcal{L}t}\right)_{\alpha_0\alpha_0',\alpha_N\alpha_N'} = \sum_{(\alpha_1\alpha_1')\cdots(\alpha_N\alpha_N')} \prod_{j=1}^{N} \left(e^{-i\mathcal{L}\tau_j}\right)_{\alpha_{j-1}\alpha_{j-1}',\alpha_j\alpha_j'} . \tag{5.8}$$

The density matrix (or observable) can thus be calculated not by application of a single evolution operator, but by application of sequential operators $e^{-i\mathcal{L}\tau_j}$ which

propagate the dynamics from time t_{j-1} to t_j. In this way, the dynamics from time zero to time t is calculated in a single simulation - there is no need to perform a separate simulation for each time step. Already, this is a huge improvement over the Dyson integral equation method.

However, the short-time propagators in Eq. (5.8) are still difficult to implement in this form. The Dyson operator identity is thus invoked again, but this time for a short-time propagator, and not the entire evolution operator, giving

$$\begin{aligned} e^{-i\mathcal{L}(t_j-t_{j-1})} &= e^{-i\mathcal{L}^0(t_j-t_{j-1})} \\ &+ \int_{t_{j-1}}^{t_j} dt' e^{-i\mathcal{L}^0(t_j-t_{j-1}-t')} J e^{-i\mathcal{L}t'} \ . \end{aligned} \tag{5.9}$$

Note that the subscripts denoting the states should be included in the equation above, but they have been momentarily dropped to make the equations clearer.

At this point, the short-time propagator in Eq. (5.9) is treated in no way differently to the way the total evolution operator is treated in the Dyson integral equation method, as it still requires an iterative solution. However, because the time-steps τ_j are of arbitrary length, they can be chosen to be sufficiently small such that the Dyson series can be truncated at first order, and the integrand on the right-hand side of Eq. (5.9) can be approximated as constant. Letting $t' = t_j$, one obtains

$$\begin{aligned} e^{-i\mathcal{L}\tau_j} &= e^{-i\mathcal{L}^0\tau_j} \\ &+ \int_{t_{j-1}}^{t_j} dt' e^{-i\mathcal{L}^0(-t_{j-1})} J e^{-i\mathcal{L}t_j} \\ &\approx e^{-i\mathcal{L}^0\tau_j} \\ &+ \int_{t_{j-1}}^{t_j} dt' e^{-i\mathcal{L}^0(-t_{j-1})} J e^{-i\mathcal{L}^0 t_j} \ , \end{aligned} \tag{5.10}$$

where in the last line above, the series has been truncated. The one point ap-

proximation for t' means that the integrand is a constant that can be taken out of the integral. Generally the J operator and the $\mathcal{L}_0$ operator do not commute, but since the series is being truncated at first order, and the term arising from their non-commutability is higher than first order, the terms can be rearranged, giving

$$\begin{aligned} e^{-i\mathcal{L}\tau_j} &= e^{-i\mathcal{L}^0\tau_j} + e^{-i\mathcal{L}^0 t_j} e^{-i\mathcal{L}^0(-t_{j-1})} J \int_{t_{j-1}}^{t_j} dt' \\ &= e^{-i\mathcal{L}^0\tau_j} \left(1 + \tau_j\, J\right) \ . \end{aligned} \tag{5.11}$$

Now the subscripts denoting the adiabatic states can be brought back, and the short-time propagator for the density matrix is

$$\begin{aligned} \left(e^{-i\mathcal{L}\tau_j}\right)_{\alpha_{j-1}\alpha'_{j-1},\alpha_j\alpha'_j} &\approx e^{-i\mathcal{L}^0_{\alpha_{j-1}\alpha'_{j-1}}\tau_j} \left(\delta_{\alpha_{j-1}\alpha_j}\delta_{\alpha'_{j-1}\alpha'_j}\right. \\ &+ \left. \tau_j J_{\alpha_{j-1}\alpha'_{j-1},\alpha_j\alpha'_j}\right) \ . \end{aligned} \tag{5.12}$$

As in the case of the Dyson series expansion for the full evolution operator, the expression for the short-term propagators comprises two terms. The first term governs the dynamics of the classical degrees of freedom. This dynamics can occur either on a single adiabatic surface (when $\alpha = \alpha'$), or on the mean of two surfaces (when $\alpha \neq \alpha'$). There is a phase factor associated with each step in the dynamics, which becomes unity when $\alpha = \alpha'$. In this way, the quantum-classical Liouville approach is a semi-hybrid of surface-hopping and mean-field methods. The second term, containing the J operator is responsible for nonadiabatic transitions in the dynamics, as well accompanying changes in the momenta of the bath degrees of freedom.

In the SSTP algorithm, at each time step, a short term propagator is implemented, which first propagates the dynamics in a classical way from time t_{j-1} to time t_j using Molecular Dynamics, and associates a phase factor with this evolution,

based on the indices α and α'. After this is done, the action of the J operator is applied in a stochastic way, with certain probabilities and pseudo-random numbers used to determine whether or not a transition occurs. This will be discussed in more detail later on.

Naturally for the algorithm to be of any use, it must be able to calculate observables of the system. For an arbitrary observable $\langle\chi\rangle$, its time evolution will be given by

$$\langle\chi\rangle(t) = \mathrm{Tr} \int\int dR\, dP\, \chi_W^{\alpha_0\alpha_0'}(R,P)\rho_W^{\alpha_0\alpha_0'}(R,P,t) \;, \tag{5.13}$$

where the trace is taken over the adiabatic states of the quantum degrees of freedom, and the double integral is over the phase space of the classical degrees of freedom in the system. The cyclic invariance property of the trace can be exploited, to give

$$\begin{aligned}
\langle\chi\rangle(t) &= \mathrm{Tr} \int dR dP\, \chi_W^{\alpha_0\alpha_0'}(R,P) e^{-iHt/\hbar} \rho_W^{\alpha_0\alpha_0'}(R,P,0) e^{iHt/\hbar} \\
&= \mathrm{Tr} \int dR dP\, e^{iHt/\hbar} \chi_W^{\alpha_0\alpha_0'}(R,P) e^{-iHt/\hbar} \rho_W^{\alpha_0\alpha_0'}(R,P,0) \\
&= \mathrm{Tr} \int dR dP\, \chi_W^{\alpha_0\alpha_0'}(R,P,t) \rho_W^{\alpha_0\alpha_0'}(R,P) \;.
\end{aligned} \tag{5.14}$$

Equations (5.13) and (5.14) provide two different pictures of the dynamics. The first representation is a Schrödinger picture, where the density matrix is propagated in time, and the operator remains constant. In Eq. (5.14), however, a Heisenberg picture is used, where the time-dependence is in the operator. It is, in fact, more convenient to utilise the latter picture for computational simulation in this case [58], because the initial density matrix can be used as a distribution function from which the initial phase space points for the trajectories can be sampled.

Thus the SSTP algorithm propagates the operator according to the evolution equation, using the time-discretised evolution operator given in Eq. (5.8):

$$\chi_W^{\alpha_0\alpha_0'}(R,P,t) \;=\; \sum_{(\alpha_1\alpha_1')\cdots(\alpha_N\alpha_N')} \prod_{j=1}^{N} \left(e^{i\mathcal{L}\tau_j}\right)_{\alpha_{j-1}\alpha_{j-1}',\alpha_j\alpha_j'} \chi_W^{\alpha_N\alpha_N'}(R,P,0)\,. \tag{5.15}$$

It then calculates the observable at each time step according to Eq. (5.14). The integration over phase space is performed using a Monte Carlo scheme, where, as mentioned previously, the initial conditions of the classical bath are sampled using the hybrid density matrix-function.

However, to implement this equation numerically, the action of the J operator needs to be performed. Currently, even though it only appears linearly in Eq. (5.12), it is still a formidable task to implement computationally. A solution that the SSTP algorithm employs is the momentum-jump approximation [34][67].

5.2.1 Momentum-Jump Approximation

The J operator is responsible for nonadiabatic transitions in the quantum subsystem being simulated. It also causes variations in the momenta of the classical degrees of freedom which accompany the transitions. In equation form, it is

$$\begin{aligned} J_{\alpha\alpha',\beta\beta'} = \;& -\; \frac{P}{M}\cdot d_{\alpha\beta}\left(1+\frac{1}{2}\frac{\Delta E_{\alpha\beta}\hat{d}_{\alpha\beta}}{\frac{P}{M}\cdot\hat{d}_{\alpha\beta}}\cdot\frac{\partial}{\partial P}\right)\delta_{\alpha'\beta'} \\ & -\; \frac{P}{M}\cdot d^*_{\alpha'\beta'}\left(1+\frac{1}{2}\frac{\Delta E_{\alpha'\beta'}\hat{d}^*_{\alpha'\beta'}}{\frac{P}{M}\cdot\hat{d}^*_{\alpha'\beta'}}\cdot\frac{\partial}{\partial P}\right)\delta_{\alpha\beta}\,. \end{aligned} \tag{5.16}$$

It comprises two terms - the first term governs changes of the first index ($\alpha \to \beta$ transitions), and the second term the second index ($\alpha' \to \beta'$ transitions). The variations in the momentum of the environment are governed by the momentum derivative terms in the round brackets. As mentioned before, it is challenging to implement the J operator in this form. Firstly, a method must be devised which

determines which transitions occur, and when they occur. This will be discussed in the next chapter on sampling schemes. Suffice to say that a stochastic scheme is implemented based on a suitable transition probability. The second problem is the quantum backreaction - the way the environmental momenta change when a quantum transition occurs. The momentum derivatives in the J operator are not easy to implement numerically. In Chapter 2, the backreaction was discussed, and it was noted that most surface-hopping schemes adjust the classical momenta in a very ad hoc manner.

One might intuitively think of determining these derivatives using a finite difference method, so that

$$d_{\alpha\beta} \cdot \nabla_P f(P) \approx (\Delta_P)^{-1} \left[f(P + d_{\alpha\beta}\Delta_P) - f(P) \right] \ . \tag{5.17}$$

However, this results in a branching of the trajectory at each nonadiabatic transition. Each branch must then be calculated until a further transition branches the trajectory again. This is prohibitively expensive computationally, as the number of branches in each trajectory grows exponentially with the number of transitions.

A more practical approach was found by making the so-called momentum-jump approximation, which resolves the issue of branching trajectories. This approximation amounts to changing the J operator from a continuous momentum derivative operator in a momentum shift operator. In this way, the momentum is changed instantaneously when a nonadiabatic transition occurs. While the SSTP algorithm shares this flaw (of unphysical instantaneous changes in momenta) with the traditional surface-hopping schemes, the momentum shifts are, at least, derived in a more rigorous fashion, and not merely by enforcing energy conservation.

There are two forms of the momentum-jump approximation; the first, given by Kapral and Ciccotti in Ref. [31] is an approximate form which does not exactly conserve the total energy of the system. A second realisation of the momentum-jump was later introduced which exactly conserves the energy. The derivations of

both are given below.

Approximate Momentum-Jump Rule

To perform the conversion of the J operator, consider just the first term:

$$J^{1st}_{\alpha\alpha',\beta\beta'} = \frac{P}{M} \cdot d_{\alpha\beta} \left(1 + \frac{1}{2} \frac{\Delta E_{\alpha\beta}(R) \hat{d}_{\alpha\beta}}{\frac{P}{M} \cdot \hat{d}_{\alpha\beta}} \cdot \frac{\partial}{\partial P} \right) \delta_{\alpha'\beta'} \, . \tag{5.18}$$

In general, the energy change of a nonadiabatic transition $\Delta E_{\alpha\beta}$ is very small compared to the kinetic energy of the environmental particles, and thus the term $\Delta E_{\alpha\beta} \hat{d}_{\alpha\beta} \left(\frac{P}{M} \cdot \hat{d}_{\alpha\beta} \right)^{-1}$ is much smaller than one. Using a first order approximation, the term in brackets can thus be written instead as an exponential:

$$\left(1 + \frac{1}{2} \frac{\Delta E_{\alpha\beta} \hat{d}_{\alpha\beta}}{\frac{P}{M} \cdot \hat{d}_{\alpha\beta}} \cdot \frac{\partial}{\partial P} \right) \approx e^{\frac{1}{2} \frac{\Delta E_{\alpha\beta} \hat{d}_{\alpha\beta}}{\frac{P}{M} \cdot \hat{d}_{\alpha\beta}} \cdot \frac{\partial}{\partial P}} \, . \tag{5.19}$$

Then, using the following identity for exponentiated derivatives,

$$e^{c \frac{\partial}{\partial x}} g(x) = g(x + c) \, , \tag{5.20}$$

where c is a constant, one obtains

$$e^{\frac{1}{2} \frac{\Delta E_{\alpha\beta} \hat{d}_{\alpha\beta}}{\frac{P}{M} \cdot \hat{d}_{\alpha\beta}} \cdot \frac{\partial}{\partial P}} f(P) \approx f \left(P + \frac{1}{2} \frac{\Delta E_{\alpha\beta} \hat{d}_{\alpha\beta}}{\frac{P}{M} \cdot \hat{d}_{\alpha\beta}} \right) \, . \tag{5.21}$$

Equation (5.21) provides a way of shifting the momenta of the classical degrees of freedom when a nonadiabatic transition occurs. In this way, the J operator has been converted from a momentum derivative operator to a momentum translation operator. The approximate momentum-jump rule is therefore

$$P \to P + \Delta^{AMJ} P \, , \tag{5.22}$$

where $\Delta^{AMJ} P$, the amount the momentum is shifted, is given by

$$\Delta^{AMJ}P = \frac{1}{2}\frac{\Delta E_{\alpha\beta}\hat{d}_{\alpha\beta}}{\frac{P}{M}\cdot\hat{d}_{\alpha\beta}}\,. \tag{5.23}$$

Note that Eq. (5.21) is only approximate, since the term multiplying the momentum derivative in the exponential contains the momentum P, and is thus not constant. This approximation is what causes the approximate momentum-jump rule to violate energy conservation. The AMJ superscript in Eqs. (5.22) and (5.23) denotes the approximate (and thus energy non-conserving) momentum-jump rule.

While the derivation above was only shown for the first term of the J operator, it applies similarly to the second term. Thus, when the approximate momentum-jump rule is applied, the J operator becomes

$$\begin{aligned} J^{AMJ}_{\alpha\alpha',\beta\beta'} = \; & - \frac{P}{M}\cdot d_{\alpha\beta}\exp\left[\frac{1}{2}\frac{\Delta E_{\alpha\beta}\hat{d}_{\alpha\beta}}{\frac{P}{M}\cdot\hat{d}_{\alpha\beta}}\cdot\frac{\partial}{\partial P}\right]\delta_{\alpha'\beta'} \\ & - \frac{P}{M}\cdot d^*_{\alpha'\beta'}\exp\left[\frac{1}{2}\frac{\Delta E_{\alpha'\beta'}\hat{d}^*_{\alpha'\beta'}}{\frac{P}{M}\cdot\hat{d}^*_{\alpha'\beta'}}\cdot\frac{\partial}{\partial P}\right]\delta_{\alpha\beta}\,. \end{aligned} \tag{5.24}$$

Exact Momentum-Jump Rule

As in the approximate momentum-jump rule derivation, to derive the exact rule, one begins by considering the first term of the J operator (Eq. 5.18). However, this time, the term in the brackets can be rewritten using a change of variables. Using the chain rule, the term becomes:

$$1 + \frac{\Delta E_{\alpha\beta}\hat{d}_{\alpha\beta}}{2\frac{P}{M}\cdot\hat{d}_{\alpha\beta}}\cdot\frac{\partial}{\partial P} = 1 + \Delta E_{\alpha\beta}M\frac{\partial}{\partial(P\cdot\hat{d}_{\alpha\beta})^2}\,. \tag{5.25}$$

Once this has been done, the momentum-jump approximation can be used, where the term is written as an exponential, using a first order approximation:

$$1 + \Delta E_{\alpha\beta}M\frac{\partial}{\partial(P\cdot\hat{d}_{\alpha\beta})^2} \approx e^{\Delta E_{\alpha\beta}M\frac{\partial}{\partial(P\cdot\hat{d}_{\alpha\beta})^2}} \tag{5.26}$$

The term multiplying the derivative no longer depends on P, and is now a constant. The identity given in Eq. (5.20) now applies exactly, giving

$$e^{\Delta E_{\alpha\beta} M \frac{\partial}{\partial (P\cdot\hat{d}_{\alpha\beta})^2}} f\left((P\cdot\hat{d}_{\alpha\beta})^2\right) = f\left((P\cdot\hat{d}_{\alpha\beta})^2 + \Delta E_{\alpha\beta} M\right) \tag{5.27}$$

Again, the J operator has been converted from a derivative operator to a translation operator. This time, however, instead of shifting the momentum, it shifts the variable $(P\cdot\hat{d}_{\alpha\beta})^2$ by an amount $\Delta E_{\alpha\beta} M$. The rule needs to be able to describe how P changes, though, and not how $(P\cdot\hat{d}_{\alpha\beta})^2$ changes, and to this end, the momentum P can be rewritten in terms of its components parallel and perpendicular to $\hat{d}_{\alpha\beta}$:

$$\begin{aligned} P &= \hat{d}^{\perp}_{\alpha\beta}\left(P\cdot\hat{d}^{\perp}_{\alpha\beta}\right) + \hat{d}_{\alpha\beta}\left(P\cdot\hat{d}_{\alpha\beta}\right) \\ &= \hat{d}^{\perp}_{\alpha\beta}\left(P\cdot\hat{d}^{\perp}_{\alpha\beta}\right) + \hat{d}_{\alpha\beta}\,\mathrm{sign}\left(P\cdot\hat{d}_{\alpha\beta}\right)\sqrt{\left(P\cdot\hat{d}_{\alpha\beta}\right)^2} \end{aligned} \tag{5.28}$$

Thus, applying the translation operator in Eq. (5.27) to a function of momentum P, gives

$$\begin{aligned} & e^{\Delta E_{\alpha\beta} M \partial/\partial (P\cdot\hat{d}_{\alpha\beta})^2} f(P) \\ = \;& e^{\Delta E_{\alpha\beta} M \frac{\partial}{\partial (P\cdot\hat{d}_{\alpha\beta})^2}} f\left(\hat{d}^{\perp}_{\alpha\beta}\left(P\cdot\hat{d}^{\perp}_{\alpha\beta}\right) + \hat{d}_{\alpha\beta}\,\mathrm{sign}\left(P\cdot\hat{d}_{\alpha\beta}\right)\sqrt{\left(P\cdot\hat{d}_{\alpha\beta}\right)^2}\right) \\ = \;& f\left(\hat{d}^{\perp}_{\alpha\beta}\left(P\cdot\hat{d}^{\perp}_{\alpha\beta}\right) + \hat{d}_{\alpha\beta}\,\mathrm{sign}\left(P\cdot\hat{d}_{\alpha\beta}\right)\sqrt{\left(P\cdot\hat{d}_{\alpha\beta}\right)^2 + \Delta E_{\alpha\beta} M}\right) \\ = \;& f\left(P - \hat{d}_{\alpha\beta}(P\cdot\hat{d}_{\alpha\beta}) + \hat{d}_{\alpha\beta}\,\mathrm{sign}(P\cdot\hat{d}_{\alpha\beta})\sqrt{(P\cdot\hat{d}_{\alpha\beta})^2 + \Delta E_{\alpha\beta} M}\right) . \end{aligned} \tag{5.29}$$

The exact momentum-shift rule is then given by

$$P \to P + \Delta^{EMJ} P \,, \tag{5.30}$$

with

$$\Delta^{EMJ} P_j = -\hat{d}_{\alpha\beta}(P \cdot \hat{d}_{\alpha\beta}) + \hat{d}_{\alpha\beta}\,\mathrm{sign}(P \cdot \hat{d}_{\alpha\beta})\sqrt{(P \cdot \hat{d}_{\alpha\beta})^2 + \Delta E_{\alpha\beta} M}\,, \tag{5.31}$$

where the EMJ superscript denotes the exact momentum-jump rule. This rule exactly conserves the total energy of the system at each nonadiabatic transition. Just as previously, the above derivation can be applied to the second term of the J operator to give

$$\begin{aligned} J_{\alpha\alpha',\beta\beta'} = \; & - \; \frac{P}{M} \cdot d_{\alpha\beta} \exp\left[\Delta E_{\alpha\beta} M \frac{\partial}{\partial \left(P \cdot \hat{d}_{\alpha\beta}\right)^2}\right] \delta_{\alpha'\beta'} \\ & - \; \frac{P}{M} \cdot d^*_{\alpha'\beta'} \exp\left[\Delta E_{\alpha'\beta'} M \frac{\partial}{\partial \left(P \cdot \hat{d}^*_{\alpha'\beta'}\right)^2}\right] \delta_{\alpha\beta}\,. \end{aligned} \tag{5.32}$$

The SSTP thus calculates Eq. (5.14) in the following way. Swarms of trajectories are propagated (see Fig. 5.1), each with initial conditions sampled from the phase space distribution for the bath, obtained from the partial Wigner transform of the density matrix for the bath degrees of freedom. At each time step, a trajectory is propagated adiabatically with a phase-factor associated with this propagation which depends on the states α and α'. At the end of each time step, pseudo-random numbers are used to sample whether or not a transition occurs, according to a suitable transition probability $\mathcal{P}$. If a transition occurs, the running value of the observable for the trajectory is multiplied by a weight of $1/\mathcal{P}$. If a transition is rejected, the observable is multiplied by a factor of $1/(1-\mathcal{P})$. In the two level

subsystem case, transitions occur simply between the ground state and excited state. When the subsystem comprises more than two distinct states, however, weights are associated with each state which determine the probabilities that govern the final state of the transition. When transitions occur, the bath momentum is adjusted according to the momentum-jump rule (approximated rule or exact rule). Finally, taking the trace over the product with the density matrix of the quantum subsystem, and averaging over all trajectories results in the statistical average for the observable.

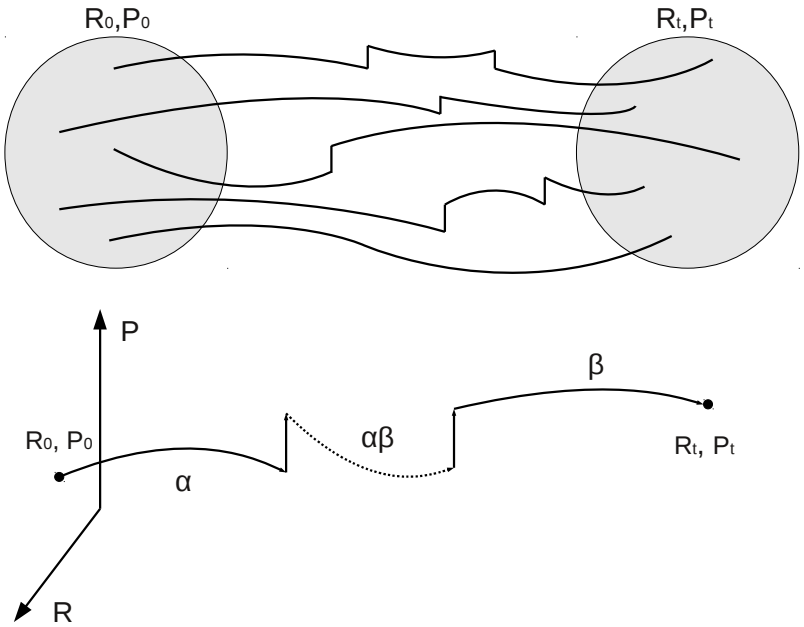

Figure 5.1: At the top of the figure is a diagrammatic representation of how the SSTP algorithm works. Swarms of trajectories are propagated from sampled initial phase space points, and may undergo nonadiabatic transitions. The observable is obtained by averaging over all the trajectories. At the bottom of the figure is an example of a single trajectory. The trajectory begins at phase space point (R_0, P_0) on adiabatic surface α. It then undergoes a transition, and begins propagating coherently on the mean of surfaces α and β. After it undergoes another transition, it propagates adiabatically again potential energy surface B, before reaching phase space point (R_t, P_t).

While each trajectory can undergo any number of nonadiabatic transitions, in practice, trajectories that undergo a large number cause significant error. Both the SSTP and TBQC algorithm from the next section thus employ a limit on the number of transitions that may occur in a single trajectory. When at a time t_i in

the calculation a transition would occur in a trajectory that has already undergone the maximum number of transitions, the trajectory is truncated, and is not included in the calculation of the observable beyond t_i. In general accounting for a maximum of two nonadiabatic transitions per trajectory is sufficient to obtain good agreement with numerically exact methods. At much longer times, however, more transitions may need to be included, especially in cases where coupling between the quantum subsystem and bath is strong.

The SSTP algorithm suffers from a similar problem as the Dyson integral equation method in that it becomes unstable at longer times, especially when there is a high level of nonadiabaticity in the dynamics being simulated. This instability is caused by the growth of weights in the observable as a result of the action of the J operator. This growth stems from the factors of $1/\mathcal{P}$ and $1/(1-\mathcal{P})$ that enter the calculation of the observable, and causes some trajectories to be weighted more heavily in the Monte Carlo integration than they should be. This problem is exacerbated by the oscillating sign of phase factors, and results in significant statistical error at longer simulation times. It is possible to dramatically reduce this error through use of intelligent transition sampling schemes, which will be discussed in the next chapter. It is also possible that treating the short-time propagators in a different way will reduce the error somewhat, and the Trotter Based Quantum-Classical Algorithm was developed to be an improvement over the SSTP algorithm.

5.3 Trotter Based Quantum-Classical Algorithm

An alternative to the SSTP method for quantum-classical dynamics within the quantum-classical Liouville approach is found in the Trotter Based Quantum-Classical, or TBQC, algorithm [35]. The TBQC algorithm is similar to the SSTP algorithm in that it is also based on segmenting the quantum-classical propagator into many short-time propagators, according to Eq. (5.8). However, it differs in the way the short-time propagators are treated.

In the SSTP, a truncated Dyson series expansion was used to split the $\mathcal{L}^0$ and J operators, however, in the TBQC case, as the name implies, Trotter factorisation is used. The short-time propagator is approximated as

$$\left(e^{i\mathcal{L}\tau_j}\right)_{\alpha_{j-1}\alpha'_{j-1},\alpha_j\alpha'_j} \approx e^{i\mathcal{L}^0_{\alpha_{j-1}\alpha'_{j-1}}\tau/2}\left(e^{-J\tau}\right)_{\alpha_{j-1}\alpha'_{j-1},\alpha_j\alpha'_j} e^{i\mathcal{L}^0_{\alpha_j\alpha'_j}\tau/2}. \tag{5.33}$$

The dynamics of each time step thus occurs in a different order to the SSTP method. Each time step is propagated for half a time step ($\tau/2$) on the mean of adiabatic energy surfaces α_{j-1} and α'_{j-1} with associated phase factor $\mathcal{W}_{\alpha_{j-1}\alpha'_{j-1}}(t_{j-1}, t_{j-1}+\frac{\tau}{2})$. As before, if $\alpha_{j-1} = \alpha'_{j-1}$, the system propagates adiabatically on state α_{j-1}, and the phase factor is unity. After this initial half step, the J operator acts, and potential nonadiabatic transitions may occur, along with bath momentum changes. Once this has been performed, the system is again propagated for half a time-step, but this time on the mean of states α_j and α'_j, with phase-factor $\mathcal{W}_{\alpha_j\alpha'_j}(t_{j-1}+\frac{\tau}{2}, t_j)$. associated with the evolution. Note that the main difference between the truncated Dyson method and the Trotter factorisation is that the J operator still appears in an exponential when the Trotter factorisation is used. As was mentioned previously, it is difficult to deal with the J operator numerically in this form, and thus some modifications are required before it can be implemented. To this end, it is convenient to split the J operator into two terms, $J = J_1 + J_2$, with

$$J_{1\alpha\alpha',\beta\beta'} = -\left(d_{\alpha\beta}\delta_{\alpha'\beta'} + d^*_{\alpha'\beta}\delta_{\alpha\beta}\right)\cdot\frac{P}{M}\,, \tag{5.34}$$

and

$$J_{2\alpha\alpha',\beta\beta'} = -\frac{1}{2}\left[\Delta E_{\alpha\beta}d_{\alpha\beta}\delta_{\alpha'\beta'} + \Delta E_{\alpha'\beta'}d^*_{\alpha'\beta'}\delta_{\alpha\beta}\right]\cdot\frac{\partial}{\partial P}\,. \tag{5.35}$$

Although the TBQC can be extended to be able to simulate subsystems of more than two states, it is convenient to just consider two-state subsystems for the fol-

lowing derivation.

Defining the initial state of the system ($\alpha\alpha'$) and the final state of the system ($\beta\beta'$) as matrix indices, the operators J_1 and J_2 can be written as matrices, with elements $J_{1(\alpha\alpha'),(\beta\beta')}$ and $J_{2(\alpha\alpha'),(\beta\beta')}$. Each index, corresponding to a pair of states can take on four values: (11), (12), (21) and (22). The matrices J_1 and J_2 are thus 4×4.

First, consider the matrix J_1:

$$J_{1_{(\alpha\alpha'),(\beta\beta')}} = \begin{pmatrix} J_{1_{11,11}} & J_{1_{11,12}} & J_{1_{11,21}} & J_{1_{11,22}} \\ J_{1_{12,11}} & J_{1_{12,12}} & J_{1_{12,21}} & J_{1_{12,22}} \\ J_{1_{21,11}} & J_{1_{21,12}} & J_{1_{21,21}} & J_{1_{21,22}} \\ J_{1_{22,11}} & J_{1_{22,12}} & J_{1_{22,21}} & J_{1_{22,22}} \end{pmatrix}$$

$$= \begin{pmatrix} -\frac{P}{M} \cdot (d_{11} + d_{11}^*) & -\frac{P}{M} \cdot d_{12}^* & -\frac{P}{M} \cdot d_{12} & 0 \\ -\frac{P}{M} \cdot d_{21}^* & -\frac{P}{M} \cdot (d_{11} + d_{22}^*) & 0 & -\frac{P}{M} \cdot d_{12} \\ -\frac{P}{M} \cdot d_{21} & 0 & -\frac{P}{M} \cdot (d_{22} + d_{11}^*) & -\frac{P}{M} \cdot d_{12}^* \\ 0 & -\frac{P}{M} \cdot d_{21} & -\frac{P}{M} \cdot d_{21}^* & -\frac{P}{M}(d_{22} + d_{22}^*) \end{pmatrix} . \tag{5.36}$$

Assuming that the adiabatic basis is real, the following rules apply for the nonadiabatic coupling matrix:

$$\begin{aligned} d_{\alpha\beta}^* &= d_{\alpha\beta} \,, \\ d_{00} = d_{11} &= 0 \,, \\ d_{\alpha\beta} &= -d_{\beta\alpha} \,. \end{aligned} \tag{5.37}$$

Using these rules, the matrix in Eq. (5.36) can be simplified to

$$
\begin{aligned}
J_{1_{(\alpha\alpha'),(\beta\beta')}} &= \begin{pmatrix} 0 & 1 & 1 & 0 \\ -1 & 0 & 0 & 1 \\ -1 & 0 & 0 & 1 \\ 0 & -1 & -1 & 0 \end{pmatrix} \frac{P}{M} \cdot d_{21}(R) \\
&\equiv \mathbf{A} \frac{P}{M} \cdot d_{21}(R) \, . \qquad (5.38)
\end{aligned}
$$

The matrix J_2 can be evaluated in a similar way:

$$
J_{2_{(\alpha\alpha'),(\beta\beta')}} = \begin{pmatrix} J_{2_{11,11}} & J_{2_{11,12}} & J_{2_{11,21}} & J_{2_{11,22}} \\ J_{2_{12,11}} & J_{2_{12,12}} & J_{2_{12,21}} & J_{2_{12,22}} \\ J_{2_{21,11}} & J_{2_{21,12}} & J_{2_{21,21}} & J_{2_{21,22}} \\ J_{2_{22,11}} & J_{2_{22,12}} & J_{2_{22,21}} & J_{2_{22,22}} \end{pmatrix}
$$

$$
= -\frac{1}{2} \begin{pmatrix} 0 & \Delta E_{12} d_{12} \cdot \frac{\partial}{\partial P} & \Delta E_{12} d_{12} \cdot \frac{\partial}{\partial P} & 0 \\ \Delta E_{21} d_{21} \cdot \frac{\partial}{\partial P} & 0 & 0 & \Delta E_{12} d_{12} \cdot \frac{\partial}{\partial P} \\ \Delta E_{21} d_{21} \cdot \frac{\partial}{\partial P} & 0 & 0 & \Delta E_{12} d_{12} \cdot \frac{\partial}{\partial P} \\ 0 & \Delta E_{21} d_{21} \cdot \frac{\partial}{\partial P} & \Delta E_{21} d_{21} \cdot \frac{\partial}{\partial P} & 0 \end{pmatrix} . \qquad (5.39)
$$

Using $\Delta E_{12} = -\Delta E_{21}$ and $d_{12} = -d_{21}$, this becomes

$$
\begin{aligned}
J_{2_{(\alpha\alpha'),(\beta\beta')}} &= -\begin{pmatrix} 0 & 1 & 1 & 0 \\ 1 & 0 & 0 & 1 \\ 1 & 0 & 0 & 1 \\ 0 & 1 & 1 & 0 \end{pmatrix} \frac{1}{2}\Delta E_{21} d_{21}(R) \cdot \frac{\partial}{\partial P} \\
&\equiv -\frac{1}{2}\mathbf{B}\Delta E_{21} d_{21}(R) \cdot \frac{\partial}{\partial P} \qquad (5.40)
\end{aligned}
$$

Simply substituting these terms for J_1 and J_2 is not useful, as it would still result in an exponentiated form for J. Instead, the term $e^{-J\tau}$ can be approximated to first order in τ as the product of exponentials for J_1 and J_2:

$$
e^{-J\tau} \approx e^{-J_1\tau} e^{-J_2\tau} \qquad (5.41)
$$

This is convenient because it allows the exponentials of J_1 and J_2 to be evaluated separately and obtain $e^{-J\tau}$ by simple multiplication at the end. First, consider the term $e^{-J_1\tau}$. With the thought of expanding the exponential as a Taylor series, it would be useful to know how the powers of the matrix $\mathbf{A}$ progress. The matrix $\mathbf{A}$ is given by

$$
\mathbf{A} = \begin{pmatrix} 0 & 1 & 1 & 0 \\ -1 & 0 & 0 & 1 \\ -1 & 0 & 0 & 1 \\ 0 & -1 & -1 & 0 \end{pmatrix}. \qquad (5.42)
$$

The square and cube of $\mathbf{A}$ are then given by

$$\begin{pmatrix} 0 & 1 & 1 & 0 \\ -1 & 0 & 0 & 1 \\ -1 & 0 & 0 & 1 \\ 0 & -1 & -1 & 0 \end{pmatrix} \begin{pmatrix} 0 & 1 & 1 & 0 \\ -1 & 0 & 0 & 1 \\ -1 & 0 & 0 & 1 \\ 0 & -1 & -1 & 0 \end{pmatrix} = \begin{pmatrix} -2 & 0 & 0 & 2 \\ 0 & -2 & -2 & 0 \\ 0 & -2 & -2 & 0 \\ 2 & 0 & 0 & -2 \end{pmatrix}, \quad (5.43)$$

and

$$\begin{aligned} \begin{pmatrix} -2 & 0 & 0 & 2 \\ 0 & -2 & -2 & 0 \\ 0 & -2 & -2 & 0 \\ 2 & 0 & 0 & -2 \end{pmatrix} \begin{pmatrix} 0 & 1 & 1 & 0 \\ -1 & 0 & 0 & 1 \\ -1 & 0 & 0 & 1 \\ 0 & -1 & -1 & 0 \end{pmatrix} &= \begin{pmatrix} 0 & -4 & -4 & 0 \\ 4 & 0 & 0 & -4 \\ 4 & 0 & 0 & -4 \\ 0 & 4 & 4 & 0 \end{pmatrix} \\ &= -4\mathbf{A}\,, \end{aligned} \quad (5.44)$$

respectively. Therefore, every odd power of $\mathbf{A}$ is a multiple of $\mathbf{A}$, and every even power of $\mathbf{A}$ is a multiple of $\mathbf{A}^2$. Using this, a Taylor series expansion for $e^{-J_1\tau}$ can now be performed. To obtain a more compact notation, the definition $a = \frac{P}{M} \cdot d_{21}(R)\tau$ is made.

$$\begin{aligned} e^{-J_1\tau} &= 1 - \mathbf{A}a + \frac{\mathbf{A}^2a^2}{2!} - \frac{\mathbf{A}^3a^3}{3!} + \frac{\mathbf{A}^4a^4}{4!} - \frac{\mathbf{A}^5a^5}{5!} + \frac{\mathbf{A}^6a^6}{6!} + \dots \\ &= 1 - \mathbf{A}a + \mathbf{A}^2\frac{a^2}{2!} + \mathbf{A}\frac{4a^3}{3!} - \mathbf{A}^2\frac{4a^4}{4!} - \mathbf{A}\frac{16a^5}{5!} + \mathbf{A}^2\frac{16a^6}{6!} + \dots \\ &= 1 - \mathbf{A}\left(a - \frac{4a^3}{3!} + \frac{16a^5}{5!} - \dots\right) + \frac{1}{2}\mathbf{A}^2\left(a^2 - \frac{8a^4}{4!} + \frac{32a^6}{6!} - \dots\right). \end{aligned} \quad (5.45)$$

By inspection, the series in the two sets of brackets are the Taylor series for $\cos a \sin a$ and $\sin^2 a$. Equation (5.45) becomes

$$
\begin{aligned}
e^{-J_1\tau} &= 1 + \mathbf{A}\left(\cos a \sin a\right) + \mathbf{A}^2\left(\frac{1}{2}\sin^2 a\right) \\
&= \begin{pmatrix} 1 & 0 & 0 & 0 \\ 0 & 1 & 0 & 0 \\ 0 & 0 & 1 & 0 \\ 0 & 0 & 0 & 1 \end{pmatrix} \\
&\quad + \begin{pmatrix} 0 & -\cos a \sin a & -\cos a \sin a & 0 \\ \cos a \sin a & 0 & 0 & -\cos a \sin a \\ \cos a \sin a & 0 & 0 & -\cos a \sin a \\ 0 & \cos a \sin a & \cos a \sin a & 0 \end{pmatrix} \\
&\quad + \begin{pmatrix} -\sin^2 a & 0 & 0 & \sin^2 a \\ 0 & -\sin^2 a & -\sin^2 a & 0 \\ 0 & -\sin^2 a & -\sin^2 a & 0 \\ \sin^2 a & 0 & 0 & -\sin^2 a \end{pmatrix} \\
&= \begin{pmatrix} \cos^2 a & -\cos a \sin a & -\cos a \sin a & \sin^2 a \\ \cos a \sin a & \cos^2 a & -\sin^2 a & -\cos a \sin a \\ \cos a \sin a & -\sin^2 a & \cos^2 a & -\cos a \sin a \\ \sin^2 a & \cos a \sin a & \cos a \sin a & \cos^2 a \end{pmatrix} .
\end{aligned}
\tag{5.46}
$$

While it is possible to treat the term $e^{-J_2\tau}$ in a similar way, it is not ideal to do so, because the resulting matrix causes shifts in the momentum in such a way that results in a branching of trajectories [35] similar to that discussed in the previous section. Instead a first order approximation in τ can be made:

$$
e^{-J_2\tau} \approx 1 - J_2\tau \, . \tag{5.47}
$$

Substitution of Eq. (5.47) into Eq. (5.41) yields

$$\begin{aligned} e^{-J\tau} &= e^{-J_1\tau} - e^{-J_1\tau} J_2 \tau \\ &= e^{-J_1\tau} + e^{-J_1\tau}\mathbf{B}\frac{\Delta E_{21} d_{21}(R)\tau}{2} \cdot \frac{\partial}{\partial P}\,. \end{aligned} \tag{5.48}$$

This form is not yet convenient for numerical implementation for the same reason as was discussed in the previous section on the SSTP algorithm - it results in branching of trajectories which is prohibitively expensive. Instead, the matrix elements of $e^{-J\tau}$ can be written explicitly:

$$\left(e^{-J\tau}\right)_{\alpha\alpha',\beta\beta'} = \left(e^{-J_1\tau}\right)_{\alpha\alpha',\beta\beta'} + \left(e^{-J_1\tau}\mathbf{B}\right)_{\alpha\alpha',\beta\beta'} \frac{\Delta E_{21} d_{21}(R)\tau}{2} \cdot \frac{\partial}{\partial P}\,, \tag{5.49}$$

and, since all the elements of the matrix $(e^{-J_1\tau})$ are non-zero, each element can be treated separately, and a factor of $(e^{-J_1\tau})_{\alpha\alpha',\beta\beta'}$ can be taken out to give:

$$\left(e^{-J\tau}\right)_{\alpha\alpha',\beta\beta'} = \left(e^{-J_1\tau}\right)_{\alpha\alpha',\beta\beta'} \left(1 + \frac{\left(e^{-J_1\tau}\mathbf{B}\right)_{\alpha\alpha',\beta\beta'}}{\left(e^{-J_1\tau}\right)_{\alpha\alpha',\beta\beta'}} \frac{\Delta E_{21} d_{21}\tau}{2} \cdot \frac{\partial}{\partial P}\right) \tag{5.50}$$

A matrix $C_{\alpha\alpha',\beta\beta'}$ is now defined to be the term $\frac{\left(e^{-J_1\tau}\mathbf{B}\right)_{\alpha\alpha',\beta\beta'}}{\left(e^{-J_1\tau}\right)_{\alpha\alpha',\beta\beta'}} \frac{\Delta E_{21} d_{21}\tau}{2}$. This gives

$$\left(e^{-J\tau}\right)_{\alpha\alpha',\beta\beta'} = \left(e^{-J_1\tau}\right)_{\alpha\alpha',\beta\beta'} \left(1 + C_{\alpha\alpha',\beta\beta'} \cdot \frac{\partial}{\partial P}\right) + \mathcal{O}(\tau^2) \tag{5.51}$$

Notice that the term in brackets in Eq. (5.51) is now a linear expansion for an exponential, a fact that was exploited in the SSTP case to obtain the momentum-jump approximation. To obtain the matrix $C_{\alpha\alpha',\beta\beta'}$, consider first $e^{J_1\tau}\mathbf{B}$:

$$e^{J_1\tau}\mathbf{B} = \begin{pmatrix} -2\cos a\sin a & \cos^2 a+\sin^2 a & \cos^2 a+\sin^2 a & -2\cos a\sin a \\ \cos^2 a-\sin^2 a & 0 & 0 & \cos^2 a-\sin^2 a \\ \cos^2 a-\sin^2 a & 0 & 0 & \cos^2 a-\sin^2 a \\ 2\cos a\sin a & \cos^2 a+\sin^2 a & \cos^2 a+\sin^2 a & 2\cos a\sin a \end{pmatrix}. \tag{5.52}$$

The matrix $C_{\alpha\alpha',\beta\beta'}$ then becomes

$$C_{(\alpha\alpha'),(\beta\beta')} = \begin{pmatrix} -2\frac{\sin a}{\cos a} & \frac{-1}{\cos a\sin a} & \frac{-1}{\cos a\sin a} & -2\frac{\cos a}{\sin a} \\ \frac{\cos^2 a-\sin^2 a}{\cos a\sin a} & 0 & 0 & \frac{\sin^2 a-\cos^2 a}{\cos a\sin a} \\ \frac{\cos^2 a-\sin^2 a}{\cos a\sin a} & 0 & 0 & \frac{\sin^2 a-\cos^2 a}{\cos a\sin a} \\ 2\frac{\cos a}{\sin a} & \frac{1}{\cos a\sin a} & \frac{1}{\cos a\sin a} & 2\frac{\sin a}{\cos a} \end{pmatrix} \frac{\Delta E_{21} d_{21}\tau}{2}. \tag{5.53}$$

A first order Taylor series approximation in τ for the sine and cosine terms can be made:

$$\begin{aligned} \sin a &= a + \mathcal{O}(\tau^3) \\ \cos a &= 1 + \mathcal{O}(\tau^2), \end{aligned} \tag{5.54}$$

which then approximates the $C_{\alpha\alpha',\beta\beta'}$ matrix as

$$C_{(\alpha\alpha'),(\beta\beta')} \approx \begin{pmatrix} -a & \frac{-1}{2a} & \frac{-1}{2a} & \frac{-1}{a} \\ \frac{1}{2a} & 0 & 0 & \frac{-1}{2a} \\ \frac{1}{2a} & 0 & 0 & \frac{-1}{2a} \\ \frac{1}{a} & \frac{1}{2a} & \frac{1}{2a} & a \end{pmatrix} \Delta E_{21} d_{21}\tau$$

$$\approx \begin{pmatrix} 0 & \frac{\Delta E_{12} d_{12}}{2\frac{P}{M}\cdot d_{12}} & \frac{\Delta E_{12} d_{12}}{2\frac{P}{M}\cdot d_{12}} & \frac{\Delta E_{12} d_{12}}{\frac{P}{M}\cdot d_{12}} \\ \frac{\Delta E_{21} d_{21}}{2\frac{P}{M}\cdot d_{21}} & 0 & 0 & \frac{\Delta E_{12} d_{12}}{2\frac{P}{M}\cdot d_{12}} \\ \frac{\Delta E_{21} d_{21}}{2\frac{P}{M}\cdot d_{21}} & 0 & 0 & \frac{\Delta E_{12} d_{12}}{2\frac{P}{M}\cdot d_{12}} \\ \frac{\Delta E_{21} d_{21}}{\frac{P}{M}\cdot d_{21}} & \frac{\Delta E_{21} d_{21}}{2\frac{P}{M}\cdot d_{21}} & \frac{\Delta E_{21} d_{21}}{2\frac{P}{M}\cdot d_{21}} & 0 \end{pmatrix} \tag{5.55}$$

where the fact that $-\frac{\Delta E_{21} d_{21}}{2\frac{P}{M}\cdot d_{21}} = \frac{\Delta E_{12} d_{12}}{2\frac{P}{M}\cdot d_{12}}$ has been used. The matrix elements $C_{11,11}$ and $C_{22,22}$ were dropped because they are of the order τ^2. Now that the form of $C_{\alpha\alpha',\beta\beta'}$ is known, the momentum-jump approximation can be made in a similar way to the SSTP, by approximating the term $\left(1 + C_{\alpha\alpha',\beta\beta'} \cdot \frac{\partial}{\partial P}\right)$ as an exponential, to give

$$\begin{aligned} \left(e^{-J\tau}\right)_{\alpha\alpha',\beta\beta'} &\approx \left(e^{-J_1\tau}\right)_{\alpha\alpha',\beta\beta'} e^{C_{\alpha\alpha',\beta\beta'}\cdot\frac{\partial}{\partial P}} \\ &\equiv \mathcal{M}_{\alpha\alpha',\beta\beta'} + \mathcal{O}(\tau^2) \end{aligned} \tag{5.56}$$

The matrix $\mathcal{M}$ is given by

$$\mathcal{M}_{(\alpha\alpha'),(\beta\beta')} = \begin{pmatrix} \cos^2 a & -(\cos a \sin a) e^{S_{12}\cdot\frac{\partial}{\partial P}} & -(\cos a \sin a) e^{S_{12}\cdot\frac{\partial}{\partial P}} & (\sin^2 a) e^{2S_{12}\cdot\frac{\partial}{\partial P}} \\ (\cos a \sin a) e^{S_{21}\cdot\frac{\partial}{\partial P}} & \cos^2 a & -\sin^2 a & -(\cos a \sin a) e^{S_{12}\cdot\frac{\partial}{\partial P}} \\ (\cos a \sin a) e^{S_{21}\cdot\frac{\partial}{\partial P}} & -\sin^2 a & \cos^2 a & -(\cos a \sin a) e^{S_{12}\cdot\frac{\partial}{\partial P}} \\ (\sin^2 a) e^{2S_{21}\cdot\frac{\partial}{\partial P}} & (\cos a \sin a) e^{S_{21}\cdot\frac{\partial}{\partial P}} & (\cos a \sin a) e^{S_{21}\cdot\frac{\partial}{\partial P}} & \cos^2 a \end{pmatrix} \tag{5.57}$$

where $S_{\alpha\beta} \equiv \frac{\hbar\omega_{\alpha\beta} M \hat{d}_{\alpha\beta}}{2P\cdot\hat{d}_{\alpha\beta}}$. Note that the term $S_{\alpha\beta}$ is exactly the same as the term in brackets in the two terms of the J operator. Apart from matrix elements $\mathcal{M}_{11,22}$ and $\mathcal{M}_{22,11}$, the exponentials in the matrix $\mathcal{M}$ thus lead to exactly the same momentum-jump rules outlined in the section on the SSTP algorithm. The exponentials containing the term S_{12} correspond to upward transitions, and the terms containing S_{21} to downward transitions. The matrix elements $\mathcal{M}_{11,22}$ and $\mathcal{M}_{22,11}$ contain an

extra factor of two because they correspond to a double jump, where both indices change, either from 11 $\rightarrow$ 22, or 22 $\rightarrow$ 11. Because they are double jumps, the momentum-jump rule is slightly different to the single jump rule. It is given by

$$e^{2S_{\alpha\beta}\cdot\frac{\partial}{\partial P}} f(P) = f\left(P + \Delta P_{\alpha\rightarrow\beta}\right) \ , \tag{5.58}$$

where

$$\Delta P_{\alpha\rightarrow\beta} = \hat{d}_{\alpha\beta}\,\mathrm{sign}\left(P\cdot\hat{d}_{\alpha\beta}\right)\sqrt{\left(P\cdot\hat{d}_{\alpha\beta}\right)^2 + 2\Delta E_{\alpha\beta}M} - \hat{d}_{\alpha\beta}\left(P\cdot\hat{d}_{\alpha\beta}\right) \ . \tag{5.59}$$

The difference between the momentum shifts for single and double jumps is that for the double jump, a factor of 2 arises as a coefficient of the $\Delta E_{\alpha\beta}M$ term in the square root. Energy of the total system is also exactly conserved for this rule.

The exponential terms in the matrix $\mathcal{M}$ are therefore responsible for the change in bath momentum accompanying a transition. The sine and cosine terms are responsible for the sampling of whether a transition occurs and which transition occurs. This sampling scheme will be explained in detail in the next chapter.

Now that the short-time nonadiabatic propagator $e^{-J\tau}$ has been derived, an expression for the short-time quantum-classical propagator can be written down:

$$\begin{aligned} e^{i\mathcal{L}(t_j - t_{j-1})} &\approx \mathcal{W}_{\alpha_{j-1}\alpha'_{j-1}}(t_{j-1}, t_{j-1} + \frac{\tau}{2}) e^{iL_{\alpha_{j-1}\alpha'_{j-1}}\tau/2} \mathcal{M}_{\alpha_{j-1}\alpha'_{j-1},\alpha_j\alpha'_j} \\ &\times \mathcal{W}_{\alpha_j\alpha'_j}(t_{j-1} + \frac{\tau}{2}, t_j) e^{iL_{\alpha_j\alpha'_j}\tau/2} \end{aligned} \tag{5.60}$$

This expression for the short-time quantum-classical propagator is then used to solve Eq. (5.14). It is performed in the same way as the SSTP algorithm, in that a swarm of trajectories are propagated, with initial conditions sampled from the initial phase space distribution function using a Monte Carlo scheme. These trajectories evolve

either on adiabatic potential energy surfaces or on the mean of two surfaces, and are interspersed with nonadiabatic transitions, which are governed by the matrix $\mathcal{M}$.

The two algorithms therefore work in very similar ways, with the only two differences being the Trotter factorisation of the short-time propagator, and the way the J operator is treated. It must be noted, however, that although the Trotter factorisation for the propagator is correct to second order in τ, due to the linear approximations used in obtaining a form for the nonadiabatic propagator $e^{-J\tau}$, Eq (5.60) is correct to the same order as Eq. (5.12). The SSTP and TBQC algorithms are thus of the same order.

Chapter 6

Sampling Schemes for Nonadiabatic Transitions

6.1 Original Sampling Schemes

6.1.1 SSTP Sampling Scheme

In the SSTP algorithm, each time step involves adiabatic propagation, followed by the action of the J operator. As mentioned before, the J operator is implemented stochastically, with transition probabilities determining whether or not a transition will occur at each time step. If the probability of a transition occurring is $\mathcal{P}$, then the probability of no transition occurring is $\mathcal{Q} = 1 - \mathcal{P}$. The form of the transition probability is not rigorously specified, and for the SSTP algorithm is chosen as [34]

$$\mathcal{P}_{\alpha\beta}(R, P, \tau) = \frac{\left|\frac{P}{M} \cdot d_{\alpha\beta}(R)\right| \tau}{1 + \left|\frac{P}{M} \cdot d_{\alpha\beta}(R)\right| \tau} , \tag{6.1}$$

which then dictates the probability that a transition will not occur as

$$\mathcal{Q}_{\alpha\beta}(R, P, \tau) \;\; = \;\; 1 - \mathcal{P}_{\alpha\beta}$$

$$= \frac{1}{1+\left|\frac{P}{M}\cdot d_{\alpha\beta}(R)\right|\tau}\,. \tag{6.2}$$

Note that the probability of a transition occurring is directly proportional to $\frac{P}{M}\cdot d$. The term $d_{\alpha\beta}$ is the nonadiabatic coupling matrix element giving the strength of coupling between adiabatic states α and β. If the momentum of the bath lies along $d_{\alpha\beta}$, the chance of a nonadiabatic transition occurring is increased. The probability is also naturally proportional to the time step τ, since the longer the time that elapses, the greater the chance a transition will occur in this time.

Because the J operator is implemented in a stochastic fashion, and not a deterministic way, when a transition is accepted, the observable must be multiplied by a factor of $1/\mathcal{P}$. Likewise when a transition is rejected, the observable is multiplied by $1/\mathcal{Q}$. There is therefore a weight associated with the observable for each trajectory in the ensemble, which is the concatenation of these weights at each time step. In addition to these weights, whenever a transition occurs, the observable must be multiplied by $\frac{P}{M}\cdot d_{\alpha\beta}\tau$ due to the $J\tau$ term in the calculation of the observable (see Eq. (5.12) for the short-time quantum-classical propagator).

Now consider the J operator:

$$\begin{aligned} J_{\alpha\alpha',\beta\beta'} = &- \frac{P}{M}\cdot d_{\alpha\beta}\left(1+\frac{1}{2}\frac{\Delta E_{\alpha\beta}d_{\alpha\beta}}{\frac{P}{M}\cdot d_{\alpha\beta}}\frac{\partial}{\partial P}\right)\delta_{\alpha'\beta'} \\ &- \frac{P}{M}d^*_{\alpha'\beta'}\left(1+\frac{1}{2}\frac{\Delta E_{\alpha\beta}d^*_{\alpha'\beta}}{\frac{P}{M}\cdot d^*_{\alpha'\beta'}}\frac{\partial}{\partial P}\right)\delta_{\alpha\beta}\,, \end{aligned} \tag{6.3}$$

which contains two terms. For some state $(\alpha\alpha')$, the first term changes the first index α and the second term changes the second index α'. In the SSTP algorithm, if a transition has been accepted according to the probability above, each of the two terms is sampled using a probability of $\frac{1}{2}$. Each term thus has an equal chance of acting. Because of this, there are no so-called double jumps that occur in the SSTP algorithm, where both indices change in one transition. This is a contrast to the

TBQC sampling described in the next section. In addition, the observable must be multiplied by a factor of 2 each time a transition occurs, since only one of the two terms in the J operator acts. The weight that enters the observable when an $\alpha \to \beta$ transition is accepted is thus:

$$\begin{aligned} W_{\alpha\beta} &= 2\left(\frac{P}{M}\cdot d_{\alpha\beta}\tau\right)\frac{1}{\mathcal{P}_{\alpha\beta}} \\ &= 2\left(\frac{P}{M}\cdot d_{\alpha\beta}\tau\right)\frac{1+\left|\frac{P}{M}\cdot d_{\alpha\beta}\right|\tau}{\left|\frac{P}{M}\cdot d_{\alpha\beta}\right|\tau} \\ &= 2\,\mathrm{sign}\left(\frac{P}{M}\cdot d_{\alpha\beta}\right)\left(1+\left|\frac{P}{M}\cdot d_{\alpha\beta}\right|\tau\right), \end{aligned} \tag{6.4}$$

and the weight when no transition occurs is

$$W^{NT} = 1+\left|\frac{P}{M}\cdot d_{\alpha\beta}\right|\tau\,. \tag{6.5}$$

While the original SSTP sampling scheme yields good results at short times, it is known to completely fails at longer times. This failure is due to the concatenation of weights in the observable, and results in large statistical error [58]. This error can be reduced by devising intelligent improved sampling schemes.

6.1.2 TBQC Sampling Scheme

In the TBQC algorithm, the J operator takes the form of the matrix $\mathcal{M}$ (Eq. (5.57)). As explained in the TBQC section in Chapter 5, the exponentials in the matrix $\mathcal{M}$ are responsible for the momentum changes accompanying a transition. The sampling scheme itself is derived from the sine and cosine terms in the matrix $\mathcal{M}$, in other words, by the elements of the matrix $e^{-J_1\tau}$:

$$e^{-J_1\tau} = \begin{pmatrix} \cos^2 a & -\cos a \sin a & -\cos a \sin a & \sin^2 a \\ \cos a \sin a & \cos^2 a & -\sin^2 a & -\cos a \sin a \\ \cos a \sin a & -\sin^2 a & \cos^2 a & -\cos a \sin a \\ \sin^2 a & \cos a \sin a & \cos a \sin a & \cos^2 a \end{pmatrix} . \tag{6.6}$$

Each row of the matrix corresponds to an initial pair of states $(\alpha\alpha')$, and each column corresponds to a final pair of states $(\beta\beta')$. The absolute value of the terms in each row of this matrix are interpreted as the unnormalised probabilities for each possible transition corresponding to each set of initial states. For example, consider an initial state $(\alpha\alpha') = (11)$. The first row of the matrix corresponds to this initial state, so only this row needs to be considered when the matrix $\mathcal{M}$ acts. The absolute values of the second and third terms in the row are then the unnormalised probabilities for single jump transitions $(11) \to (12)$ and $(11) \to (21)$, and the absolute value of the fourth term is the unnormalised probability for a double jump transition $(11) \to (22)$. The first term then corresponds to no transition occurring. The normalisation factor for the probabilities is just the sum of the absolute values of all the terms in the row. This gives the general formula for the transition probabilities as:

$$\begin{aligned} \mathcal{P}_{\alpha\alpha',\beta\beta'} &= \frac{\left| \left(e^{-J_1\tau}\right)_{\alpha\alpha',\beta\beta'} \right|}{\sum_{\beta\beta'} \left| \left(e^{-J_1\tau}\right)_{\alpha\alpha',\beta\beta'} \right|} \\ &= \frac{\left| \left(e^{-J_1\tau}\right)_{\alpha\alpha',\beta\beta'} \right|}{1 + 2|\cos a \sin a|} , \end{aligned} \tag{6.7}$$

with $\alpha\alpha' \neq \beta\beta'$. The chance of no transition occurring is given by

$$\mathcal{P}_{\alpha\alpha',\alpha\alpha'} = \frac{|\cos^2 a|}{1 + 2|\cos a \sin a|} . \tag{6.8}$$

Similar to the case of the SSTP sampling, each time the algorithm samples to determine whether a transition occurs, the observable is multiplied by a factor of $1/\mathcal{P}_{\alpha\alpha',\beta\beta'}$, as well as by the corresponding matrix element $\left(e^{-J_1\tau}\right)_{\alpha\alpha',\beta\beta'}$. Again, the weight comprising these factors becomes large at later simulation times, resulting in significant statistical error. The weight entering the observable at each time step is given by

$$\begin{aligned} W_{\alpha\alpha',\beta\beta'} &= \left(e^{-J_1\tau}\right)_{\alpha\alpha',\beta\beta'} \frac{1}{\mathcal{P}_{\alpha\alpha',\beta\beta'}} \\ &= \left(e^{-J_1\tau}\right)_{\alpha\alpha',\beta\beta'} \frac{1+2|\cos a \sin a|}{\left|\left(e^{-J_1\tau}\right)_{\alpha\alpha',\beta\beta'}\right|} \\ &= \operatorname{sign}\left(\left(e^{-J_1\tau}\right)_{\alpha\alpha',\beta\beta'}\right)(1+2|\cos a \sin a|)\ . \end{aligned} \tag{6.9}$$

This weight applies for when transitions are accepted or rejected.

A benefit of the TBQC sampling scheme over the SSTP sampling scheme is that the term $\frac{P}{M}\cdot d_{\alpha\beta}\tau$ only appears in sine and cosine functions in the weights that enter the observable, as opposed to linearly. This would result in the TBQC weight growing more slowly than the SSTP weight in cases where this term is large. The TBQC sampling scheme also includes double jump transitions, which the SSTP sampling scheme does not. This difference will most likely not effect results significantly, since the probability of a double transition is approximately the square of the probability of single jump transition.

6.2 Improved Sampling Schemes

6.2.1 Observable Cutting Scheme

The observable cutting scheme was the first improvement upon the original sampling schemes [34]. It was noted that the prime source of error in the SSTP and TBQC algorithms was the growth of the numerical weight in the observable as a result of the

sampling scheme. This growth of numerical weights resulted in certain trajectories being weighted in the calculation of the observable far more heavily than they should be, resulting in large statistical error. A simple and direct approach to this problem is to set an upper bound on the weight in the observable, so that it cannot be larger than the bound.

A numerical threshold parameter, κ_t is thus defined which sets an upper bound to the magnitude of the weight. If, at time step j in the calculation of a trajectory, the magnitude of the weight W becomes larger than κ_t, it is instead set to the value of κ_t. Mathematically, this can write this as:

$$W = \begin{cases} W & \text{if } |W| < \kappa_t \\ \text{sign}(W)\kappa_t & \text{if } |W| > \kappa_t \end{cases} \tag{6.10}$$

Note that this cutting only affects the magnitude of the weight, the sign remains the same. This cutting ensures that the weight can never grow to values where a single trajectory is having an overly large effect on the value of the observable. Consequently, statistical error in the result is greatly reduced at longer times. While effective, however, this scheme does not have any physical basis, unlike the energy-conserving filtering scheme in the next section.

6.2.2 Transition Filtering Scheme

The more recently developed transition filtering scheme [36][37] attempts to solve the long time statistical error from a different angle. Essentially, it is based of filtering out nonadiabatic transitions that would result in large changes in the momentum, where the approximate momentum-shift rule (Eq. (5.23)) fails.

Consider the energy variation caused in the system when a nonadiabatic transition $\alpha \to \beta$ is calculated using the approximated momentum-jump rule:

$$\mathcal{E}_{\alpha\beta} = \sum_j \frac{P_j'^2}{2M} + E_\beta(R) - \left(\sum_j \frac{P_j^2}{2M} + E_\alpha(R) \right) , \tag{6.11}$$

where $P_j' = P_j + \Delta^{AMJ} P_j$ is the shifted momentum. Upon introduction of a numerical parameter $\kappa_\mathcal{E}$, and weight $\omega(\kappa_\mathcal{E}, \mathcal{E}_{\alpha\beta})$, a generalised transition probability [36] for the SSTP algorithm can be defined:

$$\mathcal{P}_{\alpha\beta}^{EC}(R, P, \tau) = \frac{\tau \left| \frac{P}{M} \cdot d_{\alpha\beta}(R) \right| \omega\left(\kappa_\mathcal{E}, \mathcal{E}_{\alpha\beta}\right)}{1 + \tau \left| \frac{P}{M} \cdot d_{\alpha\beta}(R) \right| \omega\left(\kappa_\mathcal{E}, \mathcal{E}_{\alpha\beta}\right)} , \tag{6.12}$$

which then defines the probability of a transition not occurring to be

$$\begin{aligned} \mathcal{Q}_{\alpha\beta}^{EC}(R, P, \tau) &= 1 - \mathcal{P}_{\alpha\beta} \\ &= \frac{1}{1 + \tau \left| \frac{P}{M} \cdot d_{\alpha\beta}(R) \right| \omega\left(\kappa_\mathcal{E}, \mathcal{E}_{\alpha\beta}\right)} , \end{aligned} \tag{6.13}$$

The numerical weight is defined as

$$\omega\left(\kappa_\mathcal{E}, \mathcal{E}_{\alpha\beta}\right) = \begin{cases} 1 & \text{if } \mathcal{E}_{\alpha\beta} \leq \kappa_\mathcal{E} \\ 0 & \text{otherwise} \end{cases} . \tag{6.14}$$

These generalised transition probabilities essentially allow control of the amplitude of energy fluctuations that would be caused by the approximate momentum-jump rule, through use of the numerical parameter $\kappa_\mathcal{E}$. Whenever a nonadiabatic transition occurring would result in an energy jump larger than the control parameter $\kappa_\mathcal{E}$, the transition probability becomes zero, and the transition cannot occur. If the virtual energy fluctuation is less than the control parameter, the transition probabilities simply reduce to those of the original SSTP algorithm. This generalisation of the original sampling scheme thus allows transitions to occur only in regions where use of the approximate momentum-shift rule would produce small energy variations. This essentially amounts to disregarding transitions which would

cause large momentum changes in the bath, since the approximate momentum-shift rule numerically coincides with the exact momentum-shift rule as the changes in the momentum approach zero. The system is thus not led to unstable regions of phase space.

The transition filtering scheme has been shown to be quite successful at reducing statistical error at longer simulations, while still maintaining the integrity of the result [36][37]. It must be noted, however, that there is a trade-off. While reducing the value of the numerical control parameter $\kappa_{\mathcal{E}}$ reduces the statistical error, values of the parameter that are too small, result in too many transitions being filtered, essentially removing the nonadiabaticity of the dynamics. This is particularly important when the coupling between the subsystem and environment is strong. Because of this, the transition filtering scheme tends to be more successful at weak and intermediate coupling strengths.

Finally, although the transition filtering scheme was originally designed for implementation in the SSTP algorithm, it is easily extended to the TBQC algorithm. Applying the weight $\omega(\kappa_{\mathcal{E}}, \mathcal{E}_{\alpha\alpha',\beta\beta'})$ in a similar way to the TBQC sampling scheme, one obtains generalised transition probabilities as:

$$\mathcal{P}_{\alpha\alpha',\beta\beta'} = \frac{\left| \left(e^{-J_1\tau}\right)_{\alpha\alpha',\beta\beta'} \right| \omega(\kappa_{\mathcal{E}}, \mathcal{E}_{\alpha\alpha',\beta\beta'})}{|\cos^2 a| + |\sin^2 a| \omega(\kappa_{\mathcal{E}}, \mathcal{E}_{\alpha\alpha',\beta\beta'}) + 2|\cos a \sin a| \omega(\kappa_{\mathcal{E}}, \mathcal{E}_{\alpha\alpha',\beta\beta'})}\,, \tag{6.15}$$

and

$$\mathcal{P}_{\alpha\alpha',\alpha\alpha'} = \frac{|\cos^2 a|}{|\cos^2 a| + |\sin^2 a| \omega(\kappa_{\mathcal{E}}, \mathcal{E}_{\alpha\alpha',\beta\beta'}) + 2|\cos a \sin a| \omega(\kappa_{\mathcal{E}}, \mathcal{E}_{\alpha\alpha',\beta\beta'})}\,. \tag{6.16}$$

6.2.3 Combination Filtering

Although both the observable cutting and transition filtering schemes have been shown to reduce statistical error at long times, they approach the problem in two different ways. It would thus be of interest to introduce a so-called combination filtering scheme which utilises both schemes in a single algorithm. This combination scheme would then have the benefits of both techniques, and perform better than either the observable cutting or transition filtering. This would then allow even further simulation times to be reliably calculated.

According to such an idea, in each simulation, nonadiabatic transitions are filtered according to the transition filtering scheme by use of the numerical control parameter $\kappa_{\mathcal{E}}$, in addition to the weight in the observable being cut when it grows too large, according to the threshold parameter κ_t.

In the results displayed in Chapter 8, a study of the three improved sampling schemes is presented, with the aim of determining which technique is superior.

Chapter 7

The Spin-Boson Model

The theory presented in the previous chapters is not system specific, and applies to general systems that comprise a quantum subsystem coupled to a classical, or classical-like, environment. However, in order to perform numerical simulations on a computer, the theory needs to be applied to some model system. A convenient model of choice is the spin-boson model, as it has the essential components of a quantum-classical system. It comprises a quantum spin, or two-level system, coupled to an environment of bosons, or harmonic oscillators. There is thus a ground state and an excited state in the subsystem. The harmonic oscillator environment can be either classical or quantum. In the quantum-classical Liouville approach, the bosonic bath is treated in a classical-like manner through use of the partial Wigner transform.

A further reason the spin-boson model is a convenient model for numerical studies is that it is an extremely well studied system [68], and it is utilised in much of the past literature on the quantum-classical Liouville model [34]-[37],[58]. This means that not only are there many simulation results with which one can compare calculations, but indeed there are also numerically 'exact' results obtained from quantum path integral calculations.

The Hamiltonian for this model in the case of a quantum environment is given by

$$\hat{H} = -\hbar\Omega\hat{\sigma}_x + \sum_{j=1}^{N}\left(\frac{\hat{P}_j^2}{2M_j} + \frac{1}{2}M_j\omega_j^2\hat{R}_j^2 - c_j\hat{R}_j\hat{\sigma}_z\right) , \tag{7.1}$$

where $\hat{\sigma}_z$ and $\hat{\sigma}_x$ are the usual Pauli matrices [69]. The summation is over the harmonic oscillators of the environment, and M_j and ω_j denote the mass and frequency of the the j^{th} oscillator. The constants c_j give the strength of coupling between the j^{th} oscillator and the quantum subsystem. The symbol Ω gives the energy gap of the two levels in the subsystem by $\Delta E = 2\hbar\Omega$.

Taking a partial Wigner transform over the environmental degrees of freedom gives the partial Wigner transformed Hamiltonian:

$$\hat{H}_W(R,P) = -\hbar\Omega\hat{\sigma}_x + \sum_{j=1}^{N}\left(\frac{P_j^2}{2M_j} + \frac{1}{2}M_j\omega_j^2R_j^2 - c_jR_j\hat{\sigma}_z\right) . \tag{7.2}$$

In this representation, the Hamiltonian now not only depends on the quantum spin degrees of freedom, but also on phase space coordinates R and P. It is thus both an operator and a function of phase space. It can be split into the isolated subsystem Hamiltonian, $\hat{h}_s$,

$$\hat{h}_s = -\hbar\Omega\hat{\sigma}_x , \tag{7.3}$$

the Hamiltonian for the harmonic environment

$$H_b(R,P) = \sum_{j=1}^{N}\left(\frac{P_j^2}{2M_j} + \frac{1}{2}M_j\omega_j^2R_j^2\right) , \tag{7.4}$$

as well as the potential arising from coupling between the subsystem and the bath:

$$\begin{aligned}\hat{V}_c(R) &= -\sum_{j=1}^{N}c_jR_j\hat{\sigma}_z \\ &\equiv \gamma(R)\hat{\sigma}_z . \end{aligned} \tag{7.5}$$

At this point, it is worthwhile noting that although the theory allows for the

masses of the oscillators to be different, for the sake of convenience, they are taken to be the same.

In the simulations that are presented, the bath was taken to have an Ohmic spectral density. An efficient way to represent an infinite bath with an Ohmic spectral density using a finite number of oscillators is provided by the work of Makri and Thompson [70]. This is done by employing the following forms for the frequencies

$$\omega_j = -\omega_c \ln\left(1 - j\frac{\omega_0}{\omega_c}\right) , \tag{7.6}$$

and coupling constants

$$c_j = \omega_j \sqrt{\xi \hbar \omega_0 M} , \tag{7.7}$$

where

$$\omega_0 = \frac{\omega_c}{N}\left(1 - e^{-\omega_{max}/\omega_c}\right) , \tag{7.8}$$

and ω_{max} is a cutoff frequency which limits the range of frequencies the oscillators may have. The symbol ξ is known as the Kondo parameter. From Eq. (7.7) it can be seen that the Kondo parameter dictates the magnitude of the coupling constants, and is thus a measure of the strength between the subsystem and environment.

7.1 Scaled Units

In general, the numbers involved in the calculations for systems on the quantum level, when using SI units, are of a magnitude ill-suited for use in simulations. For convenience, as well as accuracy, it is desirable instead to use scaled dimensionless units that are more suited to simulation of quantum-sized systems.

In the system of dimensionless units used in the simulations, the phase space coordinates are scaled according to

$$R'_j = \left(\frac{M\omega_c}{\hbar}\right)^{\frac{1}{2}} R_j, \quad P'_j = (\hbar M\omega_c)^{-\frac{1}{2}} P_j \ . \tag{7.9}$$

When represented using the dimensionless units, the partial Wigner transformed Hamiltonian becomes

$$\hat{H}'_W(R', P') = -\Omega'\hat{\sigma}_x + \sum_j \left(\frac{P_j'^2}{2} + \frac{1}{2}\omega_j'^2 R_j'^2 - c'_j\hat{\sigma}_z R'_j\right) \ , \tag{7.10}$$

with

$$\Omega' = \frac{\Omega}{\omega_c}, \quad \omega'_j = \frac{\omega_j}{\omega_c}, \quad c'_j = \omega'_j\sqrt{\xi\frac{\omega_j}{\omega_c}} \ . \tag{7.11}$$

This system of units is essentially equivalent to setting both the reduced Planck constant, and the masses of the harmonic oscillators in the bath, to unity. The inverse temperature β, as well as the time coordinate are also scaled, in the following way:

$$t' = t\omega_c, \quad \beta' = \frac{\omega_c}{k_B T} \ . \tag{7.12}$$

The scaling of units ensures that in the computational calculation, accuracy is not lost due to rounding errors. Henceforth only dimensionless units will be used, but, for convenience, the primes denoting them will be dropped.

7.2 Solving for the Adiabatic Basis

Once the Hamiltonian of the system of study has been defined, it is possible to determine the adiabatic basis, which is required for the calculations. For the spin-boson system, the adiabatic Hamiltonian within the partial Wigner representation is given by

$$\hat{h}_W(R,P) = -\Omega\hat{\sigma}_x + V_b + \gamma(R)\hat{\sigma}_z\,, \tag{7.13}$$

where γ is defined by Eq. (7.5), and V_b is the potential energy of the bath. To obtain the adiabatic eigenvectors, the characteristic equation needs to be solved for the adiabatic Hamiltonian:

$$\det(\hat{h}_W - \lambda I) = 0\,. \tag{7.14}$$

To do this, the adiabatic Hamiltonian needs to be expressed in matrix form:

$$\begin{aligned} \hat{h}_W &= \begin{pmatrix} 0 & -\Omega \\ -\Omega & 0 \end{pmatrix} + \begin{pmatrix} V_b & 0 \\ 0 & V_b \end{pmatrix} + \begin{pmatrix} \gamma & 0 \\ 0 & -\gamma \end{pmatrix} \\ &= \begin{pmatrix} V_b+\gamma & -\Omega \\ -\Omega & V_b-\gamma \end{pmatrix}. \end{aligned} \tag{7.15}$$

Substitution of Eq. (7.15) into Eq. (7.14) yields

$$\begin{aligned} \det(\hat{h}_W - \lambda I) &= \det\begin{pmatrix} V_b+\gamma-\lambda & -\Omega \\ -\Omega & V_b-\gamma-\lambda \end{pmatrix} \\ &= 0\,. \end{aligned} \tag{7.16}$$

This simplifies to the following quadratic equation:

$$V_b^2 - 2\lambda V_b - \gamma^2 + \lambda^2 - \Omega^2 = 0\,, \tag{7.17}$$

the solutions of which are the energy eigenvalues for the adiabatic basis:

$$\begin{aligned} E_{1,2}(R) &= \frac{-2V_b \pm \sqrt{4V_b^2 - 4(V_b^2 - \gamma^2 - \Omega^2)}}{2} \\ &= V_b \pm \sqrt{\gamma^2 + \Omega^2}\,. \end{aligned} \tag{7.18}$$

To obtain the adiabatic eigenvectors, one then substitutes these eigenenergies back into the characteristic equation. In the case of $E_1(R) = V_b + \sqrt{\gamma^2 + \Omega^2}$, this gives

$$\begin{pmatrix} V_b + \gamma - V_b - \sqrt{\gamma^2 + \Omega^2} & -\Omega \\ -\Omega & V_b - \gamma - V_b - \sqrt{\gamma^2 + \Omega^2} \end{pmatrix} \begin{pmatrix} x_1 \\ x_2 \end{pmatrix} = \begin{pmatrix} 0 \\ 0 \end{pmatrix}. \tag{7.19}$$

The above vector equation can then be written as two simultaneous equations,

$$(\gamma - \sqrt{\gamma^2 + \Omega^2})x_1 + (-\Omega)x_2 = 0\,, \tag{7.20}$$

and

$$(-\Omega)x_1 + (-\gamma - \sqrt{\gamma^2 + \Omega^2})x_2 = 0\,. \tag{7.21}$$

Subtracting Eq. (7.21) from Eq. (7.20) gives

$$(\gamma + \Omega - \sqrt{\gamma^2 + \Omega^2})x_1 + (\gamma - \Omega + \sqrt{\gamma^2 + \Omega^2})x_2 = 0\,. \tag{7.22}$$

By dividing through by γ, and defining $G = \frac{1}{\gamma}\left[-\Omega + \sqrt{\gamma^2 + \Omega^2}\right]$, the above

equation can be rewritten in a more compact form:

$$(1-G)x_1 + (1+G)x_2 = 0\,. \tag{7.23}$$

The first eigenvector is thus given by

$$|E_1'(R)\rangle = \begin{pmatrix} 1+G \\ -(1-G) \end{pmatrix}, \tag{7.24}$$

where the prime on the E denotes the fact that the eigenvector is not yet normalised.

Now to calculate the second eigenvector, the second eigenenergy $E_2(R) = V_b - \sqrt{\gamma^2+\Omega^2}$ must be substituted into the characteristic equation:

$$\begin{pmatrix} V_b+\gamma-V_b+\sqrt{\gamma^2+\Omega^2} & -\Omega \\ -\Omega & V_b-\gamma-V_b+\sqrt{\gamma^2+\Omega^2} \end{pmatrix} \begin{pmatrix} x_1 \\ x_2 \end{pmatrix} = \begin{pmatrix} 0 \\ 0 \end{pmatrix}, \tag{7.25}$$

which yields the following simultaneous equations:

$$(\gamma+\sqrt{\gamma^2+\Omega^2})x_1 + (-\Omega)x_2 = 0\,, \tag{7.26}$$

and

$$(-\Omega)x_1 + (-\gamma+\sqrt{\gamma^2+\Omega^2})x_2 = 0\,. \tag{7.27}$$

Adding (7.26) and (7.27), one obtains

$$(\gamma - \Omega + \sqrt{\gamma^2 + \Omega^2})x_1 + (-\gamma - \Omega + \sqrt{\gamma^2 + \Omega^2})x_2 = 0\,. \tag{7.28}$$

Dividing through by γ as before gives

$$(1 + G)x_1 - (1 - G)x_2 = 0\,. \tag{7.29}$$

The second (unnormalised) eigenvector is thus

$$|E_2'(R)\rangle = \begin{pmatrix} 1 - G \\ 1 + G \end{pmatrix}\,. \tag{7.30}$$

Now the eigenvectors need to be normalised. The normalised eigenvectors are given by

$$\frac{|E_1'(R)\rangle}{\sqrt{\langle E_1'(R)|E_1'(R)\rangle}}\,, \tag{7.31}$$

and

$$\frac{|E_2'(R)\rangle}{\sqrt{\langle E_2'(R)|E_2'(R)\rangle}}\,. \tag{7.32}$$

The inner products of the unnormalised eigenvectors need to be calculated:

$$\begin{aligned} \langle E_1'(R)|E_1'(R)\rangle &= (1 + G)^2 + (1 - G)^2 \\ &= 2(1 + G^2) \end{aligned}$$

$$= \langle E_2'(R)|E_2'(R)\rangle\,. \tag{7.33}$$

The normalised eigenvectors for the adiabatic basis are thus given by

$$|E_1(R)\rangle = \frac{1}{\sqrt{2(1+G^2)}}\begin{pmatrix} 1+G \\ -(1-G)\end{pmatrix}, \tag{7.34}$$

and

$$|E_2(R)\rangle = \frac{1}{\sqrt{2(1+G^2)}}\begin{pmatrix} 1-G \\ 1+G\end{pmatrix}. \tag{7.35}$$

7.2.1 Nonadiabatic Coupling Matrix

Now that the eigenvectors and eigenenergies have been obtained for the adiabatic basis, the nonadiabatic coupling matrix element $d_{\alpha\beta}$, as well as the Hellmann-Feynman forces for the excited state and ground state, can be derived.

Consider first the nonadiabatic matrix coupling element. By definition

$$\begin{aligned} d_{12} &= \langle E_1(R)|\frac{\partial}{\partial R}|E_2(R)\rangle\,. \\ &= \frac{1}{\sqrt{2(1+G^2)}}\begin{pmatrix} 1+G \\ -(1-G)\end{pmatrix}\cdot\frac{\partial}{\partial R}\left[\frac{1}{\sqrt{2(1+G^2)}}\begin{pmatrix} 1-G \\ 1+G\end{pmatrix}\right] \\ &= \frac{1}{\sqrt{2(1+G^2)}}\begin{pmatrix} 1+G \\ -(1-G)\end{pmatrix}\cdot \\ &\quad \left[\begin{pmatrix} 1-G \\ 1+G\end{pmatrix}\frac{\partial}{\partial R}\frac{1}{\sqrt{2(1+G^2)}} + \frac{1}{\sqrt{2(1+G^2)}}\frac{\partial}{\partial R}\begin{pmatrix} 1-G \\ 1+G\end{pmatrix}\right]. \end{aligned} \tag{7.36}$$

Since the eigenvectors are orthogonal to each other, the first term in the square brackets disappears, and one obtains

$$\begin{aligned} d_{12} &= \frac{1}{2(1+G^2)} \begin{pmatrix} 1+G \\ -(1-G) \end{pmatrix} \cdot \frac{\partial}{\partial R} \begin{pmatrix} 1-G \\ 1+G \end{pmatrix} \\ &= \frac{1}{2(1+G^2)} \begin{pmatrix} 1+G \\ -(1-G) \end{pmatrix} \cdot \begin{pmatrix} -\frac{\partial G}{\partial R} \\ \frac{\partial G}{\partial R} \end{pmatrix} \\ &= -\frac{1}{1+G^2} \frac{\partial G}{\partial R} . \end{aligned} \tag{7.37}$$

Similarly for d_{21},

$$d_{21} = \frac{1}{1+G^2} \frac{\partial G}{\partial R} . \tag{7.38}$$

Note that $d_{12} = -d_{21}$, as is expected, since the nonadiabatic coupling matrix is anti-hermitian, and the adiabatic basis is real.

7.2.2 Hellmann-Feynman Force

The Hellmann-Feynman force for a state α is defined as

$$F_W^{\alpha} = -\langle \alpha | \frac{\partial \hat{V}_W(R)}{\partial R} | \alpha \rangle . \tag{7.39}$$

The potential energy operator for the spin-boson system comprises the potential energy of the bath and the potential energy operator for the coupling between the subsystem and bath:

$$\hat{V}_W(R) = \frac{1}{2}\omega^2 R^2 - cR\hat{\sigma}_z , \tag{7.40}$$

remembering that scaled units are being used, and thus $M = 1$. Substituting this into the definition of the Hellmann-Feynman force, the force for the adiabatic energy surface corresponding to the excited state is

$$\begin{aligned} F_W^1 &= -\langle E_1(R)|\frac{\partial}{\partial R}\left(\frac{1}{2}\omega^2 R^2 - cR\hat{\sigma}_z\right)|E_1(R)\rangle \\ &= -\langle E_1(R)|\omega R|E_1(R)\rangle + \langle E_1(R)|c\hat{\sigma}_z|E_1(R)\rangle\,. \end{aligned} \tag{7.41}$$

Because R is a function and not an operator, and ω and c are constants, they can be taken out of the inner products, which gives

$$\begin{aligned} F_W^1 &= -\omega R\langle E_1(R)|E_1(R)\rangle + c\langle E_1(R)|\hat{\sigma}_z|E_1(R)\rangle \\ &= -\omega R + c\langle E_1(R)|\hat{\sigma}_z|E_1(R)\rangle\,, \end{aligned} \tag{7.42}$$

since $|E_1(R)\rangle$ is normalised and its inner product is therefore unity. The matrix $\hat{\sigma}_z$ naturally cannot be removed from the inner product, as it acts upon the ket:

$$\begin{aligned} F_W^1 &= -\omega R + c\frac{1}{2(1+G^2)}\begin{pmatrix} 1+G \\ -(1-G)\end{pmatrix}\cdot\begin{pmatrix} 1 & 0 \\ 0 & -1\end{pmatrix}\begin{pmatrix} 1+G \\ -(1-G)\end{pmatrix} \\ &= -\omega R + c\frac{1}{2(1+G^2)}\begin{pmatrix} 1+G \\ -(1-G)\end{pmatrix}\cdot\begin{pmatrix} 1+G \\ 1-G\end{pmatrix} \\ &= -\omega R + c\frac{2G}{1+G^2}\,. \end{aligned} \tag{7.43}$$

Now the expression for G can be substituted, to give the Hellmann-Feynman force in terms of Ω and $\gamma(R)$:

$$
\begin{aligned}
F_W^1 &= -\omega R + c\frac{\frac{2}{\gamma}\left[-\Omega + \left(\gamma^2+\Omega^2\right)^{\frac{1}{2}}\right]}{1+\frac{1}{\gamma^2}\left[\Omega^2 - 2\Omega\left(\gamma^2+\Omega^2\right)^{\frac{1}{2}} + \gamma^2 + \Omega^2\right]} \\
&= -\omega R + c\frac{\left[-\Omega + \left(\gamma^2+\Omega^2\right)^{\frac{1}{2}}\right]}{\frac{1}{\gamma}\left[-\Omega\left(\gamma^2+\Omega^2\right)^{\frac{1}{2}} + \gamma^2 + \Omega^2\right]} \\
&= -\omega R + c\frac{\gamma}{\left(\gamma^2+\Omega^2\right)^{\frac{1}{2}}}\,. \qquad (7.44)
\end{aligned}
$$

Similarly, the Hellmann-Feynman force for the adiabatic energy surface corresponding to the ground state is

$$
F_W^2 = -\omega R - c\frac{\gamma}{\left(\gamma^2+\Omega^2\right)^{\frac{1}{2}}}\,. \qquad (7.45)
$$

The first term of F_W^1 and F_W^2 is simply the force for an undriven, undamped oscillator. The second term is the contribution to the force on each oscillator due to the effect of the subsystem.

7.2.3 Rotation Matrices

In order to be able to represent the density matrix or operators in the adiabatic basis, one requires the associated rotation matrix. The rotation matrix is a matrix with a determinant of one, the columns of which are simply the eigenvectors of the adiabatic basis. It is thus given by:

$$
R_{ad} = \frac{1}{\sqrt{2(1+G^2)}}\begin{pmatrix} 1+G & 1-G \\ -(1-G) & 1+G \end{pmatrix}, \qquad (7.46)
$$

and its inverse is:

$$R_{ad}^{-1} = \frac{1}{\sqrt{2(1+G^2)}} \begin{pmatrix} 1+G & -(1-G) \\ 1-G & 1+G \end{pmatrix} . \tag{7.47}$$

The density matrix or arbitrary operator is then rotated into the adiabatic basis according to

$$\chi^{ad} = R_{ad}^{-1} \chi R_{ad} . \tag{7.48}$$

Chapter 8

Numerical Studies

8.1 Simulation Details

8.1.1 Propagation of Trajectories

The trajectories in the simulation are calculated using an Eulerian description, where the phase space point associated with each trajectory is propagated in time, and the observable is updated at each time step by calculating it using the updated phase space point. Due to the hybrid quantum-classical description of the dynamics, there is no single Hilbert space corresponding to the quantum subsystem, but rather, there is a two-dimensional Hilbert space associated with each phase space point. The adiabatic eigenenergies and states are thus also updated at each time step using the new calculated phase space point for the trajectory.

At time zero for each trajectory, the bath and the subsystem are initially decoupled and the interaction begins after this time. The hybrid density matrix is a simple product of the density matrix for the quantum subsystem and the distribution function for the environment:

$$\hat{\rho}(0) = \hat{\rho}_s(0)\rho_b(R,P) \; , \tag{8.1}$$

where the initial density matrix for the subsystem is given by

$$\hat{\rho}_s = \begin{pmatrix} 1 & 0 \\ 0 & 0 \end{pmatrix} , \tag{8.2}$$

and the distribution function for the environment is [71]

$$\rho_{bW}(R,P) = \prod_{j=1}^{N} \frac{\tanh(\beta\omega_j/2)}{\pi} \exp\left[-\frac{2\tanh(\beta\omega_j/2)}{\omega_j} H_b(R,P)\right] . \tag{8.3}$$

This distribution function is obtained by Wigner transforming the Bloch equation for an ensemble of quantum harmonic oscillators. The full derivation is given in Appendix B.

From the density matrix for the subsystem given in Eq. (8.2) it can be seen that the two level quantum subsystem is taken to be initially in the pure energy eigenstate corresponding to the excited state.

As was mentioned before, the initial phase space point for each trajectory is sampled from the bath distribution function using an importance sampling Monte Carlo scheme. The importance sampling function is given by

$$\rho_0 = \exp\left[-\beta\left(P^2/2 + E_\alpha\right)\right] . \tag{8.4}$$

8.1.2 The Observable

Much of the literature for simulations based on the quantum-classical Liouville approach involve calculation of the observable $\langle\hat{\sigma}_z\rangle$ [34][35] [36][37]. For reasons of consistency and ease of comparison with previous work, all the simulations performed for the following studies thus involved the calculation of this observable. In addition, numerically 'exact' results for this observable for the spin-boson system are readily available in the literature, providing a way to determine when an algorithm is performing well, or poorly.

The observable $\langle\sigma_z\rangle$ is also known as the population observable for a two-level system. This can be understood by considering the following:

$$\begin{aligned}
\langle \sigma_z \rangle &= \mathrm{Tr}\ (\rho \sigma_z) \\
&= \mathrm{Tr}\left[\begin{pmatrix} \rho_{11} & \rho_{12} \\ \rho_{21} & \rho_{22} \end{pmatrix} \begin{pmatrix} 1 & 0 \\ 0 & -1 \end{pmatrix} \right] \\
&= \mathrm{Tr} \begin{pmatrix} \rho_{11} & -\rho_{12} \\ \rho_{21} & -\rho_{22} \end{pmatrix} \\
&= \rho_{11} - \rho_{22} \ . \qquad (8.5)
\end{aligned}$$

The observable $\langle \sigma_z \rangle$ is therefore simply the difference between the populations of the two energy levels in the system.

In order for this observable to be calculated using the quantum-classical Liouville approach, the operator $\hat{\sigma}_z$ needs to be represented in the adiabatic basis. This is performed using Eq. (7.48), where the rotation matrix and its inverse are given by Eqs. (7.46) and (7.47) respectively.

Performing this rotation to the operator $\hat{\sigma}_z$ and the density matrix for the subsystem yields

$$\hat{\sigma}_z^{ad} = \frac{1}{1+G^2} \begin{pmatrix} 2G & 1-G^2 \\ 1-G^2 & -2G \end{pmatrix} , \qquad (8.6)$$

and

$$\hat{\rho}_s^{ad} = \frac{1}{2(1+G^2)} \begin{pmatrix} (1+G)^2 & 1-G^2 \\ 1-G^2 & (1-G)^2 \end{pmatrix} . \qquad (8.7)$$

The observable $\langle \sigma_z \rangle$ is then calculated according to:

$$\langle \sigma_z(t) \rangle = \frac{\int dR dP \rho_0(R,P) \left[\rho_0^{-1} \rho_{bW}(R,P) \mathrm{Tr} \left(\hat{\rho}_s^{ad} \hat{\sigma}_z^{ad}(t) \right) \right]}{\int dR dP \rho_{bW}(R,P)} . \qquad (8.8)$$

Each simulation utilised a Monte Carlo sampling size of 10^5. This is the number of phase space trajectories that were propagated in order to calculate the phase space integral in Eq. (8.8). A molecular dynamics time-step of $\tau = 0.1$ was used for all calculations. In order to determine the statistical error of each result, the simulations were run ten times with random seeds for the initial conditions. The results presented are the average of these ten calculations.

8.2 Study of the Trotter Factorisation of the Short-Time Quantum-Classical Propagator

The first study that was performed was a comparison of the two techniques the SSTP and TBQC algorithms use to factorise the short-time quantum-classical propagator. The SSTP algorithm employs the truncated Dyson series, where the J operator appears in linear form, while the TBQC algorithm utilises Trotter factorisation, where the J operator is still in an exponential. It is naturally of interest to determine which method is superior.

The first step was to apply the two algorithms to cases where the adiabatic approximation applies; in other words the J operator is set to zero. In each case, the simulations were run for a wide range of parameters, but shown here for each algorithm are three sets - one set of parameters corresponds to weak coupling, another to intermediate coupling, and the final one to strong coupling.

Figures 8.1, 8.2 and 8.3 display comparisons of the adiabatic results for the SSTP and TBQC algorithms for weak, intermediate and strong coupling respectively. The result shown in Fig. 8.1 was calculated using system parameters $\beta = 0.3$, $\xi = 0.007$, and $\Omega = 1/3$. This set of system parameters corresponds to weak coupling between the quantum subsystem and the bath. Figure 8.2 displays the result for intermediate coupling strength, with system parameters $\beta = 12.5$, $\xi = 0.09$ and $\Omega = 0.4$. The Fig. 8.3 result was simulated using $\beta = 0.25$, $\xi = 2.0$ and $\Omega = 1.2$, which is strong coupling.

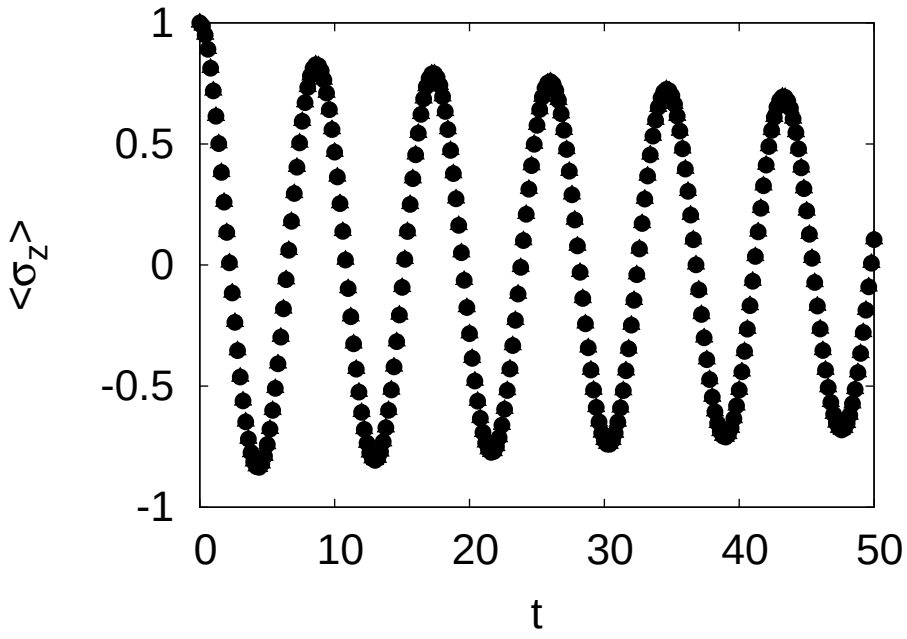

Figure 8.1: Comparison of adiabatic results for the SSTP (•) and TBQC (△) algorithms. This calculation was performed for $\beta = 0.3$, $\xi = 0.007$ and $\Omega = 1/3$, which corresponds to weak coupling. The results of the two simulations are identical, with the points for the TBQC result almost impossible to see, as they are underneath the points of the SSTP result. The error bars for both results are not seen as they are smaller than the points for the entire simulation time.

From Figs. 8.1, 8.2 and 8.3 it can be seen that, for adiabatic results at least, neither the SSTP or TBQC is superior to the other. Both algorithms can reliably simulate adiabatic calculations for long times with negligible statistical error. However, this is not the true test, as the statistical error problems encountered by the SSTP and TBQC algorithms occur when nonadiabatic transitions are included to the calculations as a result of growth of the statistical weights associated with each trajectory.

The next step was to include the nonadiabatic transitions, but in a consistent way. The J operator is implemented using two different techniques in the SSTP and TBQC algorithms, so it would not be possible to gauge which factorisation is superior, (Truncated Dyson or Trotter) simply by comparing the the nonadiabatic results of the SSTP algorithm with those of the TBQC algorithm. The truncated

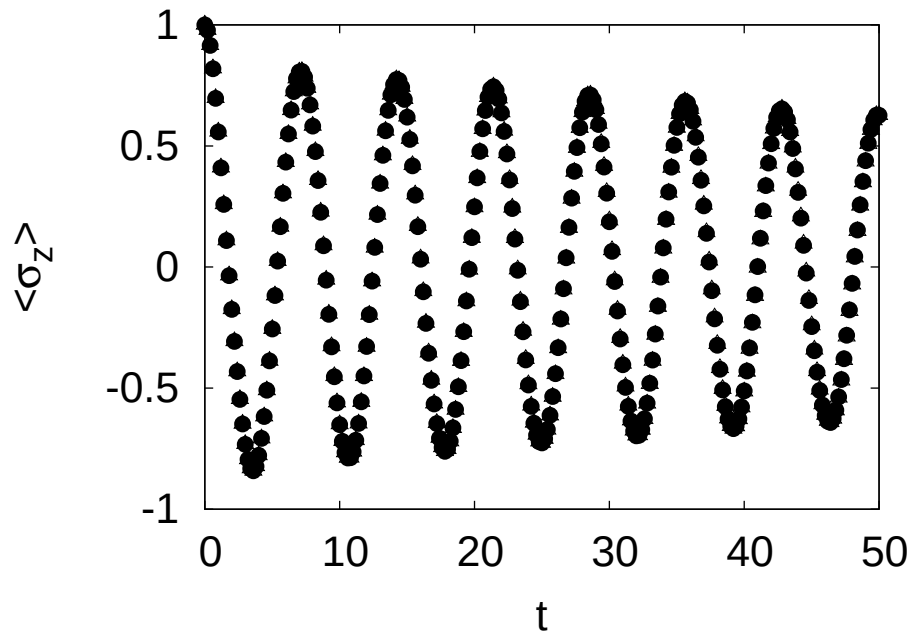

Figure 8.2: Comparison of adiabatic results for the SSTP (•) and TBQC (△) algorithms. This calculation was performed for $\beta = 12.5$, $\xi = 0.09$ and $\Omega = 0.4$, which corresponds to intermediate coupling strength. Again, the results of the two calculations are almost impossible to tell apart, and the error bars are smaller than the points.

Dyson expansion essentially amounts to a linear approximation of the exponentiated form of the J operator, since

$$\begin{aligned} e^{i\mathcal{L}\tau} &= e^{(i\mathcal{L}_0 - J)\tau} \\ &\approx e^{i\mathcal{L}_0\tau} e^{-J\tau} \\ &\approx e^{i\mathcal{L}_0\tau} (1 - J\tau) \, . \end{aligned} \tag{8.9}$$

In order to compare this to the Trotter factorisation, it is of interest to apply the Trotter factorisation to the short-time propagator, but still use the linear approximation for the J operator:

$$\begin{aligned} e^{i\mathcal{L}\tau} &\approx e^{i\mathcal{L}_0\tau/2} e^{-J\tau} e^{i\mathcal{L}_0\tau/2} \\ &\approx e^{i\mathcal{L}_0\tau/2} (1 - J\tau) \, e^{i\mathcal{L}_0\tau/2} \, . \end{aligned} \tag{8.10}$$

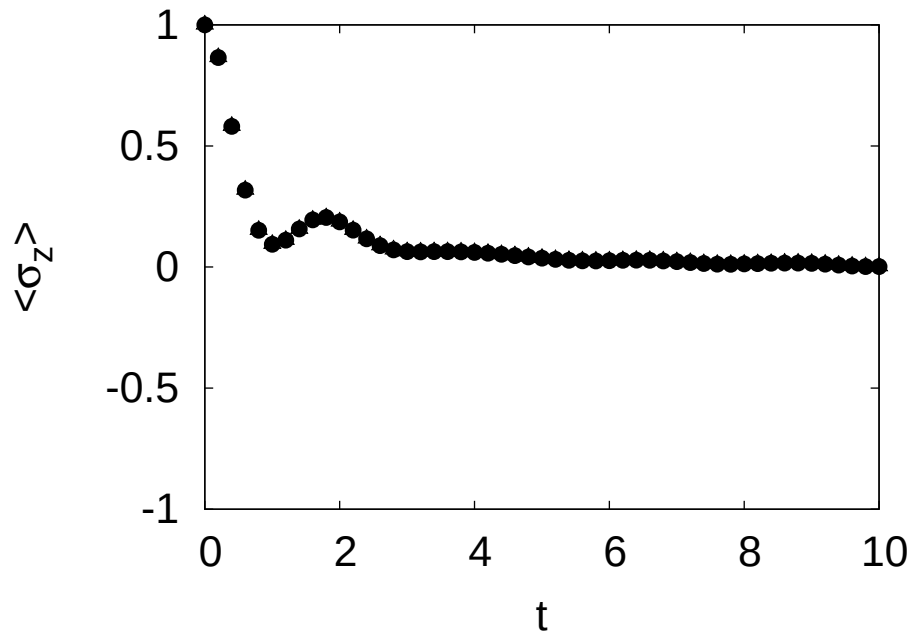

Figure 8.3: Comparison of adiabatic results for the SSTP (•) and TBQC (△) algorithms. This plot displays the results for system parameters $\beta = 0.25$, $\xi = 2.0$ and $\Omega = 1.2$, corresponding to strong coupling. As in the case of weak coupling, the two results are indistinguishable, and the error bars are smaller than the points for the entire simulation time. The result is only shown up to $t = 10$ in this case, as it does not deviate from zero.

In this way, it is possible to use the Trotter factorisation, but treat the J operator in the SSTP way. To distinguish this algorithm from the SSTP and full TBQC algorithms, this shall be named the Trotter-factorised SSTP algorithm. In the calculations of the following results, the only difference in the algorithm was thus the Trotter factorisation, and not the implementation of the J operator.

Figures 8.4 through 8.6 show the results of nonadiabatic calculations for the same sets of parameters used above. Unfortunately it is not possible to show the results for the two algorithms on the same set of axes, as it is difficult to distinguish the error bars of the two results. They are thus shown in separate plots. The results shown in Fig. 8.4 are for weak coupling calculations. Figure 8.5 displays intermediate coupling results, and finally, Fig. 8.6 gives the results for strong coupling.

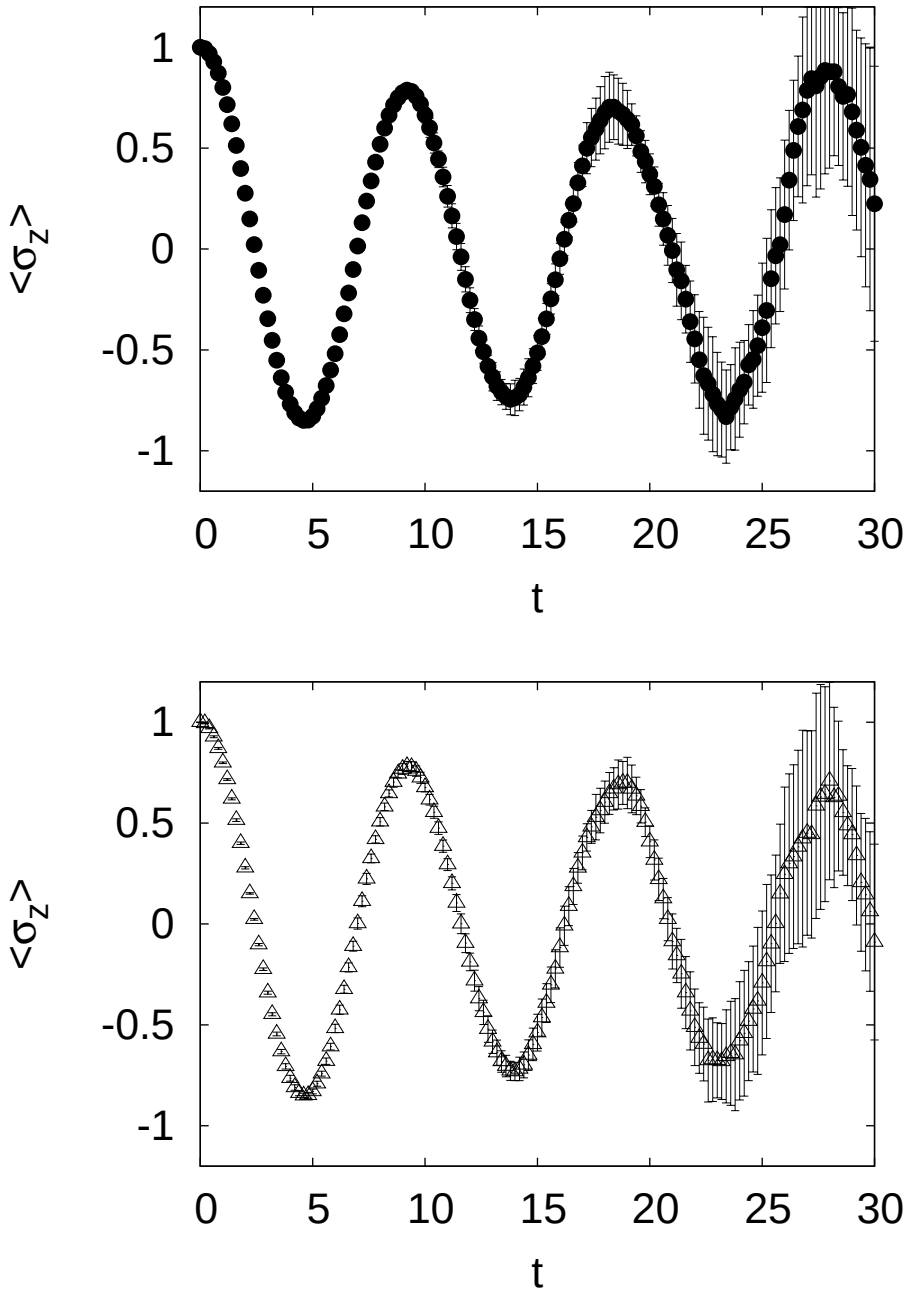

Figure 8.4: Comparison of nonadiabatic results for the SSTP (top) and Trotter-factorised SSTP algorithms (bottom), in the weak coupling regime. System parameters were $\beta = 0.3$, $\xi = 0.007$ *and* $\Omega = 1/3$. *Two nonadiabatic transitions were included for each trajectory. The calculation cannot produce reliable results for as long as in the adiabatic case. After approximately* $t = 22$, *the simulation becomes unstable, and the statistical error becomes large.*

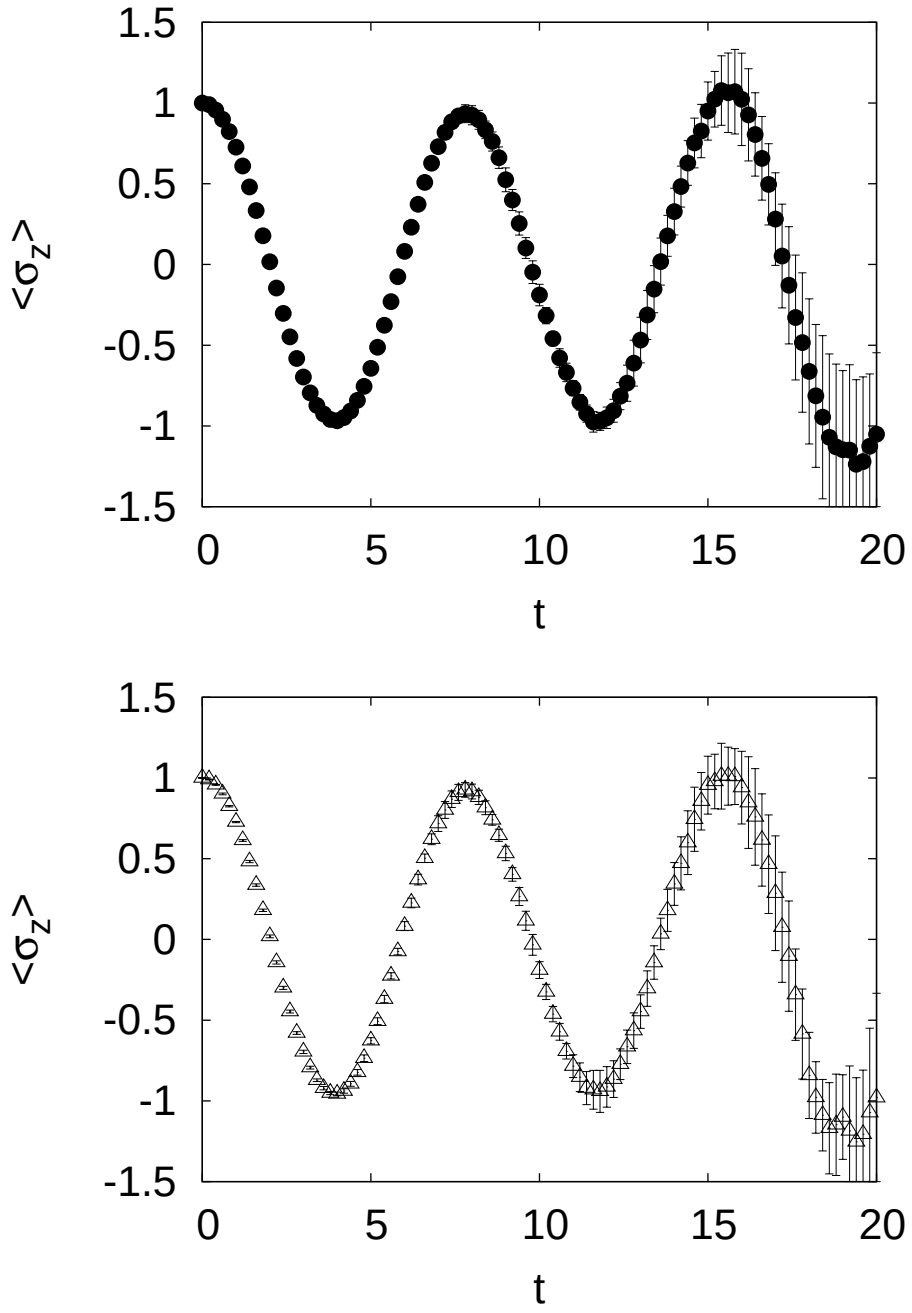

Figure 8.5: Comparison of nonadiabatic results for the SSTP (top) and Trotter-factorised SSTP algorithms (bottom), in the case of intermediate coupling. Parameters used were $\beta = 12.5$, $\xi = 0.09$ *and* $\Omega = 0.4$. *Two nonadiabatic transitions were included per trajectory. The dynamics cannot be simulated reliably for nearly as long as the adiabatic dynamics. After approximately* $t = 15$, *the simulation becomes unstable.*

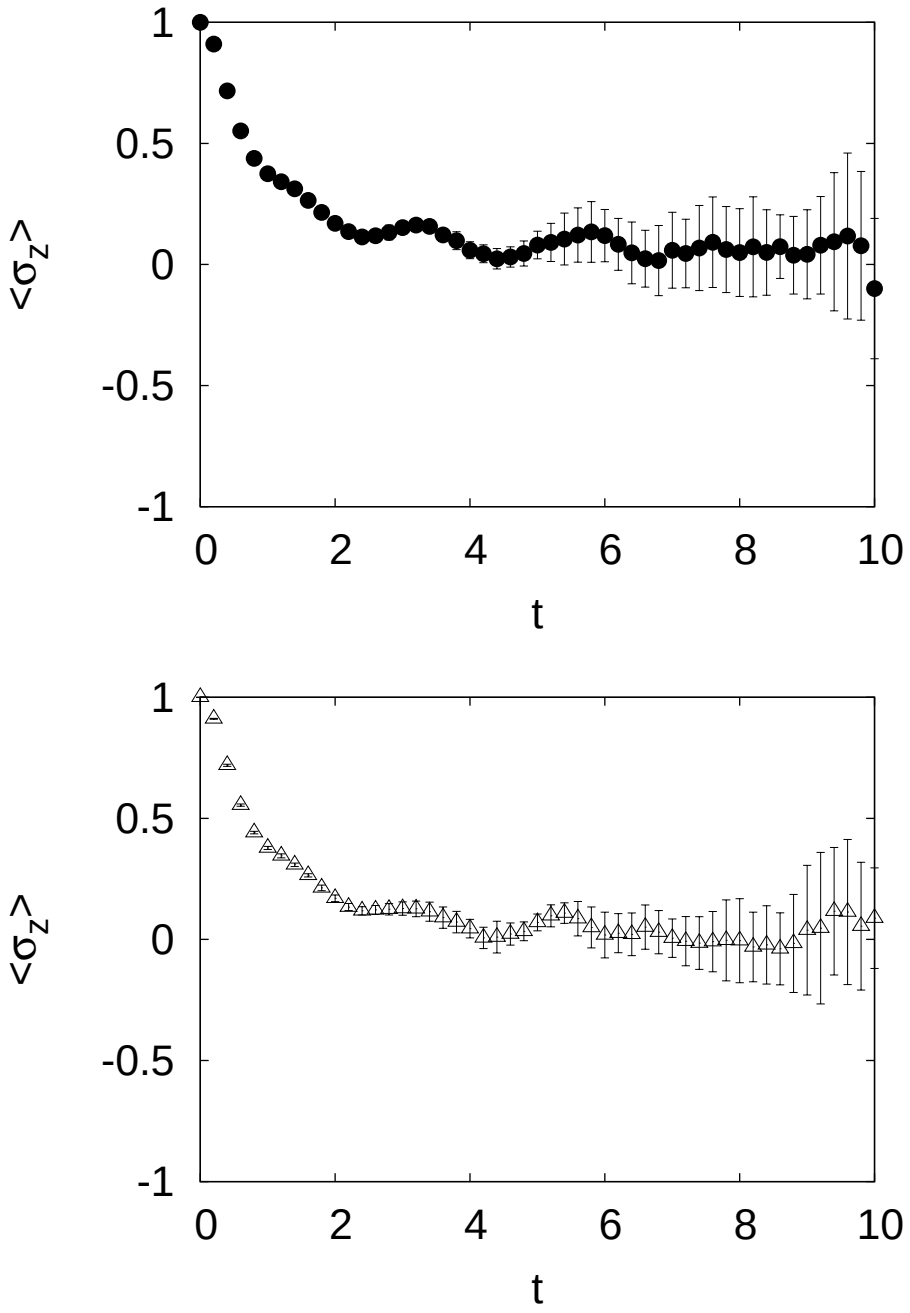

Figure 8.6: Comparison of nonadiabatic results for the SSTP (top) and Trotter-factorised SSTP algorithms (bottom), for strong coupling. System parameters of $\beta = 0.25$, $\xi = 2.0$ and $\Omega = 1.2$ were used. Two nonadiabatic transitions were included for each trajectory. The results are only reliable for very short times, as the statistical error grows quickly when the coupling is strong.

From these results, the effect of the inclusion of nonadiabatic transitions on statistical error is clear. For all three coupling regimes, the results could not be reliably simulated nearly as long as in the adiabatic case. After certain times, the simulation becomes unstable, and the statistical error grows quickly. As mentioned before, this is due to the concatenation of weights associated with the sampling of the transitions. It can be seen that the stronger the coupling strength, the shorter the time the simulation is stable. In the case of weak coupling, the statistical error begins to grow rapidly after approximately $t = 22$, but in the case of strong coupling, the calculation incurs large error before $t = 10$.

With regards to the comparison of the SSTP and Trotter-factorised SSTP algorithms, it is not apparent simply from looking at the results which is superior, as they both begin to fail at similar times for each coupling regime. In order to make a quantitative comparison of the two, it is desirable to compare the values of the statistical error for each algorithm at each time step and take an average. To this end, the following quantity can be defined:

$$\langle \varepsilon \rangle = \frac{1}{N} \sum_i \frac{\sigma_i^S - \sigma_i^T}{\max\left(\sigma_i^S, \sigma_i^T\right)}, \tag{8.11}$$

where σ_i^S and σ_i^T are the standard deviations for the i^{th} time step for the SSTP and Trotter-factorised SSTP algorithms respectively and N is the number of time steps of the simulation. This quantity gives an indication of which algorithm is superior (on average) with regards to statistical error. It has a maximum value of 1 and a minimum value of -1. If it is negative, then the SSTP algorithm is superior, and if it is positive, then the Trotter-factorised algorithm is superior. The values of $\langle \varepsilon \rangle$ for the three sets of calculations are given in Table 8.1.

Weak coupling	Intermediate coupling	Strong coupling
-2.52×10^{-2}	5.13×10^{-2}	1.36×10^{-1}

Table 8.1: Values of $\langle \varepsilon \rangle$ for different coupling strength regimes.

The values given in Table 8.1 indicate that neither algorithm is significantly superior to the other for weak and intermediate coupling strengths. In the case of strong coupling, the Trotter-factorised algorithm does in fact have a noticeable advantage over the plain SSTP algorithm, and thus the Trotter-factorisation of the short-time propagator is superior to the truncated Dyson series.

Note, however, that although the Trotter-factorisation does indeed result in smaller statistical error than the truncated Dyson series, this difference is not great enough that the Trotter-factorisation allows longer simulation times to be accessed reliably (see Figs. 8.4, 8.5, 8.6). Because implementation of the Trotter-factorisation is more computationally expensive than the truncated Dyson series, it is perhaps worth using the Dyson method over the Trotter method, as the benefits of the Trotter are not great enough to warrant the additional computational resources.

8.3 Comparison of the SSTP and TBQC Algorithms

Once this was determined, the next step was to compare results of the SSTP algorithm with those of the full TBQC algorithm, each with their original sampling scheme for the J operator, without using any of the improved techniques presented in Chapter 6.

Again, the simulations were run for a range of system parameters, but the same three sets used above are shown here to give an indication of the efficacy of the algorithms within each coupling strength regime. The comparisons between the two algorithms are given in Figs. 8.7, 8.8 and 8.9. The two results for each case are plotted on the same set of axes, however, only the error bars for the TBQC results are shown in the plots, since inclusion of the SSTP error bars would cause confusion, as the plot would become too cluttered. The error bars for the SSTP results can be seen in Figs. 8.4, 8.5 and 8.6.

In Fig. 8.7 the results for weak coupling are presented. For shorter times, the two algorithms agree very well, with their points almost indistinguishable. After

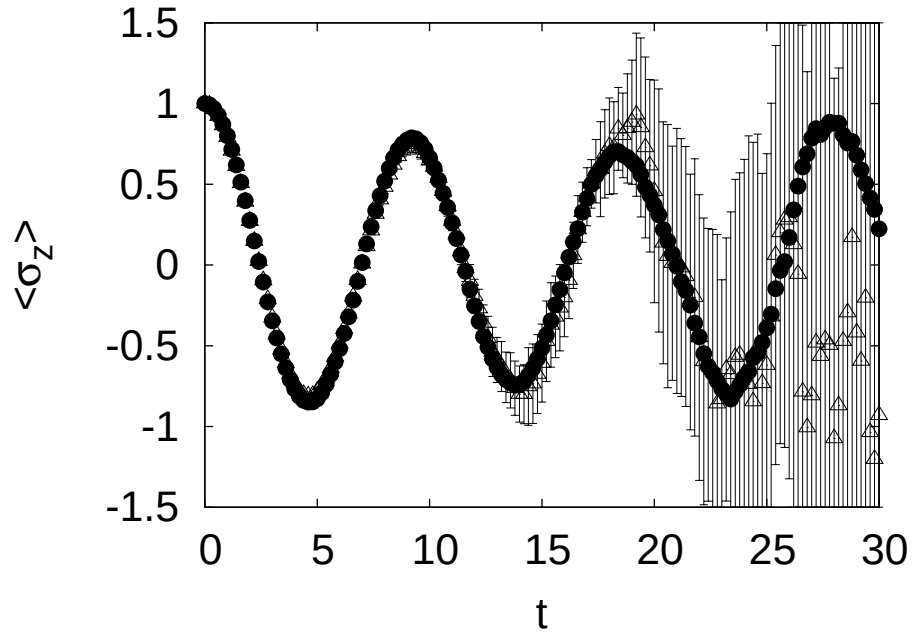

Figure 8.7: Plot illustrating a comparison of results for the SSTP (•) and TBQC (△) algorithms, in the weak coupling regime. System parameters were $\beta = 0.3$, $\xi = 0.007$ and $\Omega = 1/3$. Two nonadiabatic transitions were considered per trajectory. Although the two algorithms agree very well up until approximately $t = 17$, the TBQC result becomes unstable far more rapidly than that of the SSTP algorithm.

approximately $t = 17$, the two results deviate from each other, with increasing statistical error. The statistical error for the TBQC result actually grows faster than that of the SSTP algorithm, as the error is already large before $t = 20$. Figure 8.8, showing the result for intermediate coupling, paints a similar picture. The two results are in good agreement with one another at short times, and differ after $t = 10$. Again, the TBQC result becomes unstable significantly faster than the SSTP result. Finally, Fig. 8.9 compares the two algorithms in the strong coupling regime. This time the results agree up to $t = 5$. After this point, the algorithms deviate as the statistical error grows. As before, the TBQC algorithm is seen to incur larger statistical error than the SSTP.

The TBQC algorithm seems to be inferior to the SSTP algorithm for all three coupling strength regimes, which is surprising, since the Trotter factorisation of

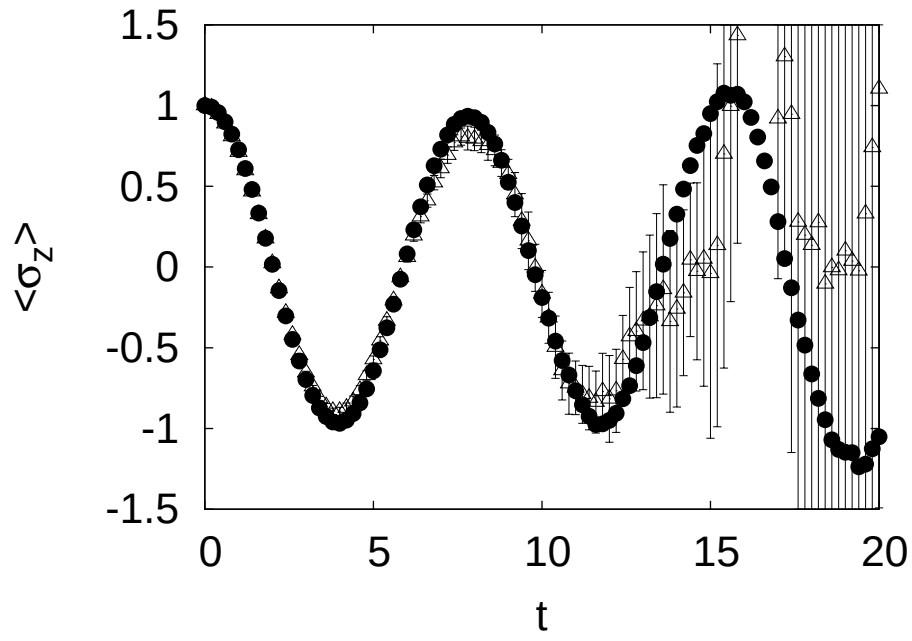

Figure 8.8: Comparison of simulation results for the SSTP (•) and TBQC (△) algorithms, for intermediate coupling strength. The system parameters were $\beta = 12.5$, $\xi = 0.09$ and $\Omega = 0.4$. Two nonadiabatic transitions were included in each trajectory. Again, the two results agree excellently at short times, but after $t = 10$ they diverge. The statistical error for the TBQC algorithm grows faster than that of the SSTP algorithm.

the short-time quantum-classical propagator was shown to perform better than the truncated Dyson series. The only difference between the Trotter-factorised SSTP algorithm shown in Figs. 8.4, 8.5 and 8.6, and the full TBQC algorithm is the implementation of the J operator, and therefore, this must be the source of the error.

This can be understood by considering the weights that enter the observable each time a transition is rejected. For the SSTP algorithm, this weight is

$$\begin{aligned} W_{SSTP}^{NT} &= 1 + \left| \frac{P}{M} \cdot d_{\alpha\beta} \right| \tau \\ &= 1 + a \,, \end{aligned} \tag{8.12}$$

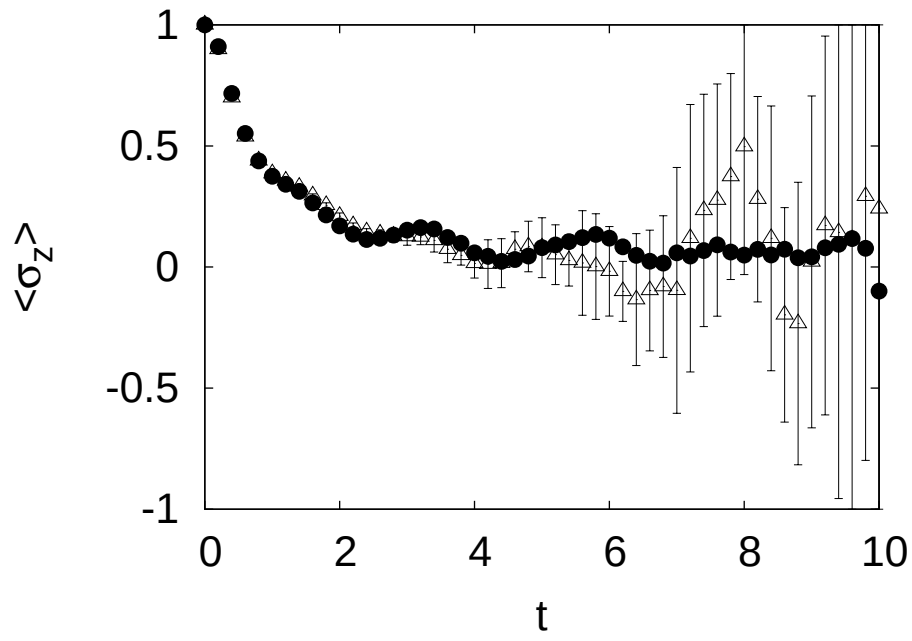

Figure 8.9: Comparison of calculations for the SSTP (•) and TBQC (△) algorithms, in the case of strong coupling. System parameters $\beta = 0.25$, $\xi = 2.0$ and $\Omega = 1.2$ were used. Two nonadiabatic transitions were considered per trajectory. The results agree strongly up until approximately $t = 5$, after which they diverge. As in the case of weak and intermediate coupling, the TBQC result has larger statistical error than the SSTP.

and for the TBQC algorithm it is

$$W_{TBQC}^{NT} = 1 + 2|\cos a \sin a| \,. \tag{8.13}$$

In cases of weak coupling, $a << 1$, and the $\cos a \sin a$ term is approximately given by a. The weight that enters the observable in the TBQC algorithm when a transition is rejected is then given by

$$W_{TBQC}^{NT} = 1 + 2a \,. \tag{8.14}$$

The observable is thus multiplied by a larger weight at each time step in the TBQC

algorithm than the SSTP algorithm, leading to greater statistical error. In fact, even in the case of the strong coupling parameters being used in the presented calculations, when $\cos a \sin a \approx a$ no longer holds, the weight for the TBQC algorithm is still larger than the SSTP. This is what causes the original SSTP algorithm to perform better than the TBQC algorithm in the results shown above.

It must be noted at this point, however, that it is still possible to achieve good results with the TBQC algorithm, when implemented with the observable cutting scheme [35]. Nevertheless, for the sake of consistency, the study presented in the next section on the three improved sampling schemes outlined in Chapter 6 was performed using only the SSTP algorithm.

8.4 Study of Improved Transition Sampling Schemes

Both improved sampling schemes, observable cutting and transition filtering have been shown to dramatically reduce statistical error in the quantum-classical Liouville approach [34][35] [36][37]. It would be of interest, however, to compare the efficacy of each technique, as well as test the newly introduced combination filtering scheme, in order to determine if any of the three are universally superior to the other two.

To this end, calculations were run, again for a range of system parameters, utilising the SSTP algorithm in conjunction with each of the three improved sampling schemes. Because it is possible that an improved scheme might reduce statistical error at the cost of result integrity, all the results were compared with known numerically exact results. The superior scheme is thus one that can eliminate the most statistical error, while still being able to agree with the numerically exact results.

Figures 8.10 and 8.11 give the results for weak coupling, with system parameters $\beta = 0.3$, $\xi = 0.007$ and $\Omega = 1/3$. From Fig. 8.10, it can be seen that both the observable cutting and transition filtering scheme produce results that agree well with the influence functional path integral calculations [70][72][73], however, at longer times

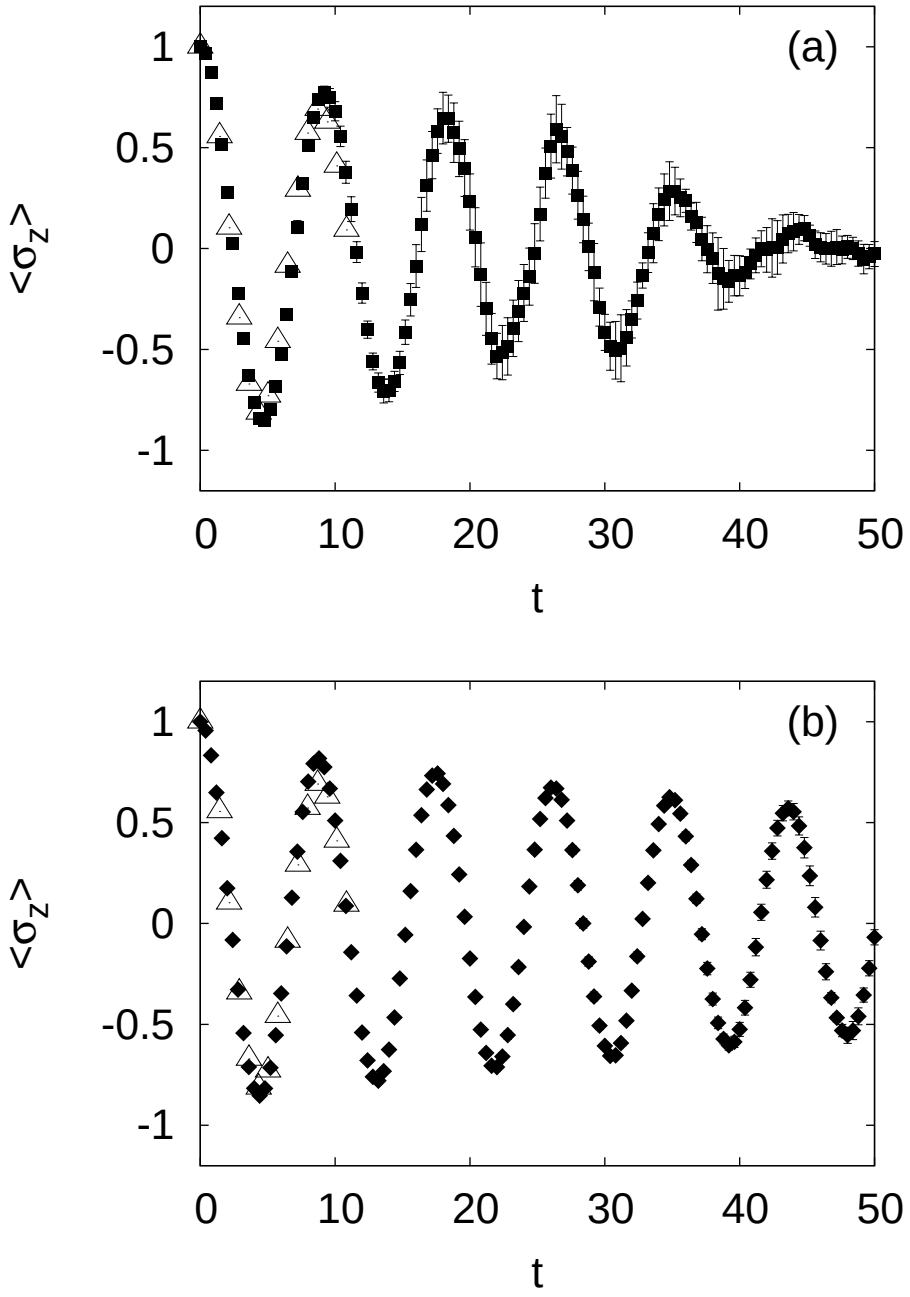

Figure 8.10: Comparison of results using the SSTP algorithm with the observable cutting (a, top) and transition filtering (b, bottom) schemes. The open triangles denote the path integral quantum results from Refs. [70][72][73]. System parameters were $\beta = 0.3$, $\xi = 0.007$ *and* $\Omega = 1/3$ *and two nonadiabatic transitions were included for each trajectory. Both techniques agree very well with the numerically exact results and are able to reduce statistical error effectively, but the error does begin to grow at later times.*

($t \approx 30$), the two results deviate from each other. In both cases, the statistical error is greatly reduced when compared with the result using the original SSTP sampling scheme, but there is still a slight growth of error at longer times. Figure 8.11 displays the weak coupling result for the combined filtering scheme. As in the case of the other two improved sampling techniques, there is excellent agreement with the influence functional results, but this time, the error bars remain smaller than the points for the entire simulation time.

In fact, the combined filtering scheme proves so effective at reducing the statistical error, the simulation remains stable for significantly longer times than previously published results [34][36][37].

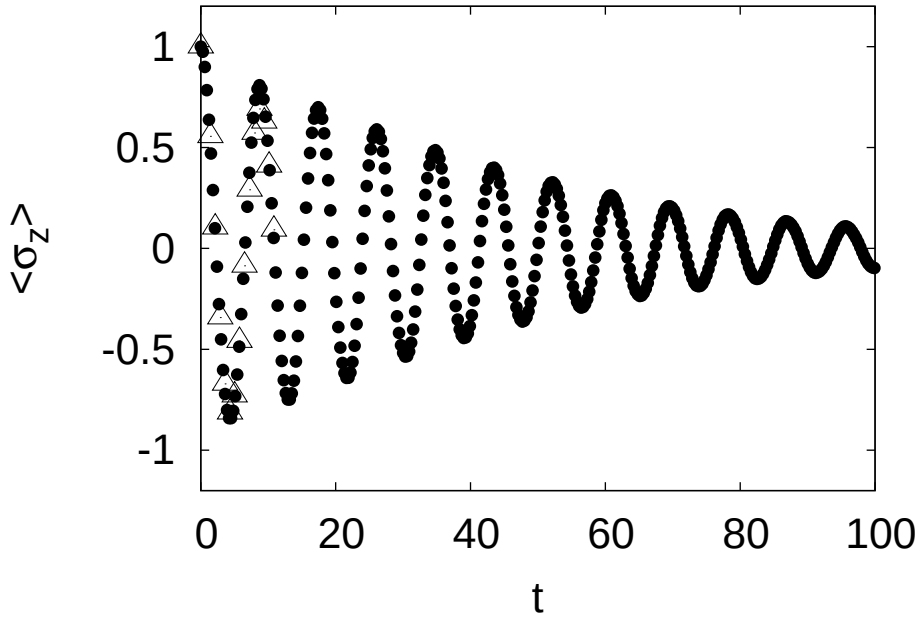

Figure 8.11: Comparison of result using the SSTP algorithm with the combined filtering scheme (•) with the path integral quantum results (open triangles) from Refs. [70][72] [73]. The system parameters were $\beta = 0.3$, $\xi = 0.007$ and $\Omega = 1/3$. Two nonadiabatic transitions were considered per trajectory. The combined filtering scheme produces results which are stable far longer than the observable cutting and transition filtering techniques.

Figures 8.12 and 8.13 show the results for intermediate coupling strength. System parameters were $\beta = 12.5$, $\xi = 0.09$ and $\Omega = 0.4$. In Fig 8.12, the observable

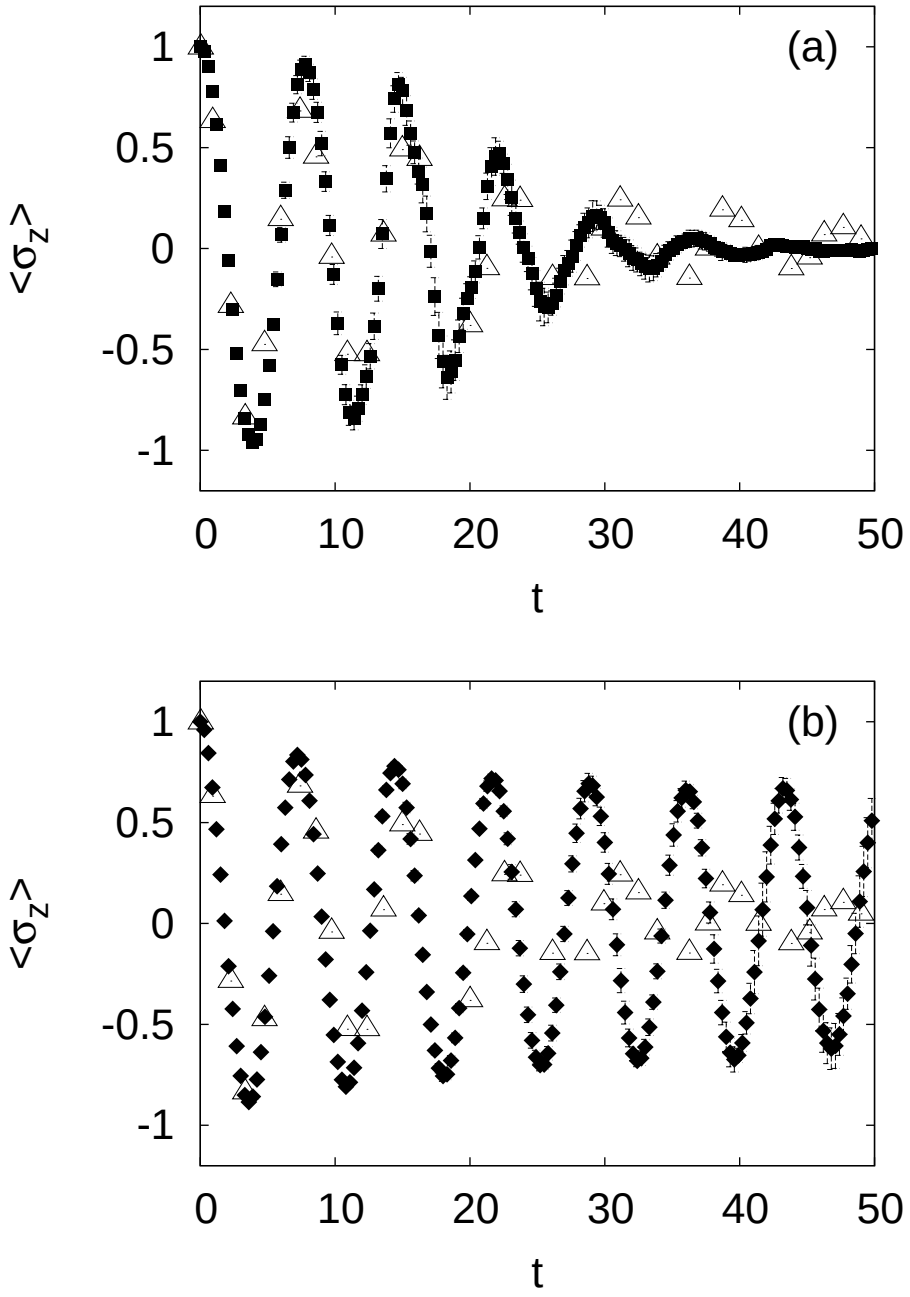

Figure 8.12: Comparison of results using the SSTP algorithm with the observable cutting (a, top) and transition filtering (b, bottom) schemes with the path integral result (open triangle) from Ref. [74]. The system parameters were $\beta = 12.5$, $\xi = 0.09$ and $\Omega = 0.4$, corresponding to intermediate coupling strength. Two nonadiabatic transitions were considered in each trajectory. Both calculations agree well with the path integral result at short times, but then deviate at longer times.

cutting and transition filtering schemes are compared with the path integral quantum result from Ref. [74]. They both agree very well with the path integral result at short times ($t < 20$), but after this time, the results deviate somewhat. In the case of the transition filtering scheme, the damping in the path integral result is not reproduced; the oscillations remain large. For the observable cutting scheme, however, the opposite is seen. The observable cutting technique damps the result too much at longer times, causing it to become zero. In Fig. 8.13, the result for the combined filtering scheme is presented. A dramatic improvement over the other two schemes can be seen, as the combined filtering result does not exhibit either of the problems encountered by the observable cutting and transition filtering techniques.

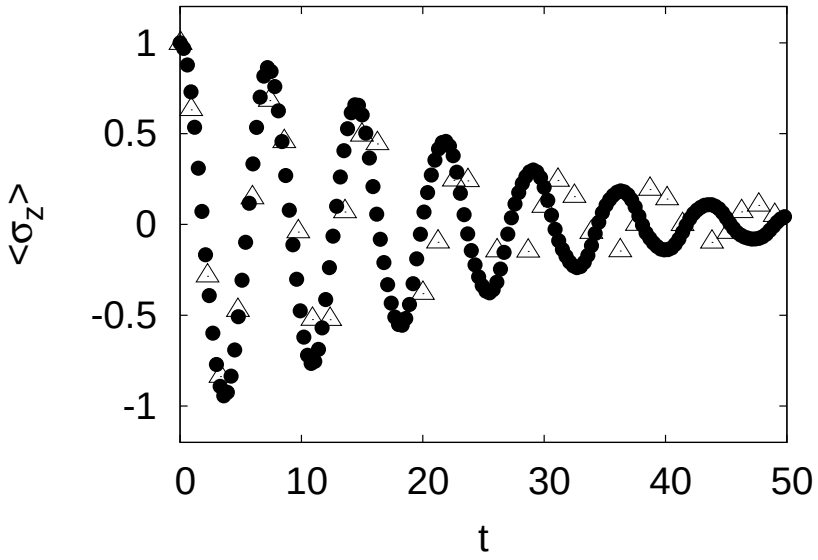

Figure 8.13: Comparison of result using the SSTP algorithm with the combined filtering scheme (•) with the path integral quantum result (open triangles) from Ref. [74]. The system parameters were $\beta = 12.5$, $\xi = 0.09$ and $\Omega = 0.4$. Two nonadiabatic transitions were included in each trajectory. The combined filtering scheme produces results which agree far better with the path integral quantum result, and is stable far longer than the observable cutting and transition filtering techniques.

The combined filtering scheme agrees far better with the path integral quantum result at longer times, and the error bars are smaller than the points for the entire simulation time.

In Figs. 8.14 and 8.15, the results for strong coupling are shown, with system parameters $\beta = 0.25$, $\xi = 2.0$ and $\Omega = 1.2$. Figure 8.14 illustrates that the observable cutting and transition filtering schemes are incapable of reproducing the quantum results of Ref. [75] even at short times. Although the two techniques are successful at reducing statistical error, it can be seen that the error bars become larger than the points at approximately $t = 2$. In Fig. 8.15, the result obtained using the combination filtering scheme for strong coupling is shown. Again, the improvement over the other two schemes is significant. In the main figure, the calculation is shown to agree excellently with the path integral result, while the inset illustrates that the simulation can be extended to long times with negligible statistical error.

The combination filtering scheme is thus not only more successful at reducing statistical error than either of the individual schemes, but agrees better with the numerically exact results as well. This is because the observable cutting scheme and transition filtering technique approach the problem of growing statistical error in different ways. The observable cutting directly cuts the weight in the calculation of the observable when it grows too large, while the transition filtering scheme disallows nonadiabatic transitions that would cause momentum changes in the environment that are too large. The combination filtering method benefits from both these improvements, thus outperforming either of the individual schemes. This results in a far more stable algorithm.

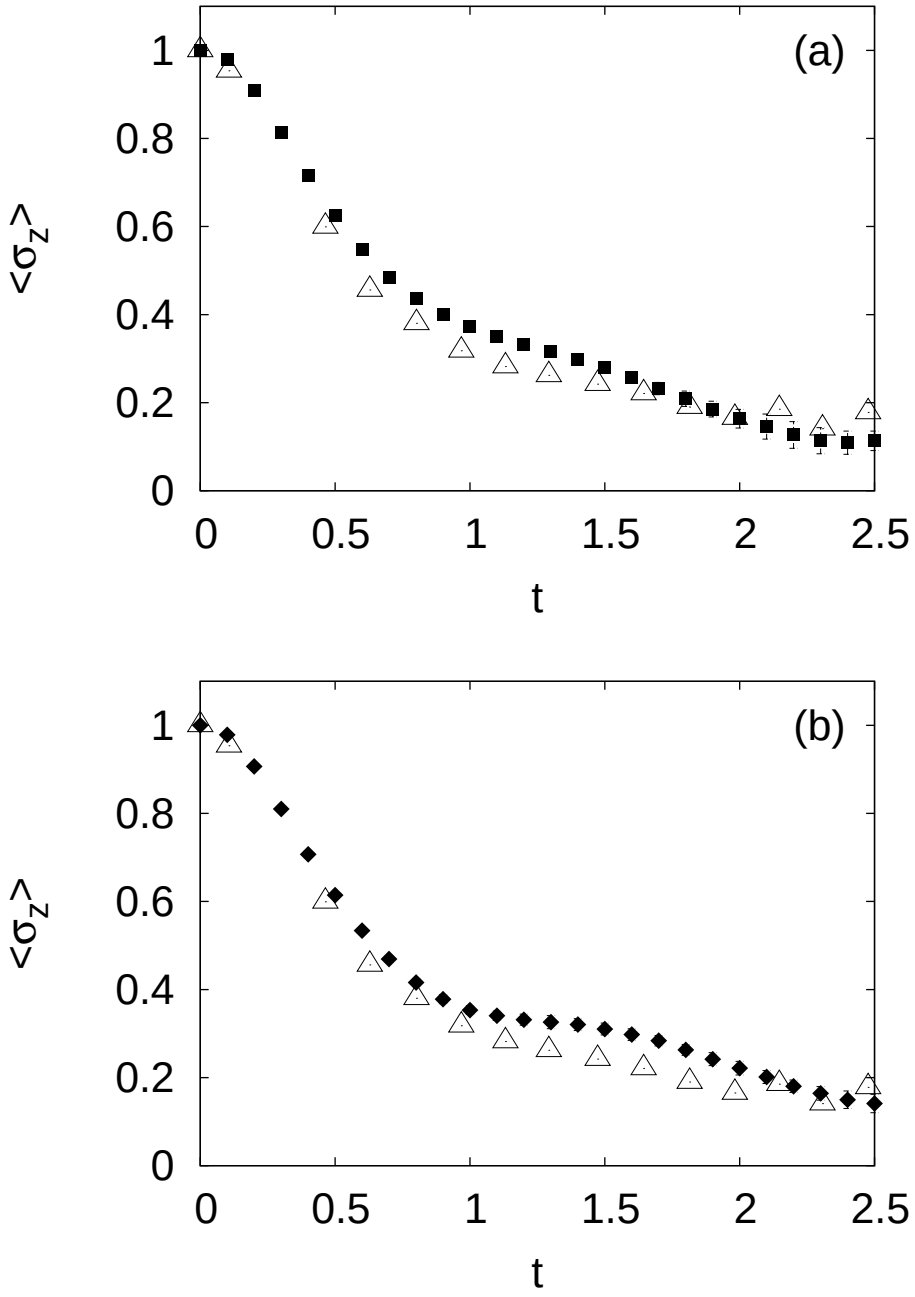

Figure 8.14: Comparison of results using the SSTP algorithm with the observable cutting (a, top) and transition filtering (b, bottom) schemes with the path integral result (open triangle) from Ref. [75]. The system parameters were $\beta = 0.25$, $\xi = 2.0$ and $\Omega = 1.2$, corresponding to the regime of strong coupling. Two nonadiabatic transitions were considered in each trajectory. Despite being able to reduce the statistical error, both sampling schemes are unable to reproduce the path integral result even at short times.

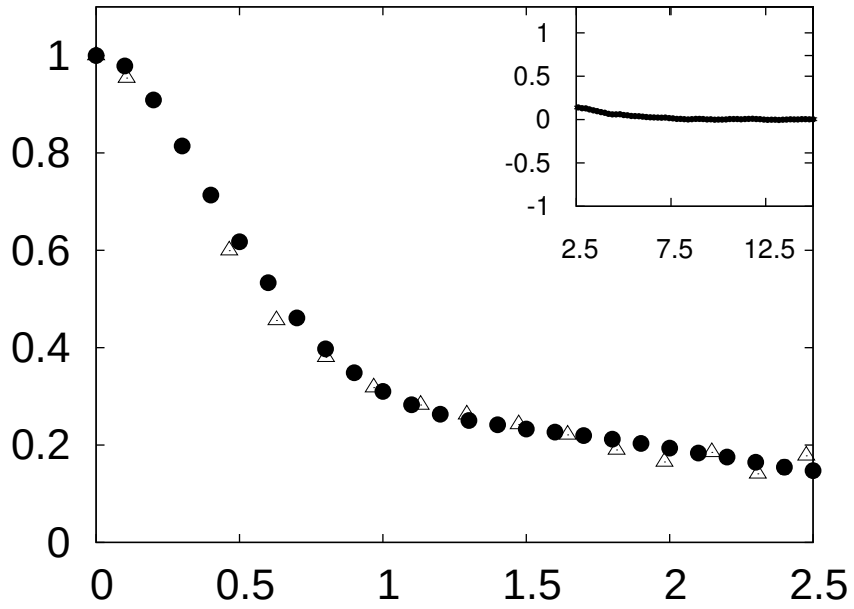

Figure 8.15: Comparison of result using the SSTP algorithm with the combined filtering scheme (•) with the path integral quantum result (open triangles) from Ref. [75]. The system parameters were $\beta = 0.25$, $\xi = 2.0$ and $\Omega = 1.2$. Two nonadiabatic transitions were included in each trajectory. Unlike the observable cutting and transition filtering schemes, the combined filtering scheme produces results which agree excellently with the path integral quantum result, while still being stable at long simulation times.

Chapter 9

Conclusions and Perspectives

The biggest problem encountered in the simulation of quantum systems is the inability to numerically calculate the dynamics of many-body interacting systems. Generally, brute force methods are impossible to perform, as the requirement on computational resources is many orders of magnitude greater than what is currently available today. Because of this, the only solution is to resort to intelligent approximations that reduce the system being studied in some way, thus making numerical calculations more feasible.

The quantum-classical approximation does just that, by partitioning the system into a quantum subsystem and a classical environment. The environment can then be simulated using well-known Monte Carlo and molecular dynamics methods, while still maintaining the quantum nature of the subsystem of interest. Naturally, due to the majority of the degrees of freedom being treated in a classical way, this greatly reduces the computational requirements for simulations.

Even within this approximation, calculations are difficult to perform when nonadiabatic effects are taken into account. This type of dynamics occurs when energy is exchanged quickly between the subsystem and environmental degrees of freedom. Many processes, such as charge transfer and photochemical reactions are inherently nonadiabatic, and thus algorithms are required that can reliably simulate this type of dynamics. More recently, there has been much interest in nonadiabatic dynamics

in biological systems, specifically in the coherent energy transfer in photosynthesis. These types of systems possibly lend themselves to a quantum-classical description, since one can think of quantum charge carriers interacting with large scale protein environments which can be treated classically.

In this thesis, two of the main quantum-classical techniques were reviewed - specifically the Ehrenfest mean-field method and surface-hopping approach by Tully. While the Ehrenfest method has its strengths, it fails to describe dynamics when the potential energy surfaces are too dissimilar. The surface-hopping approach does not have this problem, but, in general, surface-hopping schemes fail to properly describe the quantum backreaction of the subsystem on the environment.

A more recent formalism, based on the quantum-classical Liouville equation resolves this, by providing a rigorous description of the backreaction. It involves a realisation of the statistical mechanics in terms of the density matrix, not the wavefunction, and thus the ability to describe mixed states is naturally part of the formulation. This formalism was studied in detail, in addition to the Weyl transforms and partial Wigner representation required to obtain the quantum-classical Liouville equation.

Representing the quantum-classical Liouville equation in the adiabatic basis leads to a form where the terms responsible for adiabatic evolution and nonadiabatic transitions naturally separate. This separation lends itself to the development of surface-hopping algorithms. There have been two surface-hopping algorithms devised that are based on the quantum-classical Liouville equation, the sequential short-time propagation algorithm, and the Trotter based quantum-classical algorithm, which were derived and discussed in the thesis.

Both of these algorithms encounter the problem of large statistical error at long times due to the implementation of their stochastic sampling schemes for nonadiabatic transitions. This statistical error results in longer simulation times becoming inaccessible. The original sampling schemes were outlined in the thesis, and the improved sampling schemes based on observable cutting and transition filtering were

discussed. In addition to this, a new sampling scheme based on the combination of the two improved schemes was introduced.

Numerical calculations presented as part of this thesis were performed using the spin-boson model. This system is a very well studied model and can be used to study the dynamics of a generic quantum-classical system. In this thesis, the spin-boson model was outlined, and the adiabatic energies and states were derived.

The numerical studies presented comprise two primary parts. The first study was a comparison of the SSTP and TBQC algorithms. The two algorithms differ in two ways, although both are based on a segmentation of the quantum-classical propagator into many short-time propagators. The first difference is that the SSTP algorithm utilises a truncated Dyson expansion for the short-time quantum-classical propagator, while the TBQC algorithm approximates the short-time propagator using a Trotter factorisation. The second difference is in the implementation of the transition operator J.

In order to compare the effectiveness of the different factorisations of the short-time propagator, calculations were performed comparing the SSTP algorithm with an algorithm that uses the Trotter factorisation of the propagator with the SSTP implementation of the J operator. Calculations were performed for a range of system parameters, corresponding to different coupling strength regimes between the subsystem and environment. It was found that in the case of adiabatic dynamics, where $J = 0$, the two algorithms produced results that were indistinguishable. Indeed, both were able to simulate dynamics up to long times with negligible statistical error. The comparison was then extended to nonadiabatic dynamics, and it was found that overall, the Trotter factorisation performed slightly better than the truncated Dyson method. The improvement is not easily noticeable, however, and the increase in computational resources (and thus run-time) required by the Trotter factorisation is most likely not worth the small improvement.

Having found this, the SSTP algorithm was then compared to the full TBQC algorithm, including the TBQC implementation of the J operator. In each case,

no improved sampling schemes were used. Results were presented for nonadiabatic calculations, and it was illustrated that in fact, the TBQC algorithm performs more poorly than the SSTP algorithm. This was shown to be due to the weight that enters the calculation of the observable at each time step. The numerical weight for each time step is bigger for the TBQC algorithm than the SSTP algorithm, and this results in a faster growth of the statistical error.

The second study performed was a comparison of improved sampling schemes. The previous methods based on observable cutting and transition filtering have been shown to significantly improve the performance of the SSTP and TBQC algorithms by reducing the statistical error at long times. The newly devised combination filtering scheme attempts to improve upon these techniques by combining the advantages of each.

Nonadiabatic calculations were performed using each of the improved sampling techniques for the SSTP algorithm, and compared to path integral results found in the literature. The results demonstrated a clear superiority of the combined filtering technique over the observable cutting and transition filtering methods. In the case of weak coupling, all three sampling schemes were able to reproduce the path integral result. Although the observable cutting and transition filtering methods were able to reduce statistical error, the error still began to grow at longer simulation times. The combination filtering scheme, however, was able to produce results for over twice as long as the other two schemes with error bars remaining smaller than the points used in the plot of the result. For intermediate coupling strength, the transition filtering and observable cutting methods only agreed with the quantum path integral result for short simulation times. At longer simulation times, both results deviated - the observable cutting result became too damped, and went to zero, while the transition filtering result was too undamped. The combined filtering scheme did not demonstrate either of these issues, and was able to follow the path integral result very well. Finally, for strong coupling between the subsystem and the bath, the observable cutting and transition filtering techniques were not able to

reproduce the quantum path integral result even at short simulation times, although they did reduce the statistical error. Again, the combined filtering scheme was shown to be superior - it agreed excellently with the path integral result, while negligible statistical error is observed even at long simulation times.

The combined filtering technique thus proves itself as a valuable tool for improving the effectiveness of the surface-hopping algorithms within the quantum-classical Liouville approach, in the case of nonadiabatic dynamics. It allows far longer simulation times to be accessed reliably than have previously been published, and thus allows for study of more complicated systems, at longer times.

One of the current issues with the quantum-classical Liouville equation approach is that the theory for explicitly time-dependent Hamiltonians is not well formulated. The inclusion of explicit time-dependence proves to be a challenge, as the quantum-classical Liouville operator becomes time-dependent as well, complicating the theory, as well as making it far more difficult to devise algorithms. In future work, it is hoped that the approach based on the quantum-classical Liouville equation can be extended to systems with explicitly time-dependent Hamiltonians, and algorithms developed to simulate the dynamics of such systems. The ability to simulate nonadiabatic dynamics of systems with time-dependent Hamiltonians is of great interest to areas of research such as quantum control, where the dynamics of quantum systems are influenced by external fields. Naturally, the new sampling technique outlined in this thesis will aid in making such simulations a possibility.

Appendix A

Representation of the Quantum-Classical Liouville Equation in the Adiabatic Basis

In this appendix, the full derivation is presented for rotating the quantum-classical Liouville equation into the adiabatic basis.

The first step is to take the matrix elements of both sides of Eq. (4.9):

$$\begin{aligned}\langle\alpha|\frac{\partial\rho_W}{\partial t}|\alpha'\rangle &= -\frac{i}{\hbar}\langle\alpha|\left[\hat{H}_W,\hat{\rho}_W\right]|\alpha'\rangle + \frac{1}{2}\langle\alpha|\{\hat{H}_W,\hat{\rho}_W\}|\alpha'\rangle \\ &- \frac{1}{2}\langle\alpha|\{\hat{\rho}_W,\hat{H}_W\}|\alpha'\rangle\ , \end{aligned} \tag{A.1}$$

For sake of clarity, it is easier to deal with each term individually. Expanding the first term on the right hand side of Eq. (A.1) gives

$$\langle\alpha|\left[\hat{H}_W,\hat{\rho}_W\right]|\alpha'\rangle = -\frac{i}{\hbar}\left[\langle\alpha|\hat{H}_W\hat{\rho}_W|\alpha'\rangle - \langle\alpha|\hat{\rho}_W\hat{H}_W|\alpha'\rangle\right]\ . \tag{A.2}$$

Now using the fact that $\hat{H}_W = P^2/2M + \hat{h}_W$, and $\hat{h}_W|\alpha\rangle = E_\alpha|\alpha\rangle$, this becomes

$$\frac{i}{\hbar}\left[\langle\alpha|\hat{H}_W\hat{\rho}_W|\alpha'\rangle - \langle\alpha|\hat{\rho}_W\hat{H}_W|\alpha'\rangle\right] = -\frac{i}{\hbar}\left[E_\alpha\langle\alpha|\hat{\rho}_W|\alpha'\rangle - E_{\alpha'}\langle\alpha|\hat{\rho}_W|\alpha'\rangle\right] = -i\omega_{\alpha\alpha'}\rho_W^{\alpha\alpha'}\ , \tag{A.3}$$

where $\langle\alpha|\hat{\rho}_W|\alpha'\rangle = \rho_W^{\alpha\alpha'}$. The second term of Eq. (A.1) can now be expanded as well:

$$\langle\alpha|\{\hat{H}_W,\hat{\rho}_W\}|\alpha'\rangle = \langle\alpha|\frac{\partial\hat{H}_W}{\partial R}\frac{\partial\hat{\rho}_W}{\partial P}|\alpha'\rangle - \langle\alpha|\frac{\partial\hat{H}_W}{\partial P}\frac{\partial\hat{\rho}_W}{\partial R}|\alpha'\rangle\ . \tag{A.4}$$

Using the completeness relation, this becomes

$$\begin{aligned}\langle\alpha|\{\hat{H}_W,\hat{\rho}_W\}|\alpha'\rangle &= \langle\alpha|\frac{\partial\hat{H}_W}{\partial R}\sum_\beta|\beta\rangle\langle\beta|\frac{\partial\hat{\rho}_W}{\partial P}|\alpha'\rangle \\ &- \langle\alpha|\frac{\partial\hat{H}_W}{\partial P}\sum_\beta|\beta\rangle\langle\beta|\frac{\partial\hat{\rho}_W}{\partial R}|\alpha'\rangle \\ &= -\sum_\beta F_W^{\alpha\beta}\frac{\partial\rho_W^{\beta\alpha'}}{\partial P} - \sum_\beta\frac{P}{M}\delta_{\alpha\beta}\langle\beta|\frac{\partial\hat{\rho}_W}{\partial R}|\alpha'\rangle\ ,\end{aligned} \tag{A.5}$$

where the fact that $\langle\alpha|\beta\rangle = \delta_{\alpha\beta}$ has been used, as well as $\partial\hat{H}_W/\partial R = \partial\hat{V}_W/\partial R$ and $\partial\hat{H}_W/\partial P = P/M$. The Hellmann-Feynman matrix elements in the partial Wigner representation are given by

$$F_W^{\alpha\beta} = -\langle\alpha|\frac{\partial\hat{V}_W}{\partial R}|\beta\rangle\ . \tag{A.6}$$

The third term in Eq. (A.1) can be similarly expanded to yield

$$\langle\alpha|\{\hat{\rho}_W,\hat{H}_W\}|\alpha'\rangle = \sum_\beta\langle\alpha|\frac{\partial\hat{\rho}_W}{\partial R}|\beta\rangle\frac{P}{M}\delta_{\alpha'\beta} + \sum_\beta\frac{\partial\rho_W^{\alpha\beta}}{\partial P}F_W^{\beta\alpha'}\ . \tag{A.7}$$

Adding equations (A.3), (A.5) and (A.7) gives

$$\begin{aligned}
\frac{\partial \rho_W^{\alpha\alpha'}}{\partial t} &= -i\omega_{\alpha\alpha'}\rho_W^{\alpha\alpha'} - \frac{1}{2}\sum_\beta \left(F_W^{\alpha\beta}\frac{\partial \rho_W^{\beta\alpha'}}{\partial P} + \frac{\partial \rho_W^{\alpha\beta}}{\partial P}F_W^{\beta\alpha'} \right) \\
&- \frac{1}{2}\sum_\beta \left(\frac{P}{M}\langle\alpha|\frac{\partial \hat{\rho}_W}{\partial R}|\beta\rangle\delta_{\alpha\beta} + \frac{P}{M}\langle\beta|\frac{\partial \hat{\rho}_W}{\partial R}|\alpha'\rangle \right) \\
&= -i\omega_{\alpha\alpha'}\rho_W^{\alpha\alpha'} - \frac{1}{2}\sum_\beta \left(F_W^{\alpha\beta}\frac{\partial \rho_W^{\beta\alpha'}}{\partial P} + \frac{\partial \rho_W^{\alpha\beta}}{\partial P}F_W^{\beta\alpha'} \right) \\
&- \frac{P}{M}\langle\alpha|\frac{\partial \hat{\rho}_W}{\partial R}|\alpha'\rangle \, . \qquad \text{(A.8)}
\end{aligned}$$

The term on the last line of the above equation can not be written simply as $\frac{P}{M}\frac{\partial \rho_W^{\alpha\alpha'}}{\partial R}$, since the adiabatic basis states are dependent on the bath position coordinate R. Consider therefore

$$\begin{aligned}
\frac{\partial}{\partial R}\langle\alpha|\hat{\rho}_W|\alpha'\rangle &= \langle\frac{\partial \alpha}{\partial R}|\hat{\rho}_W|\alpha'\rangle + \langle\alpha|\frac{\partial \hat{\rho}_W}{\partial R}|\alpha'\rangle + \langle\alpha|\hat{\rho}_W|\frac{\partial \alpha'}{\partial R}\rangle \\
&= \langle\frac{\partial \alpha}{\partial R}|\sum_\beta |\beta\rangle\langle\beta|\hat{\rho}_W|\alpha'\rangle + \langle\alpha|\frac{\partial \hat{\rho}_W}{\partial R}|\alpha'\rangle \\
&+ \langle\alpha|\hat{\rho}_W\sum_\beta |\beta\rangle\langle\beta|\frac{\partial \alpha'}{\partial R}\rangle \\
&= \langle\alpha|\frac{\partial \hat{\rho}_W}{\partial R}|\alpha'\rangle + \sum_\beta \left(\langle\frac{\partial \alpha}{\partial R}|\beta\rangle\rho_W^{\beta\alpha'} + \rho_W^{\alpha\beta}\langle\beta|\frac{\partial \alpha'}{\partial R}\rangle \right) \, , \\
& \qquad \text{(A.9)}
\end{aligned}$$

where the completeness relation has again been used. By definition, $\langle\beta|\frac{\partial \alpha'}{\partial R}\rangle = \langle\beta|\frac{\partial}{\partial R}|\alpha'\rangle = d_{\beta\alpha'}$, but to simplify the term $\langle\frac{\partial \alpha}{\partial R}|\beta\rangle$, one must consider that

$$\frac{\partial}{\partial R}\langle\alpha|\beta\rangle = 0 \, , \qquad \text{(A.10)}$$

since $\langle\alpha|\beta\rangle = \delta_{\alpha\beta}$. But

$$\frac{\partial}{\partial R}\langle\alpha|\beta\rangle = \langle\frac{\partial \alpha}{\partial R}|\beta\rangle + \langle\alpha|\frac{\partial \beta}{\partial R}\rangle \, . \qquad \text{(A.11)}$$

This yields the following identity:

$$\begin{aligned}\langle\frac{\partial\alpha}{\partial R}|\beta\rangle &= -\langle\alpha|\frac{\partial\beta}{\partial R}\rangle \\ &= -d_{\alpha\beta}\ . \end{aligned} \tag{A.12}$$

Using this identity for Eq. (A.9), and rearranging to make $\langle\alpha|\frac{\partial\hat{\rho}_W}{\partial R}|\alpha'\rangle$ the subject of the formula now gives

$$\langle\alpha|\frac{\partial\hat{\rho}_W}{\partial R}|\alpha'\rangle = \frac{\partial\rho_W^{\alpha\alpha'}}{\partial R} - \sum_\beta\left(\rho_W^{\alpha\beta}d_{\beta\alpha'} - d_{\alpha\beta}\rho_W^{\beta\alpha'}\right)\ . \tag{A.13}$$

Substituting this expression for $\langle\alpha|\frac{\partial\hat{\rho}_W}{\partial R}|\alpha'\rangle$ back into Eq. (A.8), one arrives at the following equation for the time derivative of the density matrix elements -

$$\begin{aligned}\frac{\partial\rho_W^{\alpha\alpha'}(R,P,t)}{\partial t} &= -i\omega_{\alpha\alpha'}\rho_W^{\alpha\alpha'} - \frac{1}{2}\sum_\beta\left(F_W^{\alpha\beta}\frac{\partial\rho_W^{\beta\alpha'}}{\partial P} + \frac{\partial\rho_W^{\alpha\beta}}{\partial P}F_W^{\beta\alpha'}\right) \\ &- \frac{P}{M}\frac{\partial\rho_W^{\alpha\alpha'}}{\partial R} + \frac{P}{M}\sum_\beta\left(\rho_W^{\alpha\beta}d_{\beta\alpha'} - d_{\alpha\beta}\rho_W^{\beta\alpha'}\right) \\ &= \sum_{\beta\beta'}\Big[-i\omega_{\alpha\alpha'}\delta_{\alpha\beta}\delta_{\alpha'\beta} - \frac{1}{2}\left(F_W^{\alpha\beta}\delta_{\alpha'\beta'}\cdot\frac{\partial}{\partial P} + F_W^{\beta'\alpha'}\delta_{\alpha\beta}\cdot\frac{\partial}{\partial P}\right) \\ &- \frac{P}{M}\cdot\frac{\partial}{\partial R}\delta_{\alpha\beta}\delta_{\alpha'\beta'} + \frac{P}{M}\cdot\left(d_{\beta'\alpha'}\delta_{\alpha\beta} - d_{\alpha\beta}\delta_{\alpha'\beta'}\right)\Big]\rho_W^{\beta\beta'}(R,P,t) \\ &= \sum_{\beta\beta'} -i\mathcal{L}_{\alpha\alpha',\beta\beta'}\rho_W^{\beta\beta'}(R,P,t)\ . \end{aligned} \tag{A.14}$$

In the last line of the above equation, the quantum-classical Liouville operator has been defined. Now to cast it in the form given in Eq. (4.18). To do this, one first defines the classical-like Liouville operator [31]:

$$iL_{\alpha\alpha'} = \frac{P}{M}\cdot\frac{\partial}{\partial R} + \frac{1}{2}\left(F_W^{\alpha} + F_W^{\alpha'}\right)\cdot\frac{\partial}{\partial P}\ , \tag{A.15}$$

which describes the classical evolution of the bath coordinates, and is given in terms

of the Hellmann-Feynman forces for the adiabatic states α and α' [58]. The quantum-classical Liouville operator can now be written in the form

$$\begin{aligned} -i\mathcal{L}_{\alpha\alpha',\beta\beta'} &= -(i\omega_{\alpha\alpha'} + iL_{\alpha\alpha'})\delta_{\alpha\beta}\delta_{\alpha'\beta'} + \left[\frac{P}{M}\cdot(d_{\beta'\alpha'}\delta_{\alpha\beta} - d_{\alpha\beta}\delta_{\alpha'\beta'})\right. \\ &- \left.\frac{1}{2}\left(F_W^{\alpha\beta}\delta_{\alpha'\beta'} + F_W^{\beta'\alpha'}\delta_{\alpha\beta} - (F_W^{\alpha} + F_W^{\alpha'})\delta_{\alpha\beta}\delta_{\alpha'\beta'}\right)\cdot\frac{\partial}{\partial P}\right] . \end{aligned} \tag{A.16}$$

The terms in the square brackets now constitute the operator $J_{\alpha\alpha',\beta\beta'}$. The next step is to to obtain from these terms, the form for the J operator given by Eq. (4.21). To do this, all the terms with a $\delta_{\alpha'\beta'}$ coefficient are grouped together, and all the terms with a $\delta_{\alpha\beta}$ coefficient are grouped together, to give

$$\begin{aligned} J_{\alpha\alpha',\beta\beta'} &= \left[-\frac{P}{M}\cdot d_{\alpha\beta} - \frac{1}{2}\left(F_W^{\alpha\beta} - F_W^{\alpha}\delta_{\alpha\beta}\right)\cdot\frac{\partial}{\partial P}\right]\delta_{\alpha'\beta'} \\ &+ \left[\frac{P}{M}\cdot d_{\beta'\alpha'} - \frac{1}{2}\left(F_W^{\beta'\alpha'} - F_W^{\alpha'}\delta_{\alpha'\beta'}\right)\cdot\frac{\partial}{\partial P}\right]\delta_{\alpha\beta} . \end{aligned} \tag{A.17}$$

Now consider the derivative with respect to the bath position coordinate R, of the matrix elements of the Hamiltonian -

$$\begin{aligned} -\frac{\partial}{\partial R}\langle\alpha|\hat{H}_W|\beta\rangle &= -\langle\frac{\partial\alpha}{\partial R}|\hat{H}_W|\beta\rangle - \langle\alpha|\frac{\partial\hat{H}_W}{\partial R}|\beta\rangle - \langle\alpha|\hat{H}_W|\frac{\partial\beta}{\partial R}\rangle \\ &= -\langle\frac{\partial\alpha}{\partial R}|\left(\frac{P^2}{2M} + \hat{h}_W\right)|\beta\rangle - \langle\alpha|\left(\frac{\partial}{\partial R}\left(\frac{P^2}{2M} + \hat{h}_W\right)\right)|\beta\rangle \\ &- \langle\alpha|\left(\frac{P^2}{2M} + \hat{h}_W\right)|\frac{\partial\beta}{\partial R}\rangle \\ &= \langle\alpha|\frac{\partial}{\partial R}\hat{h}_W|\beta\rangle - \langle\alpha|\left(\frac{\partial\hat{h}_W}{\partial R}\right)|\beta\rangle - \langle\alpha|\hat{h}_W\frac{\partial}{\partial R}|\beta\rangle , \end{aligned} \tag{A.18}$$

where the fact that the bath momentum commutes with the adiabatic states (which only depend on R) and $d_{\alpha\beta} = -d_{\beta\alpha}$ has been used. Using $\langle\alpha|\hat{h}_W = E_\alpha$, $\hat{h}_W|\beta\rangle = E_\beta$, and $-\langle\alpha|\left(\frac{\partial\hat{h}_W}{\partial R}\right)|\beta\rangle = F_W^{\alpha\beta}$, the above equation becomes

$$\begin{aligned} -\frac{\partial}{\partial R}\langle\alpha|\hat{H}_W|\beta\rangle &= E_\beta\langle\alpha|\frac{\partial}{\partial R}|\beta\rangle + F_W^{\alpha\beta} - E_\alpha\langle\alpha|\frac{\partial}{\partial R}|\beta\rangle \\ &= F_W^{\alpha\beta} - (E_\alpha - E_\beta)\, d_{\alpha\beta} \; . \end{aligned} \tag{A.19}$$

But

$$\begin{aligned} -\frac{\partial}{\partial R}\langle\alpha|\hat{H}_W|\beta\rangle &= -\frac{\partial}{\partial R}\left[\langle\alpha|\frac{P^2}{2M}|\beta\rangle + \langle\alpha|\hat{h}_W|\beta\rangle\right] \\ &= -\frac{\partial}{\partial R}E_\beta\delta_{\alpha\beta} \\ &= F_W^{\beta}\delta_{\alpha\beta} = F_W^{\alpha}\delta_{\alpha\beta} \; . \end{aligned} \tag{A.20}$$

Substituting this expression for $-\frac{\partial}{\partial R}\langle\alpha|\hat{H}_W|\beta\rangle$ back into Eq. (A.19) yields the identity

$$F_W^{\alpha\beta} - F_W^{\alpha}\delta_{\alpha\beta} = (E_\alpha - E_\beta)d_{\alpha\beta} \; . \tag{A.21}$$

Upon use of this identity, Eq (A.17) becomes

$$\begin{aligned} J_{\alpha\alpha',\beta\beta'} &= \left[-\frac{P}{M}\cdot d_{\alpha\beta} - \frac{1}{2}\,(E_\alpha - E_\beta)\, d_{\alpha\beta}\cdot\frac{\partial}{\partial P}\right]\delta_{\alpha'\beta'} \\ &+ \left[\frac{P}{M}\cdot d_{\beta'\alpha'} + \frac{1}{2}\,(E_\alpha - E_{\beta'})\, d_{\beta'\alpha'}\cdot\frac{\partial}{\partial P}\right]\delta_{\alpha\beta} \; . \end{aligned} \tag{A.22}$$

Note that $d_{\beta'\alpha'} = -d^*_{\alpha'\beta'}$, since the matrix for the nonadiabatic coupling vector is anti-hermitian. Making this substitution for $d_{\beta'\alpha'}$, and taking out common factors of $-\frac{P}{M}\cdot d_{\alpha\beta}$ and $-\frac{P}{M}\cdot d^*_{\alpha'\beta'}$ from the first and second pair of square brackets respectively,

gives

$$
\begin{aligned}
J_{\alpha\alpha',\beta\beta'} = \; & - \quad \frac{P}{M} \cdot d_{\alpha\beta} \left(1 + \frac{1}{2} \frac{\Delta E_{\alpha\beta} d_{\alpha\beta}}{\frac{P}{M} \cdot d_{\alpha\beta}} \frac{\partial}{\partial P} \right) \delta_{\alpha'\beta'} \\
& - \quad \frac{P}{M} \cdot d^*_{\alpha'\beta'} \left(1 + \frac{1}{2} \frac{\Delta E_{\alpha\beta} d^*_{\alpha'\beta}}{\frac{P}{M} \cdot d^*_{\alpha'\beta'}} \cdot \frac{\partial}{\partial P} \right) \delta_{\alpha\beta} \; , \qquad \text{(A.23)}
\end{aligned}
$$

which is the form for the J operator defined by Eq. (4.21).

Appendix B

Derivation of the Phase Space Distribution Function

In this appendix, the full derivation for the distribution function of a canonical ensemble of quantum harmonic oscillators [71] is performed. It is this distribution function that is used to sampled the initial conditions for the harmonic bath in the spin-boson system simulations.

First consider the canonical ensemble. The density matrix is given by

$$\hat{\rho} = \frac{1}{Z(\beta)} e^{-\beta \hat{H}} \equiv \frac{1}{Z(\beta)} \hat{\Omega} \,, \tag{B.1}$$

where $\beta = 1/kT$, k is the Boltzmann constant, and $Z(\beta)$ is the canonical partition function $Z(\beta) = \mathrm{Tr}\left(e^{-\beta \hat{H}}\right)$. The right hand of Eq. (B.1) defines the unnormalised density matrix $\hat{\Omega}$. If the initial condition $\hat{\Omega}\left(\beta = 0\right) = \hat{I}$ is satisfied, where $\hat{I}$ is the identity matrix, the unnormalised density matrix then satisfies the Bloch equation -

$$\frac{\partial \hat{\Omega}}{\partial \beta} = -\hat{H}\hat{\Omega} = -\hat{\Omega}\hat{H} \,. \tag{B.2}$$

Applying the Wigner transform, and using the identity given in Eq. (3.17), this equation becomes -

$$\begin{aligned}\frac{\partial \Omega_W(q,p)}{\partial \beta} &= -H_W(q,p)e^{\frac{\hbar\Lambda}{2i}}\Omega_W(q,p) \\ &= -\Omega_W(q,p)e^{\frac{\hbar\Lambda}{2i}}H_W(q,p)\ , \end{aligned} \tag{B.3}$$

where Λ is the negative of the Poisson bracket and (q,p) are phase space coordinates. Using Eq. (B.3), in conjunction with Eq. (3.17), yields

$$H_W(q,p)e^{\frac{\hbar\Lambda}{2i}}\Omega_W(q,p) = H_W(q,p)e^{-\frac{\hbar\Lambda}{2i}}\Omega_W(q,p)\ . \tag{B.4}$$

The Wigner transformed Bloch equation can thus be rewritten as

$$\frac{\partial \Omega_W(q,p)}{\partial \beta} = \frac{1}{2}\left[-H_W(q,p)e^{\frac{\hbar\Lambda}{2i}}\Omega_W(q,p) - H_W(q,p)e^{-\frac{\hbar\Lambda}{2i}}\Omega_W(q,p)\right]\ . \tag{B.5}$$

The complex exponentials above can be expanded using the Euler formula, giving

$$\begin{aligned}\frac{\partial \Omega_W(q,p)}{\partial \beta} &= \frac{1}{2}\left[-H_W\left(\cos\left(\frac{\hbar\Lambda}{2}\right) - i\sin\left(\frac{\hbar\Lambda}{2}\right)\right)\Omega_W\right. \\ &- \left. H_W\left(\cos\left(\frac{\hbar\Lambda}{2}\right) + i\sin\left(\frac{\hbar\Lambda}{2}\right)\right)\Omega_W\right] \\ &= -H_W(q,p)\cos\left(\frac{\hbar\Lambda}{2}\right)\Omega_W(q,p)\ . \end{aligned} \tag{B.6}$$

Equation (B.6) applies for a general Hamiltonian, but consider now the Wigner-transformed Hamiltonian for an ensemble of harmonic oscillators:

$$H_W = \frac{p^2}{2m} + \frac{1}{2}m\omega^2 q^2\ . \tag{B.7}$$

where a multidimensional notation $(q,p) = (q_1, q_2, ..., p_1, p_2, ...)$ is being used. Sub-

stitution of this Hamiltonian into the Wigner transformed Bloch equations gives

$$\frac{\partial \Omega_W}{\partial \beta} = -\left(\frac{p^2}{2m} + \frac{1}{2}m\omega^2 q^2\right) \cos\left(\frac{\hbar}{2}\left[\frac{\overleftarrow{\partial}}{\partial q}\frac{\overrightarrow{\partial}}{\partial p} - \frac{\overleftarrow{\partial}}{\partial p}\frac{\overrightarrow{\partial}}{\partial q}\right]\right) \Omega_W \ . \tag{B.8}$$

The next step is to approximate the cosine term using a series expansion to second order in $\hbar$:

$$\cos\left(\frac{\hbar}{2}\left(\frac{\overleftarrow{\partial}}{\partial q}\frac{\overrightarrow{\partial}}{\partial p} - \frac{\overleftarrow{\partial}}{\partial p}\frac{\overrightarrow{\partial}}{\partial q}\right)\right) \approx 1 - \frac{1}{2}\left(\frac{\hbar}{2}\right)^2 \left(\frac{\overleftarrow{\partial}}{\partial q}\frac{\overrightarrow{\partial}}{\partial p} - \frac{\overleftarrow{\partial}}{\partial p}\frac{\overrightarrow{\partial}}{\partial q}\right)^2 \ . \tag{B.9}$$

Expanding the square of the derivative terms in the round brackets gives

$$\begin{aligned}
\left(\frac{\overleftarrow{\partial}}{\partial q}\frac{\overrightarrow{\partial}}{\partial p} - \frac{\overleftarrow{\partial}}{\partial p}\frac{\overrightarrow{\partial}}{\partial q}\right)^2 &= \frac{\overleftarrow{\partial}}{\partial q}\frac{\overrightarrow{\partial}}{\partial p}\frac{\overleftarrow{\partial}}{\partial q}\frac{\overrightarrow{\partial}}{\partial p} - \frac{\overleftarrow{\partial}}{\partial q}\frac{\overrightarrow{\partial}}{\partial p}\frac{\overleftarrow{\partial}}{\partial p}\frac{\overrightarrow{\partial}}{\partial q} \\
&- \frac{\overleftarrow{\partial}}{\partial p}\frac{\overrightarrow{\partial}}{\partial q}\frac{\overleftarrow{\partial}}{\partial q}\frac{\overrightarrow{\partial}}{\partial p} + \frac{\overleftarrow{\partial}}{\partial p}\frac{\overrightarrow{\partial}}{\partial q}\frac{\overleftarrow{\partial}}{\partial p}\frac{\overrightarrow{\partial}}{\partial q} \\
&= \frac{\overleftarrow{\partial^2}}{\partial q^2}\frac{\overrightarrow{\partial^2}}{\partial p^2} - \frac{\overleftarrow{\partial^2}}{\partial q \partial p}\frac{\overrightarrow{\partial^2}}{\partial q \partial p} - \frac{\overleftarrow{\partial^2}}{\partial p \partial q}\frac{\overrightarrow{\partial^2}}{\partial q \partial p} \\
&+ \frac{\overleftarrow{\partial^2}}{\partial p^2}\frac{\overrightarrow{\partial^2}}{\partial q^2} \\
&= \frac{\overleftarrow{\partial^2}}{\partial q^2}\frac{\overrightarrow{\partial^2}}{\partial p^2} - 2\,\frac{\overleftarrow{\partial^2}}{\partial q \partial p}\frac{\overrightarrow{\partial^2}}{\partial q \partial p} + \frac{\overleftarrow{\partial^2}}{\partial p^2}\frac{\overrightarrow{\partial^2}}{\partial q^2} \ .
\end{aligned} \tag{B.10}$$

Subsequent substitution of this second order expression for the cosine term into Eq. (B.8) yields

$$\begin{aligned}
\frac{\partial \Omega_W}{\partial \beta} &= -\frac{p^2}{2m}\left[1 - \frac{\hbar^2}{8}\left(\frac{\overleftarrow{\partial^2}}{\partial q^2}\frac{\overrightarrow{\partial^2}}{\partial p^2} - 2\,\frac{\overleftarrow{\partial^2}}{\partial q \partial p}\frac{\overrightarrow{\partial^2}}{\partial q \partial p} + \frac{\overleftarrow{\partial^2}}{\partial p^2}\frac{\overrightarrow{\partial^2}}{\partial q^2}\right)\right] \Omega_W \\
&- \frac{m\omega^2 q^2}{2}\left[1 - \frac{\hbar^2}{8}\left(\frac{\overleftarrow{\partial^2}}{\partial q^2}\frac{\overrightarrow{\partial^2}}{\partial p^2} - 2\,\frac{\overleftarrow{\partial^2}}{\partial q \partial p}\frac{\overrightarrow{\partial^2}}{\partial q \partial p} + \frac{\overleftarrow{\partial^2}}{\partial p^2}\frac{\overrightarrow{\partial^2}}{\partial q^2}\right)\right] \Omega_W
\end{aligned}$$

$$= -\left(\frac{p^2}{2m} - \frac{1}{2}m\omega^2 q^2\right)\Omega_W + \frac{\hbar^2}{8m}\frac{\partial^2\Omega_W}{\partial q^2} + \frac{\hbar^2}{8}m\omega^2\frac{\partial^2\Omega_W}{\partial p^2} \ . \tag{B.11}$$

This is the Wigner transformed Bloch equation for the harmonic oscillator. Note that because the harmonic Hamiltonian only contains terms that are second order in q and p, the Wigner transformed Bloch equation using the second order approximation for the cosine term (Eq. (B.11) is exact. The higher order terms of the cosine expansion only contain derivatives of order higher than two, which when acted upon the Hamiltonian give zero.

However, despite the approximation made for the cosine term, Eq. (B.11) is still difficult to solve in its current form. To resolve this, an ansatz can be made for the form of Ω_W:

$$\Omega_W(q,p) = e^{-A(\beta)H_W(q,p)+B(\beta)} \ , \tag{B.12}$$

where the functions A and B are subject to initial conditions $A(0) = B(0) = 0$. To obtain the unnormalised density matrix, the functions $A(\beta)$ and $B(\beta)$ thus need to be determined. To this end, the derivatives of Ω_W with respect to the spatial coordinate are calculated:

$$\frac{\partial\Omega_W}{\partial q} = \Omega_W\left(-A\frac{\partial H_W}{\partial q}\right) \ ,$$

$$\begin{aligned} \Rightarrow \frac{\partial^2\Omega_W}{\partial q^2} &= \frac{\partial\Omega_W}{\partial q}\left(-A\frac{\partial H_W}{\partial q}\right) - A\Omega_W\frac{\partial^2 H_W}{\partial q^2} \\ &= \left(-A\frac{\partial H_W}{\partial q}\right)^2\Omega_W - A\Omega_W\frac{\partial^2 H_W}{\partial q^2} \\ &= \left(A^2m^2\omega^4q^2 - Am\omega^2\right)\Omega_W \ , \end{aligned} \tag{B.13}$$

as well as the derivatives with respect to the momentum coordinate:

$$\frac{\partial \Omega_W}{\partial p} = -A\frac{\partial H_W}{\partial p}\Omega_W \ ,$$

$$\begin{aligned}
\Rightarrow \frac{\partial^2 \Omega_W}{\partial p^2} &= -A\frac{\partial^2 H_W}{\partial p^2}\Omega_W - A\frac{\partial H_W}{\partial p}\frac{\partial \Omega_W}{\partial p} \\
&= -A\frac{\partial^2 H_W}{\partial p^2}\Omega_W + \left(A\frac{\partial H_W}{\partial p}\right)^2 \\
&= -\frac{A}{m}\Omega_W + \left(A\frac{p}{m}\right)^2 \Omega_W \\
&= -\frac{A}{m}\Omega + A^2\frac{p^2}{m^2}\Omega_W \ , \qquad \text{(B.14)}
\end{aligned}$$

and finally with respect to β:

$$\frac{\partial \Omega_W}{\partial \beta} = \left(-\frac{\partial A}{\partial \beta}H_W + \frac{\partial B}{\partial \beta}\right)\Omega_W \ . \qquad \text{(B.15)}$$

Substituting Eqs. (B.13), (B.14) and (B.15) back into the the Wigner transformed Bloch equation, and dividing through by Ω_W, the equation becomes

$$\begin{aligned}
-\frac{\partial A}{\partial \beta}H_W + \frac{\partial B}{\partial \beta} &= -\left(\frac{p^2}{2m} + \frac{1}{2}m\omega^2 q^2\right) + \frac{\hbar^2}{8}A^2 m\omega^4 q^2 - \frac{\hbar}{8}A\omega^2 \\
&- \frac{\hbar^2}{8}\omega^2 A + \frac{\hbar^2}{8}\omega^2 A^2\frac{p^2}{m} \\
&= -H_W + \frac{\hbar^2}{8}\left[A^2 m\omega^4 q^2 - A\omega^2 - \omega^2 A + \omega^2 A^2\frac{p^2}{m}\right] \\
&= -H_W + \frac{\hbar^2}{4}\left[-A\omega^2 + \omega^2 A^2\left(\frac{1}{2}m\omega^2 q^2 + \frac{p^2}{2m}\right)\right] \\
&= -H_W + \left(\frac{\hbar\omega}{2}\right)^2\left[-A + A^2 H_W\right] \ . \qquad \text{(B.16)}
\end{aligned}$$

Performing some rearranging, one obtains

$$\Rightarrow -\frac{\partial A}{\partial \beta} H_W + H_W \;\; = \;\; -\frac{\partial B}{\partial \beta} + \left(\frac{\hbar\omega}{2}\right)^2 \left[-A + A^2 H_W\right] \; ,$$

$$\Rightarrow \left[-\frac{\partial A}{\partial \beta} + 1 - \left(\frac{\hbar\omega A}{2}\right)^2\right] H_W + \left[\frac{\partial B}{\partial \beta} + \left(\frac{\hbar\omega}{2}\right)^2 A\right] = 0 \; . \tag{B.17}$$

The terms in both pairs of square brackets are dependent on β only, and not on the phase space coordinates q and p. Because of this, the equation must hold for all values of (q, p), and each set of square brackets must vanish independently. Therefore

$$\frac{dA}{d\beta} - 1 + \frac{(\hbar\omega)^2}{4} A^2 = 0 \; , \tag{B.18}$$

and

$$\frac{dB}{d\beta} + \frac{(\hbar\omega)^2}{4} A = 0 \; . \tag{B.19}$$

Consider Eq. (B.18), which only contains the function $A(\beta)$. It can be rewritten as

$$\frac{dA}{1 - \frac{(\hbar\omega)^2}{4} A^2} = d\beta \; . \tag{B.20}$$

To solve this equation, it is convenient to perform a change of variables. Letting $x = \frac{\hbar\omega}{2} A$, then $dA = \frac{2}{\hbar\omega} dx$, and the above equation becomes

$$\frac{2}{\hbar\omega}\int\frac{dx}{1-x^2} \;=\; \int d\beta\,. \tag{B.21}$$

Using the identity

$$\frac{1}{1-x^2} = \frac{1}{2}\frac{d}{dx}\ln\left(\frac{1+x}{1-x}\right)\,, \tag{B.22}$$

one obtains

$$\begin{aligned}\beta &= \frac{1}{\hbar\omega}\int dx\frac{d}{dx}\ln\left(\frac{1+x}{1-x}\right)\\ &= \frac{1}{\hbar\omega}\ln\left(\frac{1+x}{1-x}\right)\\ &= \frac{1}{\hbar\omega}\ln\left(\frac{1+\frac{\hbar\omega}{2}A}{1-\frac{\hbar\omega}{2}A}\right)\,,\end{aligned} \tag{B.23}$$

or, rewriting it in exponential form:

$$e^{\hbar\omega\beta} = \frac{1+\frac{\hbar\omega}{2}A}{1-\frac{\hbar\omega}{2}A}\,.$$

It is then a simple case of performing some rearrangement to obtain $A(\beta)$ as the subject of the formula:

$$\begin{aligned}A(\beta) &= \frac{2}{\hbar\omega}\frac{e^{\hbar\omega\beta}-1}{e^{\hbar\omega\beta}+1}\\ &= \frac{2}{\hbar\omega}\frac{e^{\frac{\hbar\omega}{2}\beta}-e^{-\frac{\hbar\omega}{2}\beta}}{e^{\frac{\hbar\omega}{2}\beta}+e^{-\frac{\hbar\omega}{2}\beta}}\\ &= \frac{2}{\hbar\omega}\tanh\left(\frac{\hbar\omega}{2}\beta\right)\,.\end{aligned} \tag{B.24}$$

To obtain the function $B(\beta)$, Eq. (B.24) must now be substituted into Eq. (B.19):

$$\frac{\partial B}{\partial \beta} + \left(\frac{\hbar\omega}{2}\right)\frac{2}{\hbar\omega}\tanh\left(\frac{\hbar\omega}{2}\beta\right) = 0\,. \tag{B.25}$$

Rearranging to make B the subject of the formula gives

$$B = -\frac{\hbar\omega}{2}\int d\beta \tanh\left(\frac{\hbar\omega\beta}{2}\right)\,. \tag{B.26}$$

In order to solve this integral, one can consider

$$\begin{aligned}\tanh x &= \frac{\sinh x}{\cosh x} \\ &= \frac{d}{dx}\ln(\cosh x)\,.\end{aligned} \tag{B.27}$$

Identifying $x = \frac{\hbar\omega\beta}{2}$, and thus $d\beta = \frac{2}{\hbar\omega}dx$, yields

$$\begin{aligned}\Rightarrow B &= -\frac{\hbar\omega}{2}\frac{2}{\hbar\omega}\int dx \tanh x \\ &= -\int dx \frac{d}{dx}\ln(\cosh x) \\ &= -\ln(\cosh x) \\ &= -\ln\left[\cosh\left(\frac{\hbar\omega\beta}{2}\right)\right]\,.\end{aligned} \tag{B.28}$$

Now that $A(\beta)$ and $B(\beta)$ have been determined, they can be substituted back into the original ansatz for the unnormalised distribution function Ω_W:

$$\begin{aligned}\Omega_W &= e^{-A(\beta)H_W(q,p)+B(\beta)} \\ &= e^{-\ln\cosh\left(\frac{\hbar\omega\beta}{2}\right)}e^{-\frac{2}{\hbar\omega}\tanh\left(\frac{\hbar\omega\beta}{2}\right)H_W(q,p)}\end{aligned}$$

$$= \frac{1}{\cosh\left(\frac{\hbar\omega\beta}{2}\right)} e^{-\frac{2}{\hbar\omega}\tanh\left(\frac{\hbar\omega\beta}{2}\right)H_W(q,p)} \,. \tag{B.29}$$

In order to obtain the full distribution function for the canonical ensemble of harmonic oscillators, all that remains is to determine the partition $Z(\beta)$. It is defined as

$$\begin{aligned} Z(\beta) &= \int\int dqdp\, \Omega_W(q,p,\beta) \\ &= \frac{1}{\cosh\left(\frac{\hbar\omega\beta}{2}\right)} \int\int dqdp\, e^{-\frac{2}{\hbar\omega}\tanh\left(\frac{\hbar\omega\beta}{2}\right)\left(\frac{p^2}{2m}+\frac{1}{2}m\omega^2q^2\right)} \,, \end{aligned} \tag{B.30}$$

where the integrals are performed over all of phase space. The integrand in the equation above can be factorised into q-dependent terms and p-dependent terms, to give

$$Z(\beta) = \frac{1}{\cosh\left(\frac{\hbar\omega\beta}{2}\right)} \int dp e^{-\frac{2}{\hbar\omega}\tanh\left(\frac{\hbar\omega\beta}{2}\right)\frac{p^2}{2m}} \int dq e^{-\frac{2}{\hbar\omega}\tanh\left(\frac{\hbar\omega\beta}{2}\right)\frac{m\omega^2}{2}q^2} \,. \tag{B.31}$$

Both the integrands are simple Gaussian functions, so

$$\begin{aligned} Z(\beta) &= \frac{1}{\cosh\left(\frac{\hbar\omega\beta}{2}\right)} \left(\frac{\pi}{\left(\frac{1}{\hbar\omega m}\right)\tanh\left(\hbar\omega\beta\right)}\right)^{\frac{1}{2}} \left(\frac{\pi}{\left(\frac{m\omega}{\hbar}\right)\tanh\left(\hbar\omega\beta\right)}\right)^{\frac{1}{2}} \\ &= \frac{1}{\cosh\left(\frac{\hbar\omega\beta}{2}\right)} \frac{\pi}{\tanh\left(\frac{\hbar\omega\beta}{2}\right)} \frac{1}{\sqrt{\frac{1}{\hbar\omega m}\frac{m\omega}{\hbar}}} \\ &= \frac{\pi\hbar}{\cosh\left(\frac{\hbar\omega\beta}{2}\right)} \frac{\cosh\left(\frac{\hbar\omega\beta}{2}\right)}{\sinh\left(\frac{\hbar\omega\beta}{2}\right)} \\ &= \frac{\pi\hbar}{\sinh\left(\frac{\hbar\omega\beta}{2}\right)} \,. \end{aligned} \tag{B.32}$$

The normalised Wigner transformed distribution function is given by

$$\rho_W(q,p,\beta) = \frac{1}{Z(\beta)}\Omega_W(q,p,\beta)\ .$$

Substituting the expressions for Ω_W and $Z(\beta)$, given by Eqs. (B.29) and (B.32) respectively, produces the final result:

$$\begin{aligned}\rho_W(q,p,\beta) &= \frac{\sinh\left(\frac{\hbar\omega\beta}{2}\right)}{\pi\hbar}\frac{e^{-\frac{2}{\hbar\omega}\tanh\left(\frac{\hbar\omega\beta}{2}\right)H}}{\cosh\left(\frac{\hbar\omega\beta}{2}\right)} \\ &= \frac{1}{\pi\hbar}\tanh\left(\frac{\hbar\omega\beta}{2}\right)e^{-\frac{2}{\hbar\omega}\tanh\left(\frac{\hbar\omega\beta}{2}\right)H}\ . \qquad \text{(B.33)}\end{aligned}$$

Bibliography

[1] H. de Raedt, Lecture Notes, Como (1995).

[2] B. J. Alder and T. E. Wainwright, J. Chem. Phys. **27**, 1208-1209 (1957).

[3] B. J. Alder and T. E. Wainwright, J. Chem. Phys. **31**, 459-466 (1959).

[4] J. C. Tully, *Classical and Quantum Dynamics in Condensed Phase Simulations* (World Scientific Publishing, 1998) pp 489, 514.

[5] J. C. Slater, Phys. Rev. **81**, 385-390 (1951).

[6] E. J. Baerends, D. E. Ellis, P. Ros, Chem. Phys. **2**, 41-51 (1973).

[7] P. Hohenberg and W. Kohn, Phys. Rev. **136**, B864-B871 (1964).

[8] W. Kohn and L. J. Sham, Phys. Rev. **140**, A1133-A1138 (1965).

[9] A. D. McLachlan, Mol. Phys. **8**, 39 (1964).

[10] J. C. Tully and R. K. Preston, J. Chem. Phys. **55**, 562 (1971).

[11] W. H. Miller and F. F. George, J. Chem. Phys. **56**, 5637-5653 (1972).

[12] D. MacKernan, G. Ciccotti and R. Kapral, J. Chem. Phys. **116**, 2346-2353 (2002).

[13] E. J. Heller, B. Segev and A. V. Sergeev, J. Phys. Chem. B **106**, 8471-8478 (2002).

[14] S. Nielsen, R. Kapral and G. Ciccotti, J. Chem. Phys. **225**, 5805-5815 (2001).

[15] T. Beth and G. Leuchs, *Quantum Information Processing - Second Edition* (Wiley-VCH, Germany, 2005).

[16] D. G. Angelakis, M. Christandl, A. Ekert, A. Kay and S. Kulik, *Quantum Information Processing - From Theory to Experiment* (IOS Press, Amsterdam, 2006).

[17] G. Grynberg, A. Aspect and C. Fabre, *Introduction to Quantum Optics: From the Semi-classical Approach to Quantized Light* (Cambridge University Press, Cambridge, 2010).

[18] P. Kok and B. W. Lovett, *Introduction to Optical Quantum Information Processing* (Cambridge University Press, Cambridge, 2010).

[19] G. Hanna and R. Kapral, Acc. Chem. Res. **39**, 21-27 (2006).

[20] R. Kapral and G. Ciccotti, "Transport Coefficients of Quantum-Classical Systems", in *Computer Simulations in Condensed Matter: From Materials to Chemical Biology - Vol. 1*, M. Ferrario, G. Ciccotti and K. Binder Eds. (Springer, Berlin, 2006).

[21] G. Hanna and R. Kapral, J. Chem. Phys. **122**, 244505 (2005).

[22] G. S. Engel, T. R. Calhoun, E. L. Read, T. Ahn, T. Mančal, Y. Cheng, R. E. Blankenship and G. R, Fleming, Nature **446**, 782-786 (2007).

[23] A. Sergi, Atti. Acc. Pelor. Pericol. Cl. Sci. Fis. Mat. Nat. **87**, C1C0901001 (2009).

[24] D. F. Coker, "Computer Simulation Methods for Nonadiabatic Dynamics in Condensed Systems", in *Computer Simulations in Chemical Physics*, M. P. Allen and D. J. Tildesley Eds. (Kluwer Academic Publishers, Netherlands, 1993).

[25] I. V. Aleksandrov, Z. Natureforsch A, **36**, 902-908 (1981).

[26] V. I. Gerasimenko, Theor. Math. Phys. **50**, 77-87 (1982).

[27] W. Boucher and J. Traschen, Phys. Rev. D, **37**, 3522-3532 (1988).

[28] W. Y. Zhang and R. Balescu, J. Plasma Phys. **40**, 199-213 (1988).

[29] C. C. Martens and J. Y. Fang, J. Chem. Phys. **106**, 4918-4930 (1996).

[30] O. V. Prezhdo and V. V. Kisil, Phys. Rev. A **56**, 162-175 (1997).

[31] R. Kapral and G. Ciccotti, J. Chem. Phys. **110**, 8919-8929 (1999).

[32] I. Horenko, C. Salzmann, B. Schmidt and C. Schutte, J. Chem. Phys. **117**, 11075-11088 (2002).

[33] Q. Shi and E. Geva, J. Chem. Phys. **121**, 3393-3404 (2004).

[34] D. MacKernan, R. Kapral and G. Ciccotti, J. Phys.:Condens. Matter **14**, 9069-9076 (2002).

[35] D. Mac Kernan, G. Ciccotti and R. Kapral, J. Phys. Chem. B **112**, 424-432 (2008).

[36] A. Sergi, F. Petruccione, Phys. Rev. E **81**, 032101 (2010).

[37] D. A. Uken, A. Sergi and F. Petruccione, Phys. Scr. **T143**, 014024 (6pp) (2011).

[38] D. A. Uken and A. Sergi, Phys. Rev. E **88**, 033301 (7pp) (2013).

[39] N. F. Mott, Proc. Cambridge Phil. Soc. **27**, 553 (1931).

[40] A. G. Redfield, Adv. Magn. Reson. **1**, 1 (1965).

[41] J. M. Jean, R. A. Friesner and G. R. Fleming, J. Chem. Phys. **96**, 5827 (1992).

[42] W. T. Pollard, A. K. Felts and R. A. Friesner, Adv. Chem. Phys. **93**, 77 (1996).

[43] P. Ehrenfest, Z. Phys. **45**, 455 (1927).

[44] P. A. M. Dirac, Proc. Cambridge Philos. Soc. **26**, 376 (1930).

[45] M. H. Mittelman, Phys. Rev. **122**, 449 (1961).

[46] W. H. Miller and C. W. McCurdy, J. Chem. Phys. **69**, 5163 (1978).

[47] H. D. Meyer and W. H. Miller, J. Chem. Phys. **72**, 2272 (1980).

[48] D. A. Micha, J. Chem. Phys. **78**, 7138 (1983).

[49] M. Morin, N. J. Levinos and A. L. Harris, J. Chem. Phys. **96**, 3950 (1992).

[50] J. C. Tully, M. Gomez and M. Head-Gordon, J. Vac. Sci. Technol. **A11**, 1914 (1993).

[51] M. Head-Gordon and J. C. Tully, J. Chem. Phys. **103**, 10137 (1995).

[52] S. Hammes-Schiffer and J. C. Tully, J. Chem. Phys. **101**, 4657-4667 (1994).

[53] L. Ballentine, *Quantum Mechanics - A Modern Development* (World Scientific Publishing, 1998).

[54] E. Wigner, Phys. Rev. **40**, 749-759 (1932).

[55] H. Weyl, *The Theory of Groups and Quantum Mechanics* (Dover, New York, 1931).

[56] W. B. Case, Am. J. Phys. **76**, 937-946 (2008).

[57] D. F. Styer *et al.*, Am. J. Phys. **70**, 288, 297 (2001).

[58] A. Sergi, D. MacKernan, G. Ciccotti and R. Kapral, Theor. Chem. Acc. **110**, 49-58 (2003).

[59] R. Kubo, M. Toda and N. Hashitsume, *Statistical Physics II: Nonequilibrium Statistical Mechanics, 2nd Ed* (Springer, London, 2012).

[60] A. Sergi, Phys. Rev. E **72**, 066125 (2005).

[61] A. Sergi and P. Giaquinta, Phys. Essays **20**, 629-639 (2007).

[62] R. Balescu, *Equilibrium and Non-equilibrium Statistical Mechanics* (John Wiley and Sons, New York, 1975).

[63] S. Nosè, Mol. Phys. **52**, 255-268 (1984).

[64] A. Sergi, J. Phys. A: Math. Theor. **40**, F347-F354 (2007).

[65] J. McCauley, *Classical Mechanics* (Cambridge University Press, Cambridge, 1977).

[66] H. Goldstein, *Classical Mechanics, 2nd Ed* (Addison-Wesley, London, 1980).

[67] D. A. Uken and A. Sergi, Mod. Phys. Lett. B **25**, 1271-1280 (2011).

[68] A. J. Leggett, S. Chakravarty, A. T. Dorsey, M. P. A. Fisher, A. Garg, W. Zwerger, Rev. Mod. Phys. **59**, 1-85 (1987).

[69] C. Cohen-Tannoudji, B. Diu and F. Laloë, *Quantum Mechanics - Volume 1* (John Wiley and Sons, New York, 1977)

[70] N. Makri and K. Thompson, Chem. Phys. Lett. **291**, 101 (1998).

[71] M. Hillery, R. F. O'Connell, M. O. Scully and E. P. Wigner, Phys. Rep. **106**, 121-167 (1984).

[72] K. Thompson and N. Makri, J. Chem. Phys. **110**, 1343-1353 (1999).

[73] N. Makri, J. Phys. Chem. B **103**, 2823-2829 (1999).

[74] D. E. Makarov. and N. Makri, Chem. Phys. Lett. **221**, 482-491 (1994).

[75] C. H. Mak and D. Chandler, Phys. Rev. A **44**, 2352-2369 (1991).